Electronic Supplementary Material (ESI) for Physical Chemistry Chemical Physics.

Supplementary Information

The activation of carbon dioxide by first row transition metals (Sc – Zn)

Kacper Blaziak,[a,b] Demeter Tzeli,[c] Sotiris S. Xantheas[d,e] and Einar Uggerud[a,*]

[a] Department of Chemistry and Hylleraas Centre for Quantum Molecular Sciences, University of Oslo, PO Box 1033, Blindern, Oslo N-0135, Norway

[b] Institute of Organic Chemistry, Polish Academy of Sciences, Kasprzaka 44/52, 01-224 Warsaw, Poland

[c] Theoretical and Physical Chemistry Institute, National Hellenic Research Foundation, 48 Vassileos Constantinou, Athens 116 35, Greece

[d] Advanced Computing, Mathematics and Data Division, Pacific Northwest National Laboratory, 902 Battelle Boulevard, P.O. Box 999, MS K1-83, WA, 99352, USA

[e] Department of Chemistry, University of Washington, Seattle, WA, 98195, USA

[*] Corresponding author. Email: einar.uggerud@kjemi.uio.no

Table of Contents

1. Experimental procedures

1.1. Sample preparation

Samples were prepared from commercially available MCl_2 salts, where M=Cr, Mn, Fe, Co, Ni, Cu, Zn, and oxalic acid (Sigma-Aldrich). Solutions of oxalic acid (1 mM) and metal (II) chloride (2 mM) in pure methanol were introduced to the electrospray ion source by direct injection using a laboratory syringe pump.

1.2. API 3000 Triple quadrupole mass spectrometer

The collision-induced dissociation (CID) experiments and carboxylation reaction experiments were performed with an API 3000 triple quadrupole mass spectrometer (TQMS) from Applied Biosystems. Model spectra are presented in the main text. The instrument is equipped with a TurboIonSpray source operated in negative ion mode. For all measurements, source parameters were as follows: capillary voltage: 4,5 kV, nebulizer gas: 8, curtain gas: 8 (arbitrary units). For each measurement, ion declustering potential (DP) and focusing potential (FP) were ramped between 5-100V and 150-300V, respectively, in order to produce the optimal intensity.

All representative CID spectra presented in the main text were recorded at one arbitrary value of collision energy (CE) of 15 eV and collision cell exit potential (CXP) was set at 15eV (lab frame). Nominal pressure of the collision gas (N_2) was set at 6 (arbitrary units), which according to the manufacturer's specification, corresponds to a pressure of approx. 2.3×10^{-3} mBar.

In order to perform bimolecular gas-phase reactions, we introduced CO_2 gas from a bottle (analytical purity) into the collision cell by an in-house gas inlet system. Appropriate *m/z* values corresponding to the MCl^- ions were filtered by the first quadrupole (Q1) and focused in the linear quadrupole collision cell (Q2), where the carboxylation reactions proceeds. All of the spectra presented in the main text were collected for 50-240 min at nominal carbon dioxide pressure of 3.5×10^{-3} mBar. Ion trap parameters were ramped between CE = 4-5 eV and CXP = 4-6 eV in the lab frame.

Original spectra from Analyst® Software 4.2 (ABSciex) are presented below.

1.2.1 Reaction spectra recorded with API 3000 (TQMS) spectrometer.

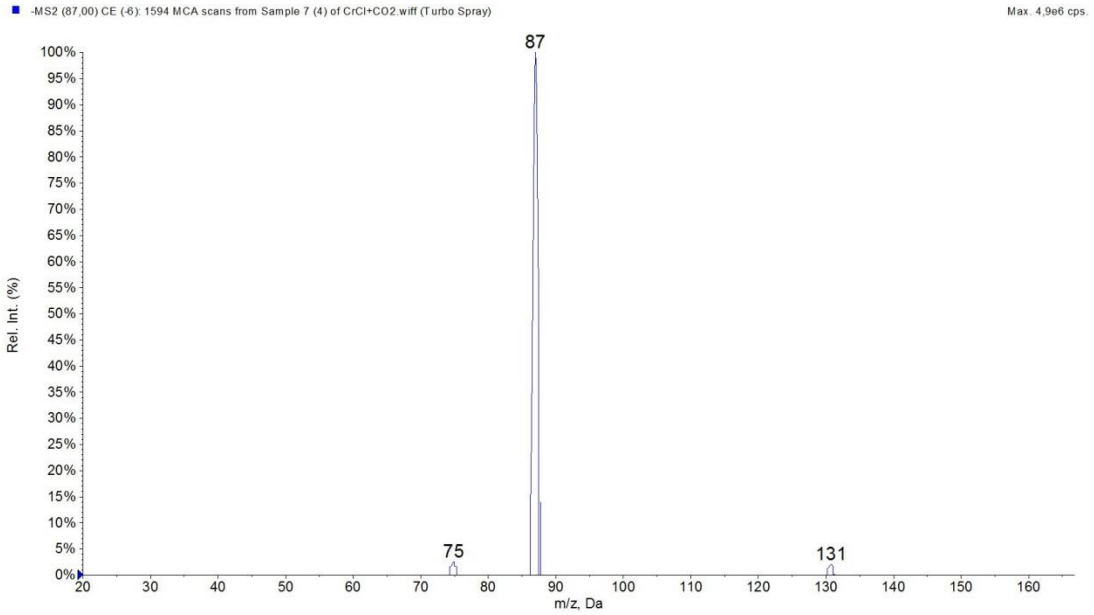

Figure S 1 Mass spectrum of the reaction between $CrCl^-$ (*m/z* 87) and CO_2 recorded at a collision energy of 1.89 eV (CM) with CO_2 at nominal pressure of 3.5×10^{-3} mBar. *Comment*: Spectrum peaks correspond to: *m/z* 75 unidentified, *m/z* 87 $[CrCl]^-$, *m/z* 131 $[ClCrCO_2]^-$.

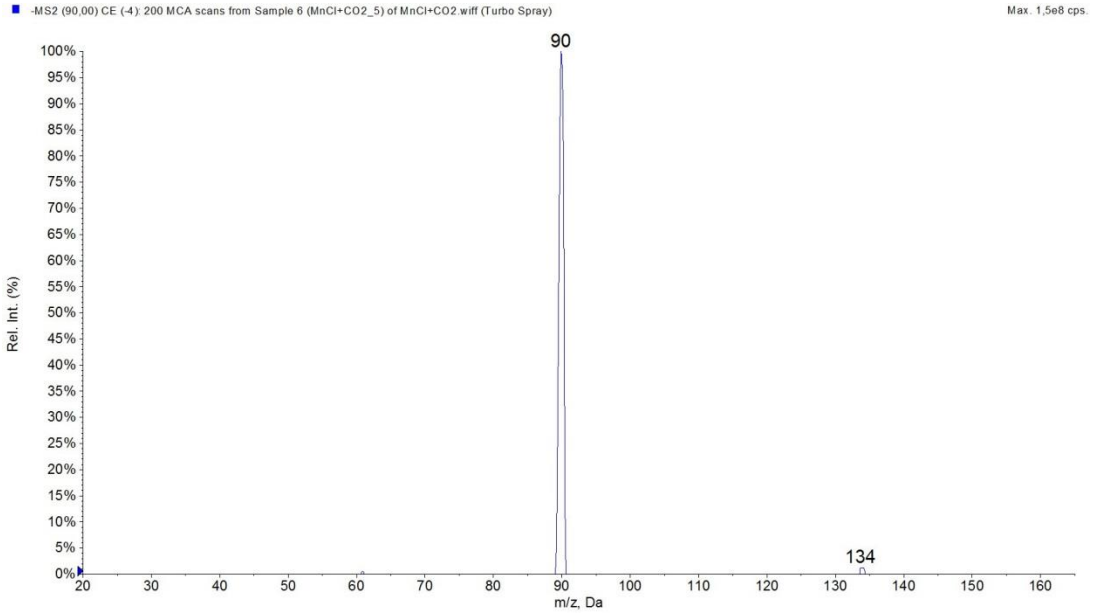

Figure S 2 Mass spectrum of the reaction between $MnCl^-$ (*m/z* 90) and CO_2 recorded at a collision energy of 1.23 eV (CM) with CO_2 at nominal pressure of 3.5×10^{-3} mBar. *Comment*: Spectrum peaks correspond to: *m/z* 90 $[MnCl]^-$, *m/z* 134 $[ClMnCO_2]^-$.

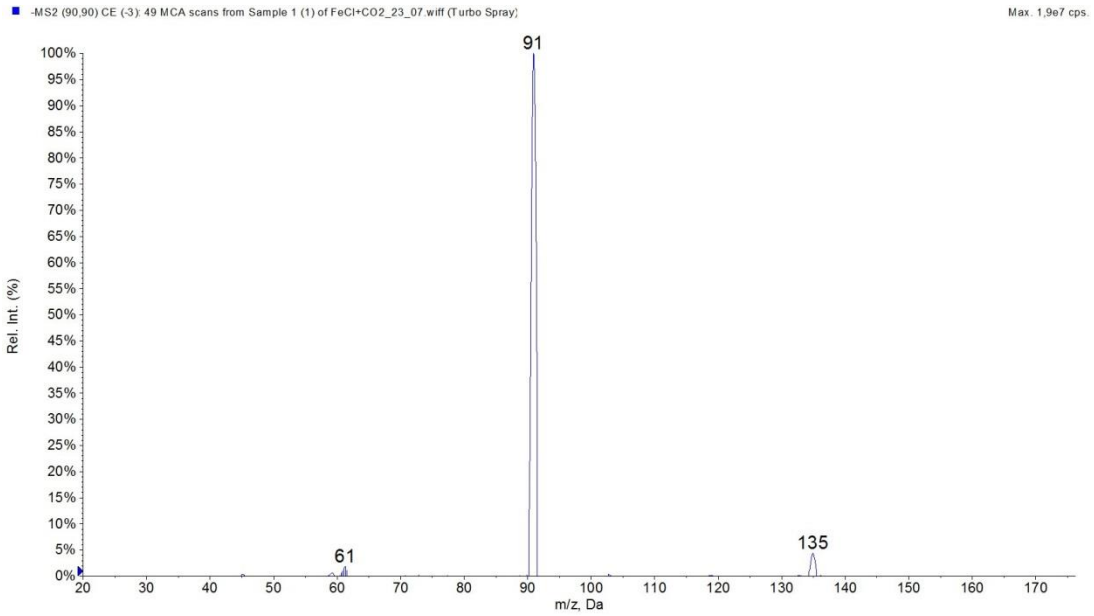

Figure S 3 Mass spectrum of the reaction between $FeCl^-$ (*m/z* 91) and CO_2 recorded at a collision energy of 1.8 eV (CM) with CO_2 at nominal pressure of 3.5×10^{-3} mBar. *Comment*: Spectrum peaks correspond to: *m/z* 61 unidentified, *m/z* 91 $[FeCl]^-$, *m/z* 135 $[ClFeCO_2]^-$.

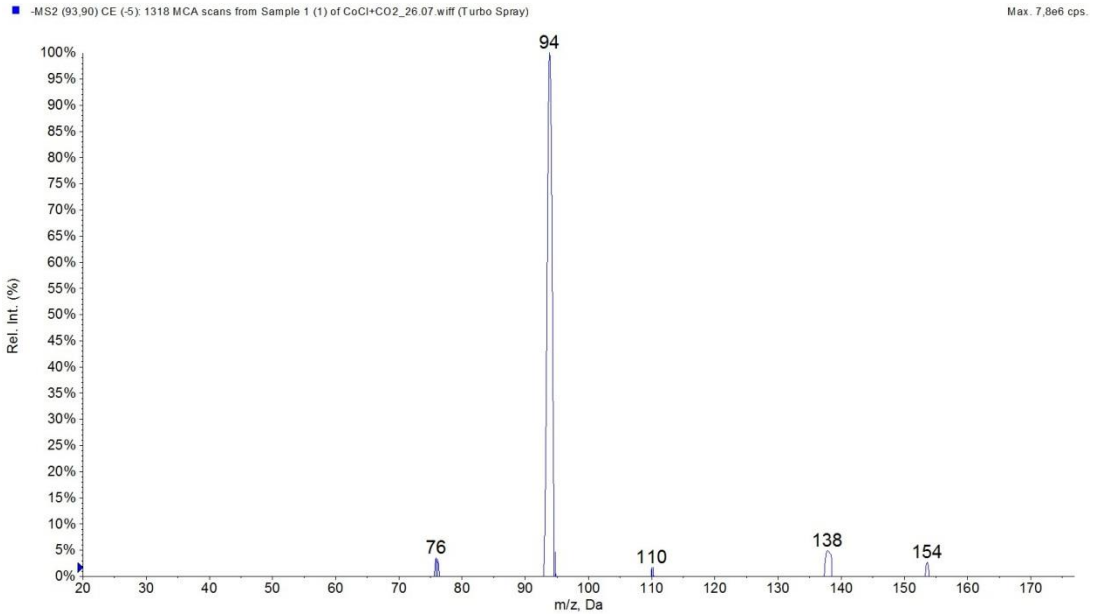

Figure S 4 Mass spectrum of the reaction between $CoCl^-$ (*m/z* 94) and CO_2 recorded at a collision energy of 1.79 eV (CM) with CO_2 at nominal pressure of 3.5×10^{-3} mBar.

Comment: Spectrum peaks correspond to: *m/z* 76 $[CoOH]^-$, *m/z* 94 $[CoCl]^-$, *m/z* 110 $[ClCoO]^-$, *m/z* 138 $[ClCoCO_2]^-$, *m/z* 154 $[ClCoOCO_2]^-$.

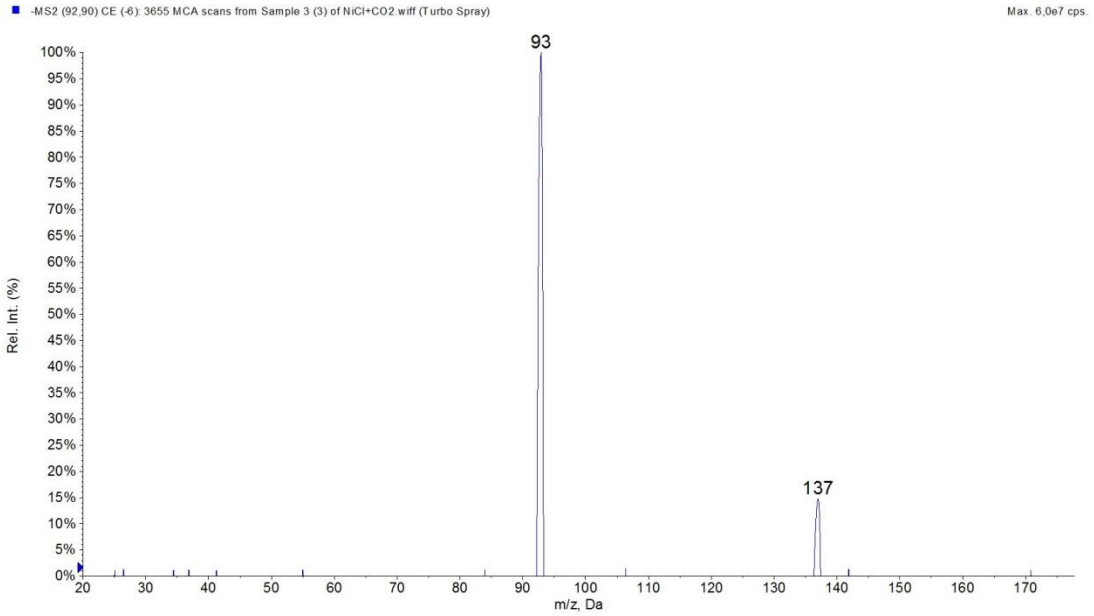

Figure S 5 Mass spectrum of the reaction between $NiCl^-$ (*m/z* 93) and CO_2 recorded at a collision energy of 1.8 eV (CM) with CO_2 at nominal pressure of 3.5×10^{-3} mBar. *Comment*: Spectrum peaks correspond to: *m/z* 93 $[NiCl]^-$, *m/z* 137 $[ClNiCO_2]^-$

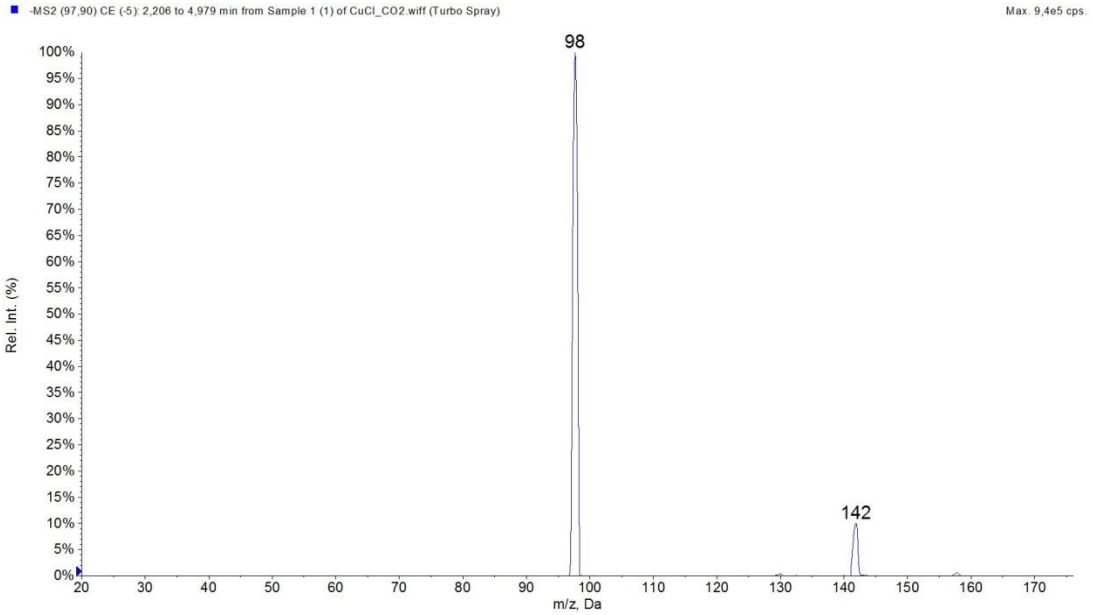

Figure S 6 Mass spectrum of the reaction between $CuCl^-$ (*m/z* 98) and CO_2 recorded at a collision energy of 1.45 eV (CM) with CO_2 at nominal pressure of 3.5×10^{-3} mBar. *Comment*: Spectrum peaks correspond to: *m/z* 98 $[CuCl]^-$, *m/z* 142 $[ClCuCO_2]^-$

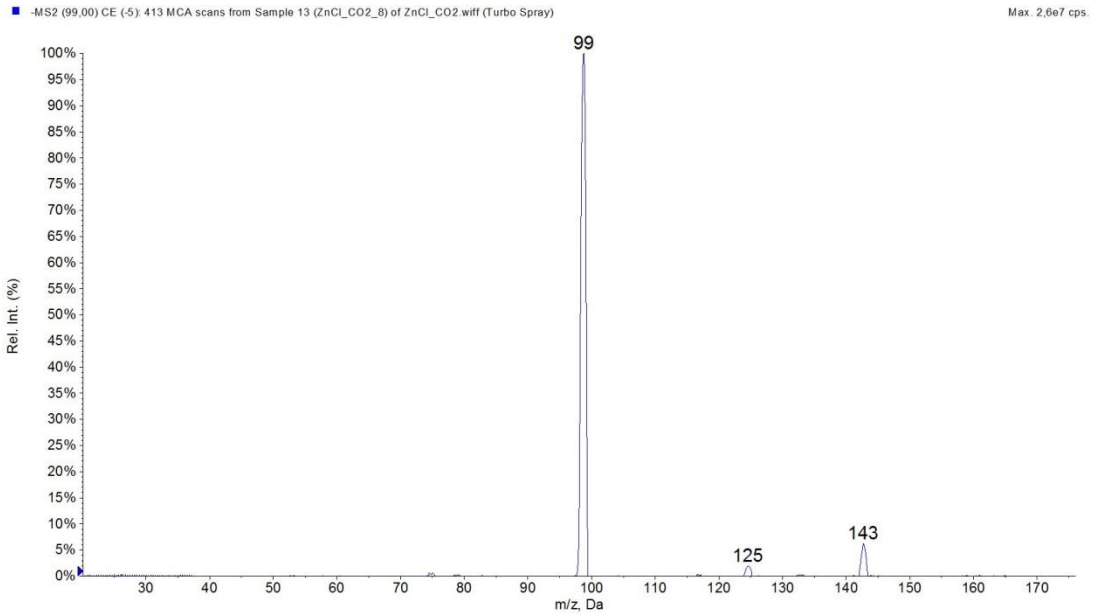

Figure S 7 Mass spectrum of the reaction between $ZnCl^-$ (*m/z* 99) and CO_2 recorded at a collision energy of 1.44 eV (CM) with CO_2 at nominal pressure of 3.5×10^{-3} mBar. *Comment*: Spectrum peaks correspond to: *m/z* 99 $[ZnCl]^-$, *m/z* 125 $[HOZnCO_2]^-$, *m/z* 143 $[ClZnCO_2]^-$

1.2.2 Model CID spectra recorded with API 3000 (TQMS) spectrometer

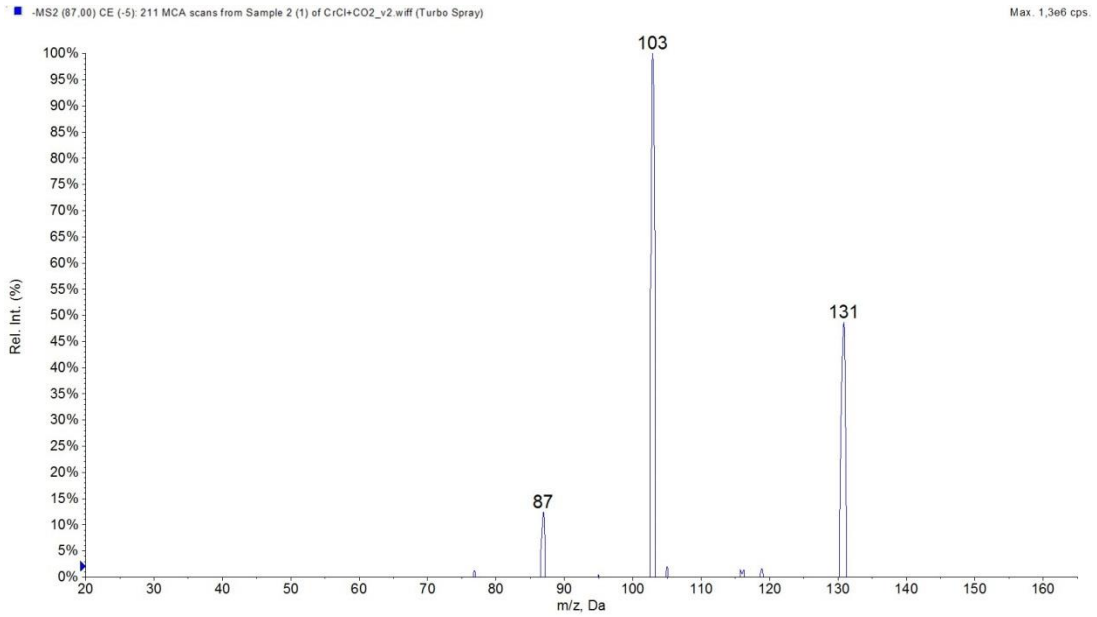

Figure S 8 Fragment ion mass spectrum of $[ClCrCO_2]^-$ (*m/z* 131) recorded at center of mass energy of 2.64 eV (CM) with nitrogen as the collision gas at nominal pressures of 2.30×10^{-3} mBar. *Comment*: Spectrum peaks correspond to: *m/z* 87 $[CrCl]^-$, *m/z* 1073$[ClCrO]^-$, *m/z* 131 $[ClCrCO_2]^-$.

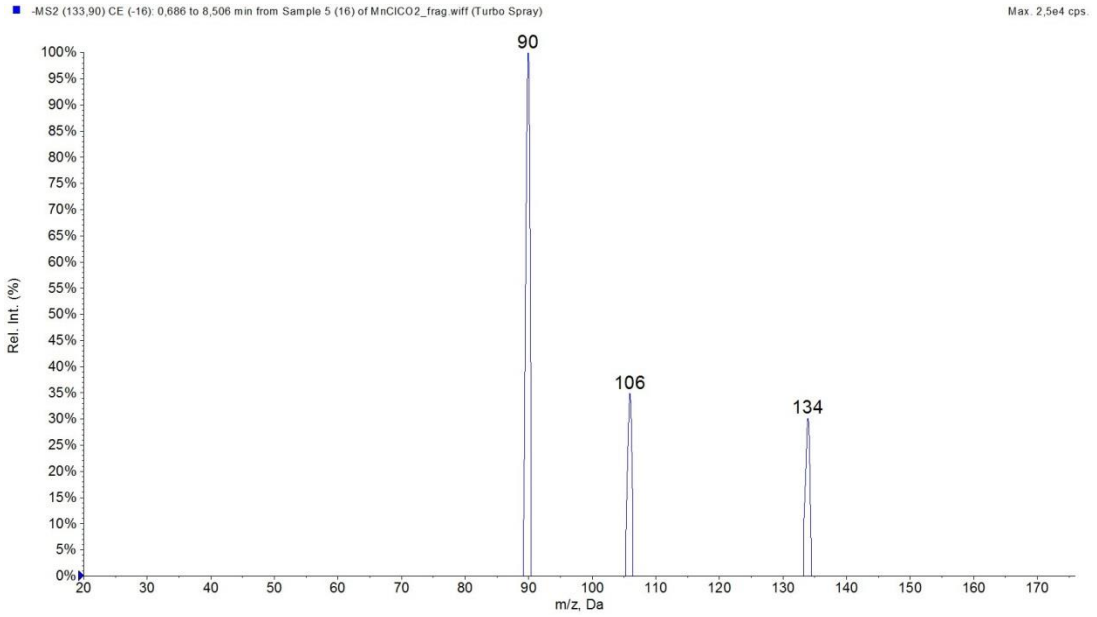

Figure S 9 Fragment ion mass spectrum of $[ClMnCO_2]^-$ (*m/z* 134) recorded at center of mass energy of 2.59 eV (CM) with nitrogen as the collision gas at nominal pressures of 2.30×10^{-3} mBar. *Comment*: Spectrum peaks correspond to: *m/z* 89 $[MnCl]^-$, *m/z* 106 $[ClMnO]^-$, *m/z* 134 $[ClMnCO_2]^-$.

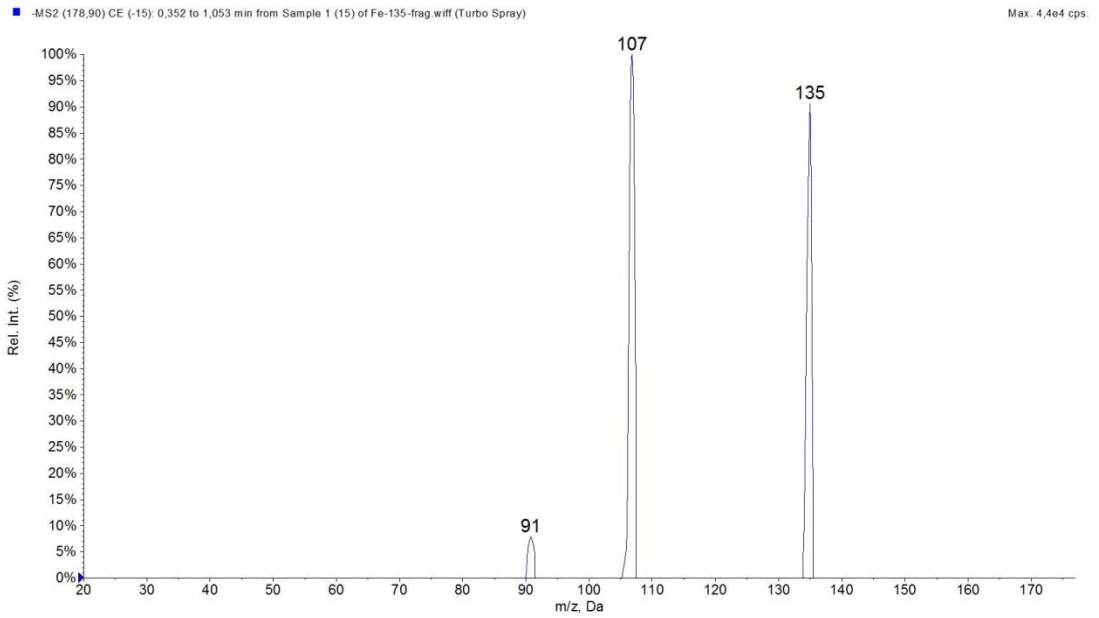

Figure S 10 Fragment ion mass spectrum of $[ClFeCO_2]^-$ (*m/z* 135) recorded at center of mass energy of 2.58 eV (CM) with nitrogen as the collision gas at nominal pressures of 2.30×10^{-3} mBar. *Comment*: Spectrum peaks correspond to: *m/z* 91 $[FeCl]^-$, *m/z* 107 $[ClFeO]^-$, *m/z* 135 $[ClFeCO_2]^-$.

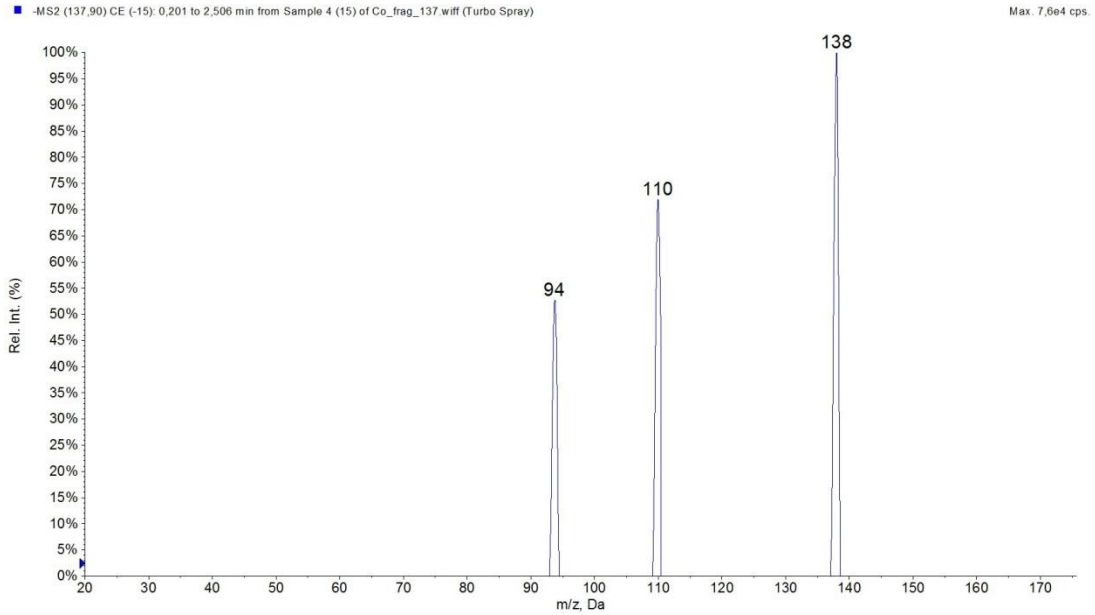

Figure S 11 Fragment ion mass spectrum of $[ClCoCO_2]^-$ (*m/z* 138) recorded at center of mass energy of 2.53 eV (CM) with nitrogen as the collision gas at nominal pressures of 2.30×10^{-3} mBar. *Comment*: Spectrum peaks correspond to: *m/z* 94 $[CoCl]^-$, *m/z* 110 $[ClCoO]^-$, *m/z* 138 $[ClCoCO_2]^-$.

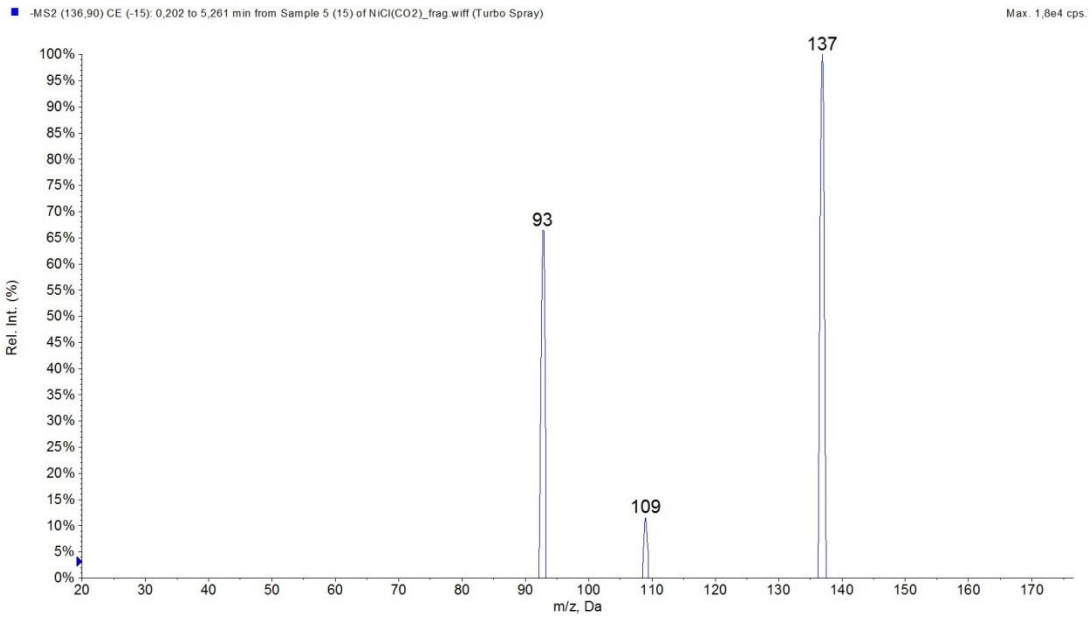

Figure S 12:Fragment ion mass spectrum of $[ClNiCO_2]^-$ (*m/z* 137) recorded at center of mass energy of 2.55 eV (CM) with nitrogen as the collision gas at nominal pressures of 2.30×10^{-3} mBar. *Comment*: Spectrum peaks correspond to: *m/z* 93 $[NiCl]^-$, *m/z* 109 $[ClNiO]^-$, *m/z* 147 $[ClNiCO_2]^-$.

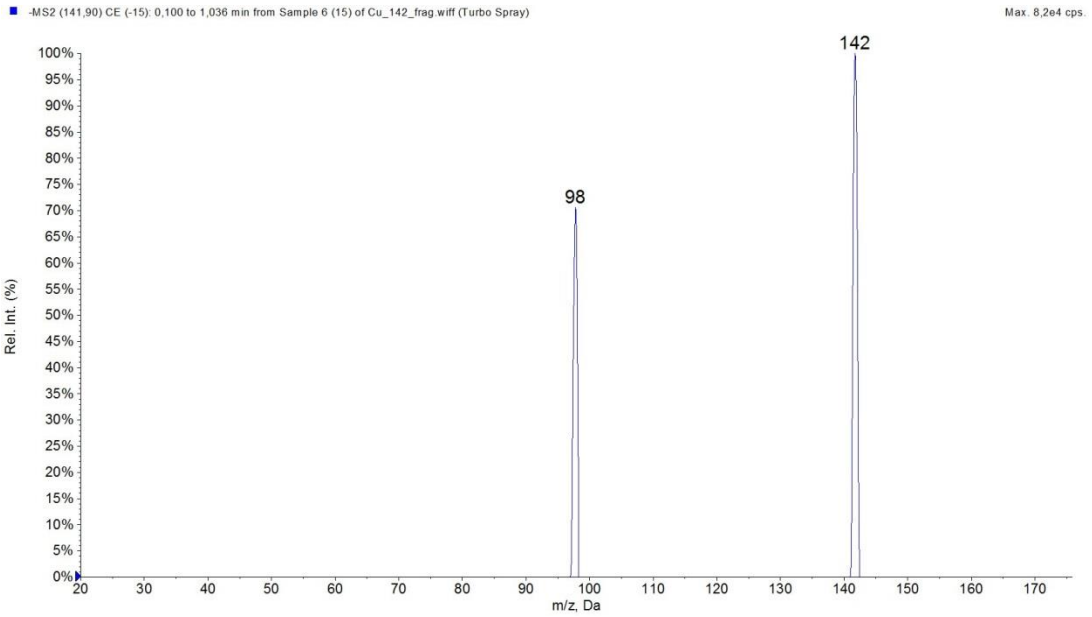

Figure S 13 Fragment ion mass spectrum of $[ClCuCO_2]^-$ (*m/z* 142) recorded at center of mass energy of 2.47 eV (CM) with nitrogen as the collision gas at nominal pressures of 2.30×10^{-3} mBar. *Comment*: Spectrum peaks correspond to: *m/z* 98 $[CuCl]^-$, *m/z* 142 $[ClCuCO_2]^-$.

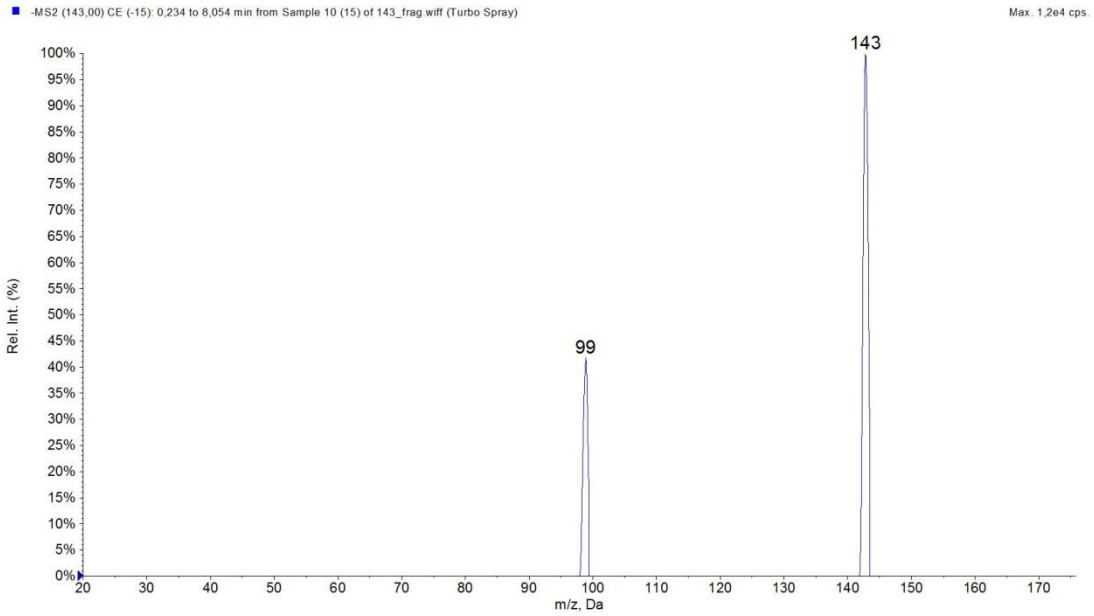

Figure S 14 Fragment ion mass spectrum of $[ClZnCO_2]^-$ (*m/z* 143) recorded at center of mass energy of 2.46 eV (CM) with nitrogen as the collision gas at nominal pressures of 2.30×10^{-3} mBar. *Comment*: Spectrum peaks correspond to: *m/z* 99 $[ZnCl]^-$, *m/z* 143 $[ClZnCO_2]^-$.

1.3 Micromass/Waters Q-ToF 2 mass spectrometer

In order to determine the onset energies for each decarboxylation reaction, collision-induced dissociation (CID) was performed with a modified Micromass/Waters Q-ToF 2 spectrometer. This instrument is a three-sector mass spectrometer with a quadrupole/hexapole/time-of-flight (ToF) geometry. The quadrupole served as a mass filter, the hexapole as the collision cell, and the time-of-flight part as the final mass analyzer. Ions were generated by the equipped ESI source operating in the negative ion mode. For the CID experiments, the collision gas (Ar) was introduced into the collision cell using an in-house gas inlet system.

Breakdown Curves

Collision spectra were recorded by varying the collision energy in incremental steps. Collision mass spectra were recorded with an energy resolution of 2–30 eV in the lab frame and 20-40 minutes of collection time at each step. Additionally, in order to avoid statistical biases, the experiments were repeated twice. Plotting of the total breakdown curves was performed using absolute peak heights. Breakdown curves at five different argon pressures are presented below.

Extrapolation Procedure

In order to determine the onset/threshold energies (at each gas pressure), so as to enable a comparison of the energetics of the observed processes, we used a simple extrapolation procedure. By performing a linear fitting of the approximately linearly rising section of the breakdown curve, we defined the onset energy at each gas pressure by calculating the energy (X value) at zero intensity (Y = 0). In order to compare the experimental and theoretical energy values, we opted also for gas pressure extrapolation. We used the energies taken from extrapolation at five different gas pressures to define the onset energy by calculation of the energy (Y value) at zero gas pressure (X = 0). All breakdown curves and summaries are presented below. We also attempted to apply kinetic extrapolation using the L-CID software[1] in order to determine onset energies from calculated cross-section values. Unfortunately, due to low intensity of the parent ions, the obtained results were unsatisfactory – please see Chapter 1.4 in this document.

Determination of experimental error

Direct determination of uncertainties for the experimentally measured energy values is not a straightforward task. There is a number of possible combinations of the experimental data points in the linear part of the breakdown curves that can be taken into account during the linear extrapolation procedure. Each data selection gives a slightly different slope of the extrapolation curves, which could lead to different onset energies at each gas pressure. Thus, the overall error cannot be determined uniformly for all measurements. In the second step of energy determination we are using the onset energies from five different gas pressures to find the value in the vacuum approximation (0 mBar). In this manner, we usually obtain reasonable, if not perfectly fitted extrapolation lines, with coefficient of determination $R^2 \in (0.76;0.99)$. Overall, we estimate that the experimental error is ca. 40% for each experimental energy value.

Breakdown curves

1.3.1 Collision-induced dissociation (CID) of $ClCr(CO_2)^-$ (*m/z* 131)

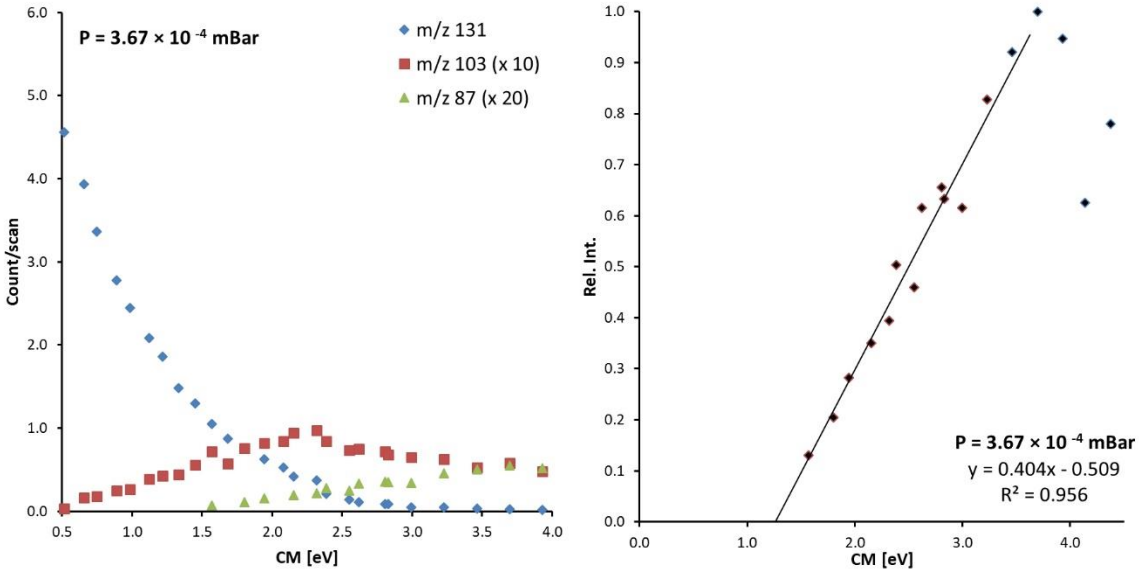

Figure S 15 Breakdown curve for $ClCr(CO_2)^-$ (*m/z* 131) (left) and extrapolation procedure for the decarboxylation of $ClCr(CO_2)^-$ (*m/z* 131) (right) recorded at argon collision gas pressure of 3.67×10^{-4} mBar.

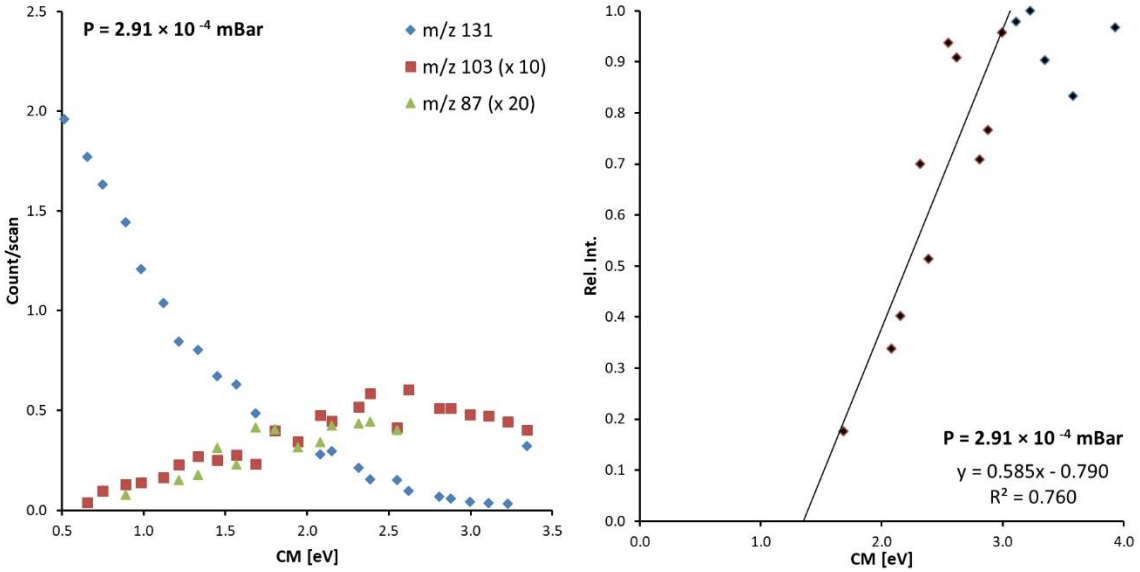

Figure S 16 Breakdown curve for $ClCr(CO_2)^-$ (*m/z* 131) (left) and extrapolation procedure for the decarboxylation of $ClCr(CO_2)^-$ (*m/z* 131) (right) recorded at argon collision gas pressure of 2.91×10^{-4} mBar.

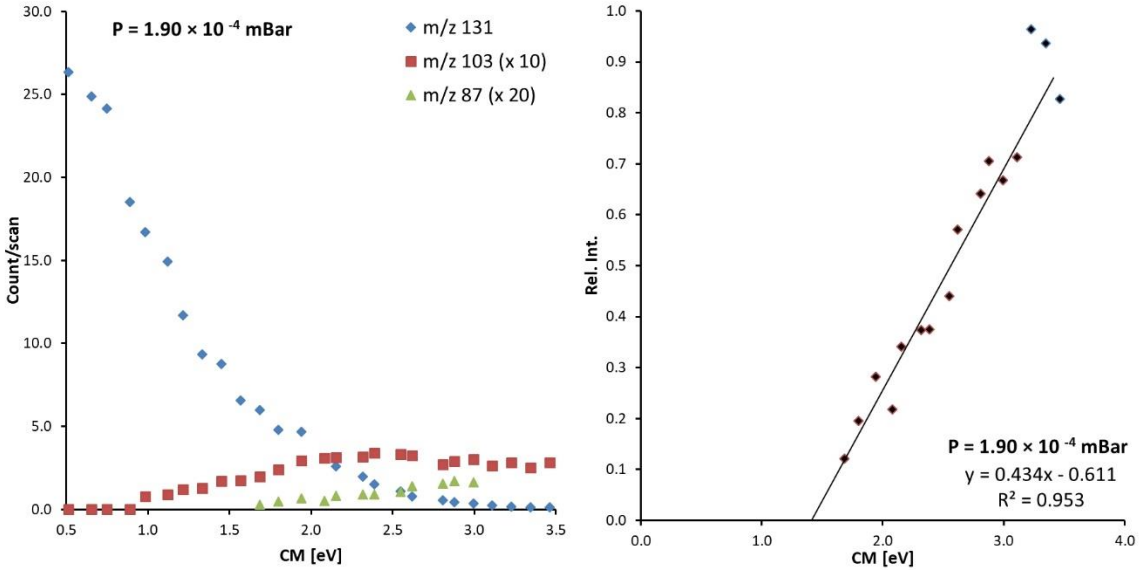

Figure S 17 Breakdown curve for $ClCr(CO_2)^-$ (*m/*z 131) (left) and extrapolation procedure for the decarboxylation of $ClCr(CO_2)^-$ (*m/*z 131) (right) recorded at argon collision gas pressure of 1.90×10^{-4} mBar.

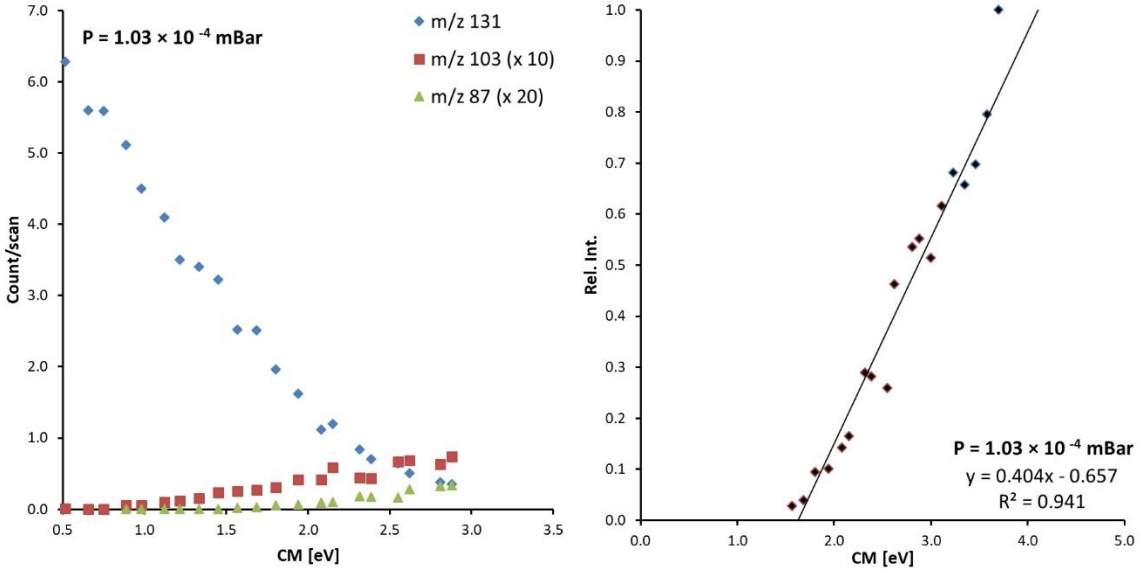

Figure S 18 Breakdown curve for $ClCr(CO_2)^-$ (*m/*z 131) (left) and extrapolation procedure for the decarboxylation of $ClCr(CO_2)^-$ (*m/*z 131) (right) recorded at argon collision gas pressure of 1.03×10^{-4} mBar.

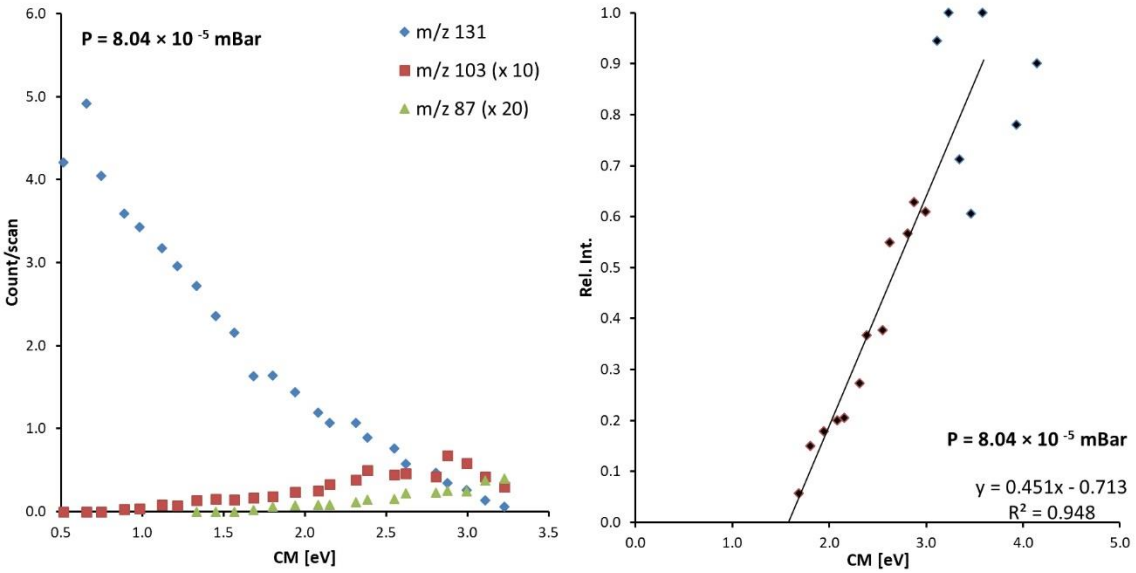

Figure S 19 Breakdown curve for $ClCr(CO_2)^-$ (*m/*z 131) (left) and extrapolation procedure for the decarboxylation of $ClCr(CO_2)^-$ (*m/*z 131) (right) recorded at argon collision gas pressure of 8.04×10^{-5} mBar.

Table S 20 Summary of the values from the extrapolation procedure for decarboxylation of $ClCr(CO_2)^-$ (*m/*z 131).

Pressure [mBar]:	Slope	Intercept	X at Y=0 [eV]	[kJ/mol]
8.04E-05	0.451	-0.713	1.581	151.8
1.03E-04	0.404	-0.657	1.627	156.2
1.90E-04	0.434	-0.611	1.408	135.2
2.91E-04	0.585	-0.790	1.351	129.7
3.67E-04	0.404	-0.509	1.261	121.1
Extrapolated pressure [mBar]:	Intercept	Slope	Y at X=0 [eV]	[kJ/mol]
0	1216.057	1.696	1.696	162.8

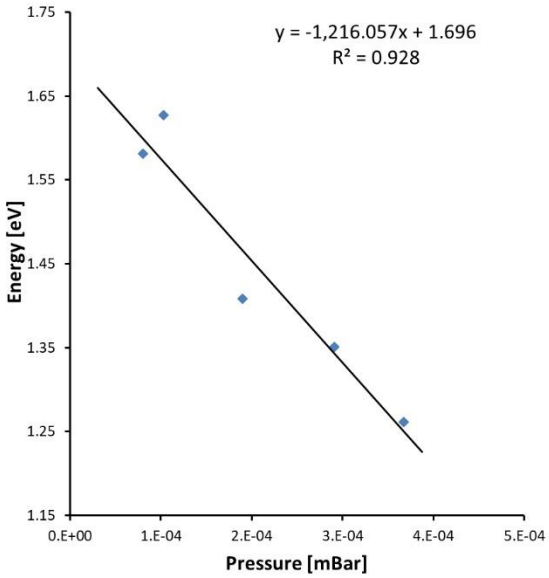

Figure S 21 Extrapolation procedure for the decarboxylation of $ClCr(CO_2)^-$ (*m/*z 131) at a gas pressure of 0 mbar.

1.3.2 Collision-induced dissociation (CID) of $ClMn(CO_2)^-$ (*m/*z 134)

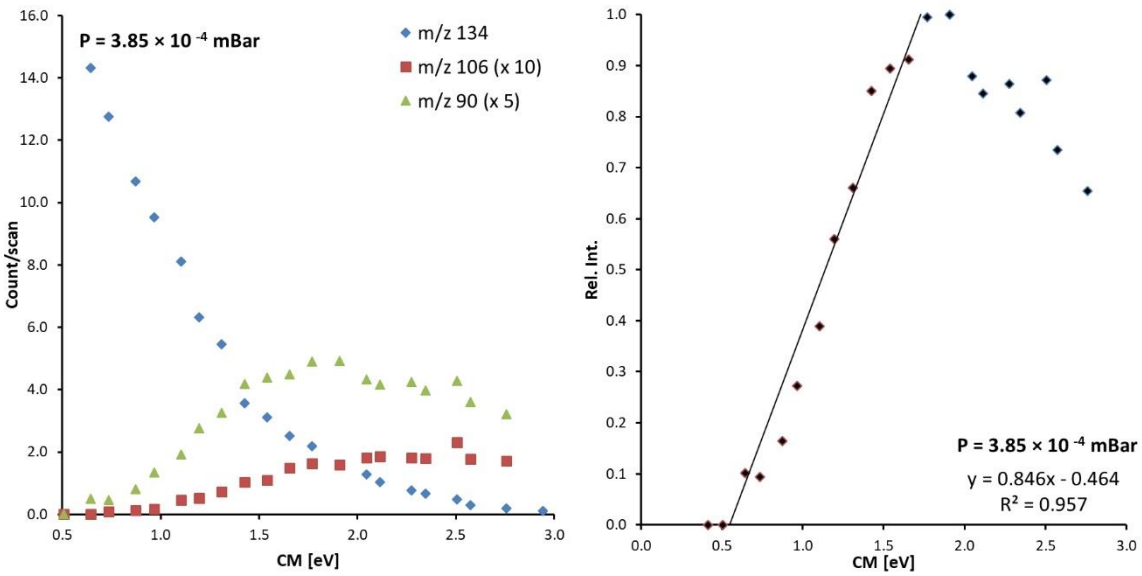

Figure S 22 Breakdown curve for $ClMn(CO_2)^-$ (*m/*z 134) (left) and extrapolation procedure for the decarboxylation of $ClMn(CO_2)^-$ (*m/*z 134) (right) recorded at argon collision gas pressure of 3.85×10^{-4} mBar.

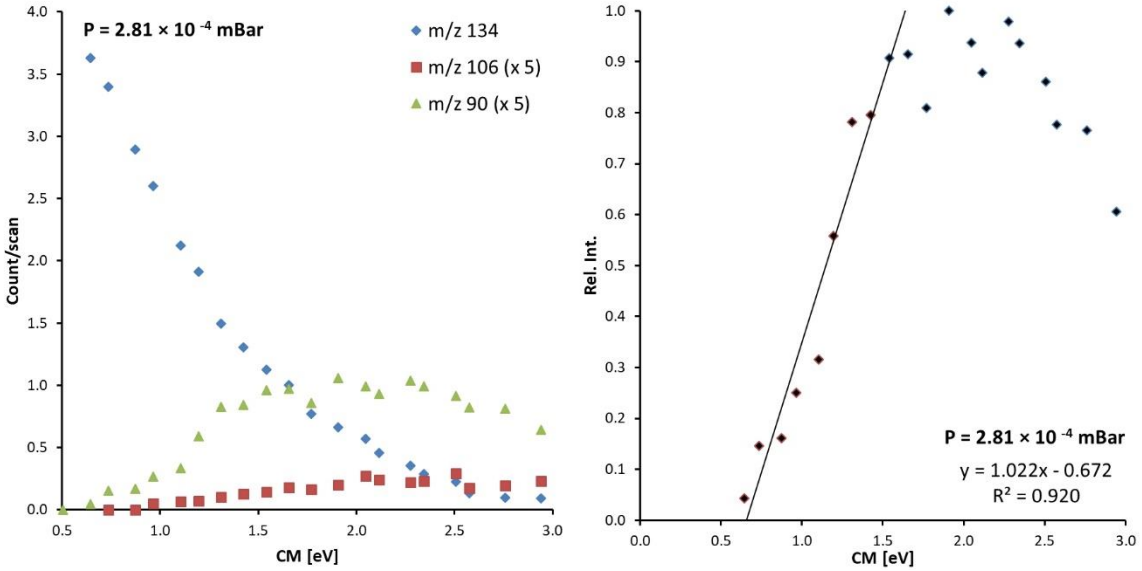

Figure S 23 Breakdown curve for $ClMn(CO_2)^-$ (*m/*z 134) (left) and extrapolation procedure for the decarboxylation of $ClMn(CO_2)^-$ (*m/*z 134) (right) recorded at argon collision gas pressure of 2.81×10^{-4} mBar.

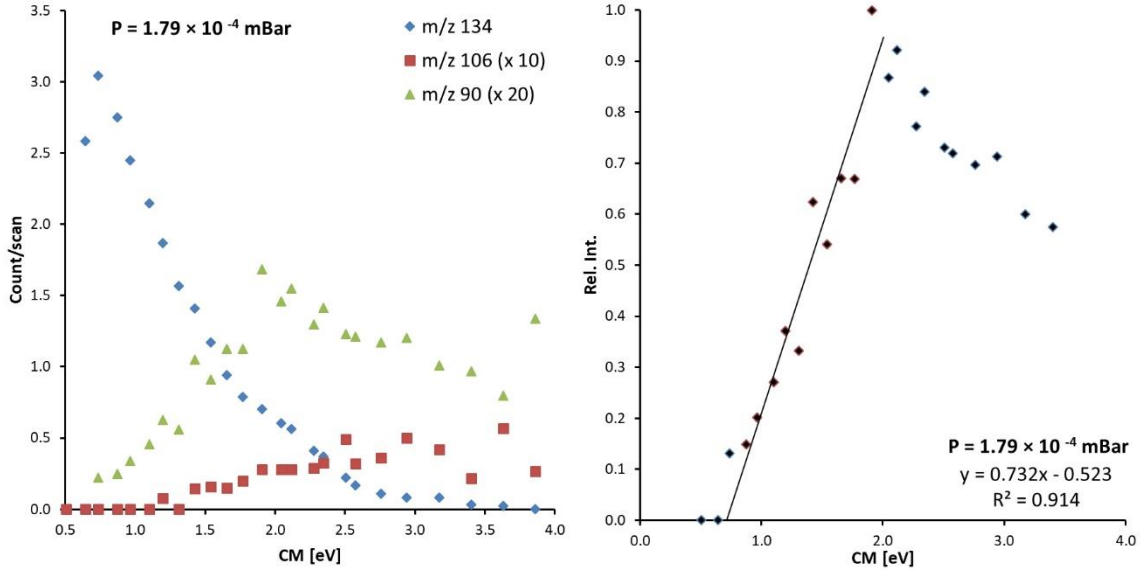

Figure S 24 Breakdown curve for $ClMn(CO_2)^-$ (*m/*z 134) (left) and extrapolation procedure for the decarboxylation of $ClMn(CO_2)^-$ (*m/*z 134) (right) recorded at argon collision gas pressure of 1.79×10^{-4} mBar.

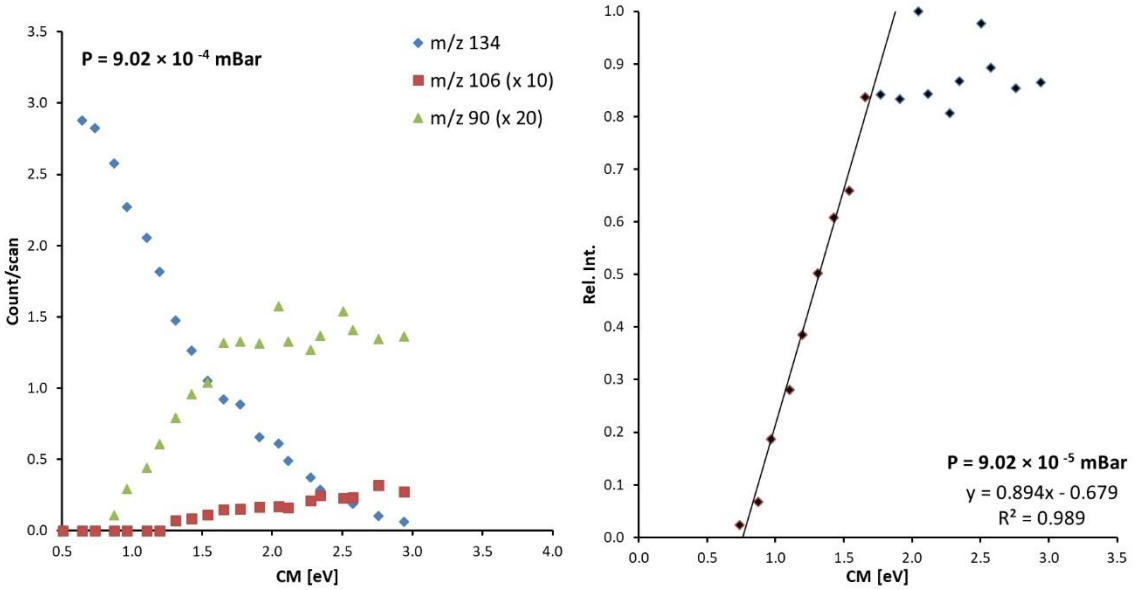

Figure S 25 Breakdown curve for $ClMn(CO_2)^-$ (*m/*z 134) (left) and extrapolation procedure for the decarboxylation of $ClMn(CO_2)^-$ (*m/*z 134) (right) recorded at argon collision gas pressure of 9.02×10^{-5} mBar.

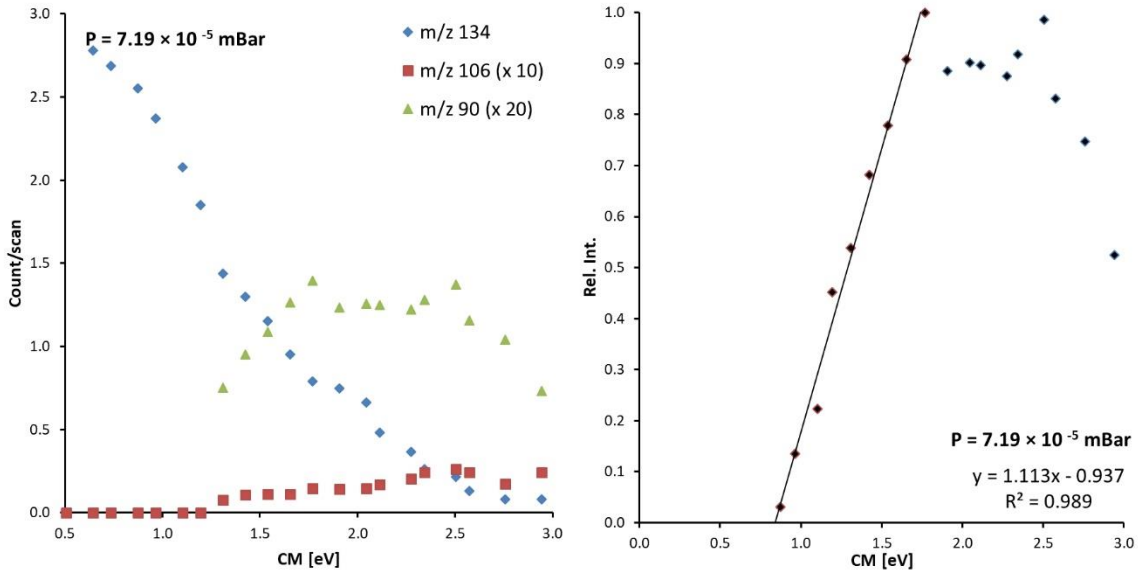

Figure S 26 Breakdown curve for $ClMn(CO_2)^-$ (*m/*z 134) (left) and extrapolation procedure for the decarboxylation of $ClMn(CO_2)^-$ (*m/*z 134) (right) recorded at argon collision gas pressure of 7.19×10^{-5} mBar.

Table S 27 Summary of the values from the extrapolation procedure for decarboxylation of $ClMn(CO_2)^-$ (*m/*z 134).

Pressure [mBar]:	Slope	Intercept	X at Y=0 [eV]	[kJ/mol]
7.19E-05	1.113	-0.937	0.842	80.8
9.02E-05	0.894	-0.679	0.759	72.9
1.79E-04	0.732	-0.523	0.715	68.6
2.81E-04	1.022	-0.672	0.658	63.2
3.85E-04	0.846	-0.464	0.548	52.6
Extrapolated pressure [mBar]:	**Intercept**	**Slope**	**Y at X=0 [eV]**	**[kJ/mol]**
0	-703.394	0.835	0.835	80.2

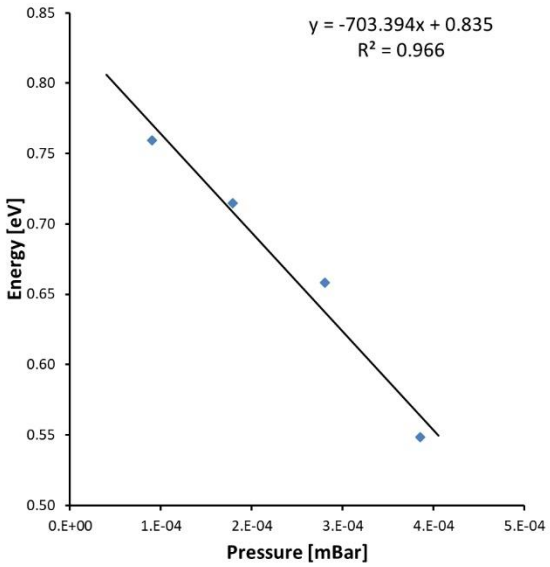

Figure S 28 Extrapolation procedure for the decarboxylation of $ClMn(CO_2)^-$ (*m/*z 134) at a gas pressure of 0 mbar.

1.3.3 Collision-induced dissociation (CID) of $ClFe(CO_2)^-$ (*m/z* 135)

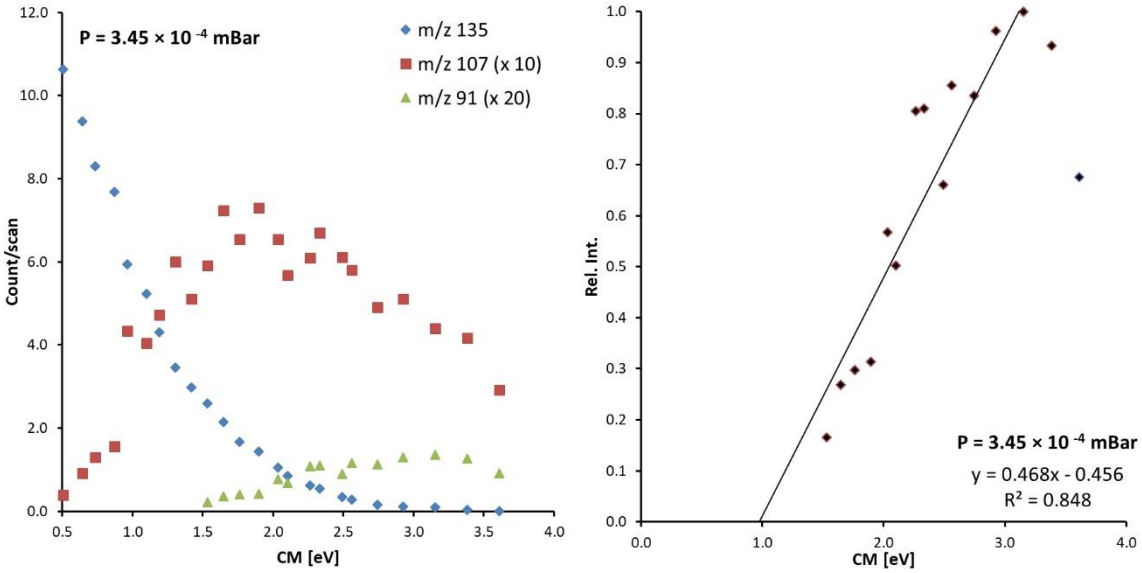

Figure S 29 Breakdown curve for $ClFe(CO_2)^-$ (*m/z* 135) (left) and extrapolation procedure for the decarboxylation of $ClFe(CO_2)^-$ (*m/z* 135) (right) recorded at argon collision gas pressure of 3.45×10^{-4} mBar.

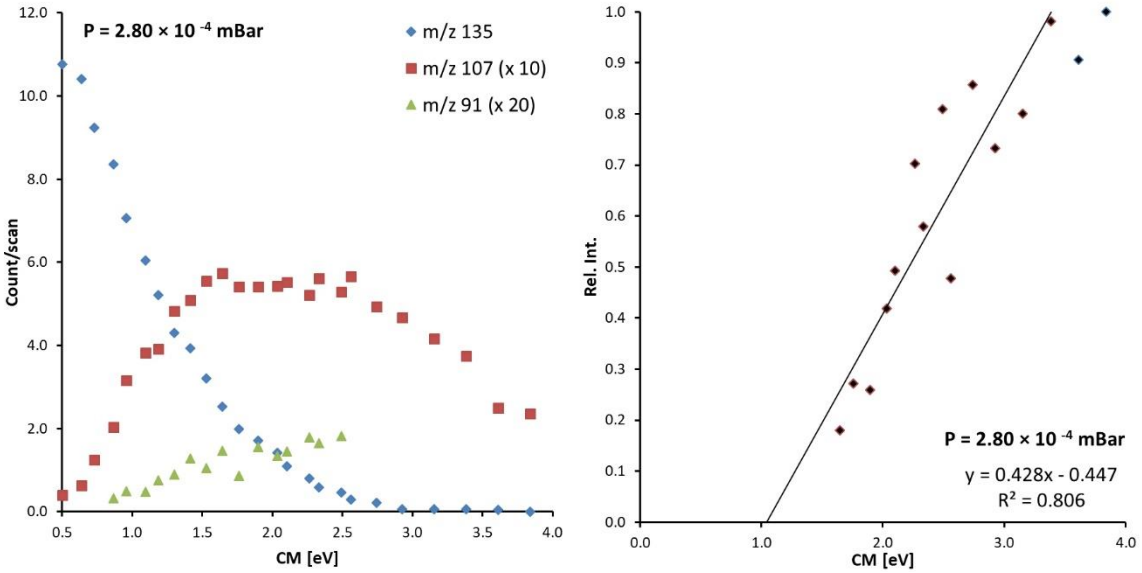

Figure S 30 Breakdown curve for $ClFe(CO_2)^-$ (*m/z* 135) (left) and extrapolation procedure for the decarboxylation of $ClFe(CO_2)^-$ (*m/z* 135) (right) recorded at argon collision gas pressure of 2.80×10^{-4} mBar.

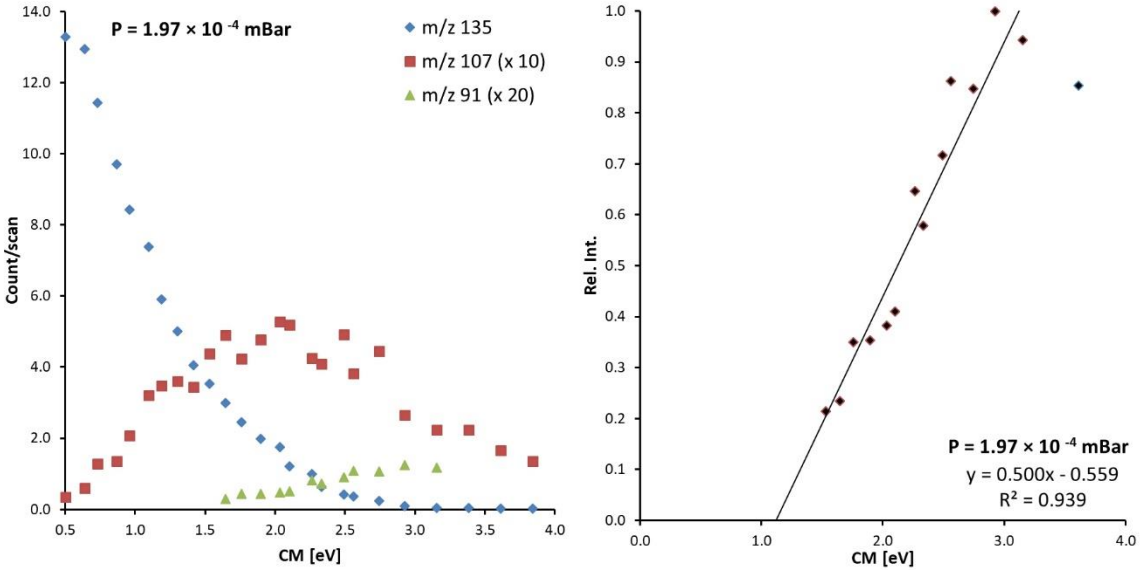

Figure S 31 Breakdown curve for $ClFe(CO_2)^-$ (*m/*z 135) (left) and extrapolation procedure for the decarboxylation of $ClFe(CO_2)^-$ (*m/*z 135) (right) recorded at argon collision gas pressure of 1.97×10^{-4} mBar.

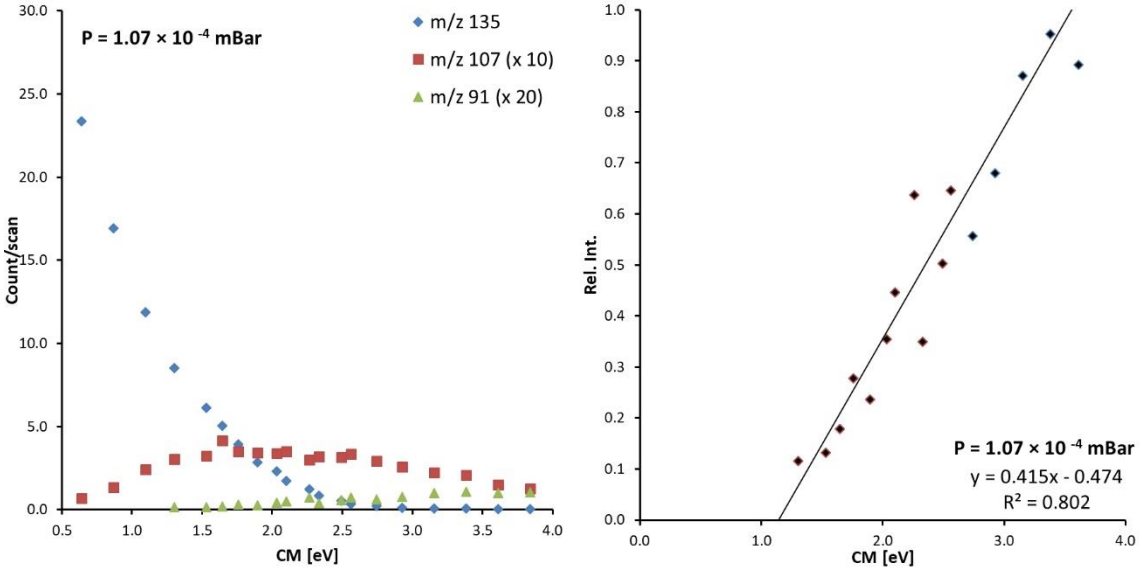

Figure S 32 Breakdown curve for $ClFe(CO_2)^-$ (*m/*z 135) (left) and extrapolation procedure for the decarboxylation of $ClFe(CO_2)^-$ (*m/*z 135) (right) recorded at argon collision gas pressure of 1.07×10^{-4} mBar.

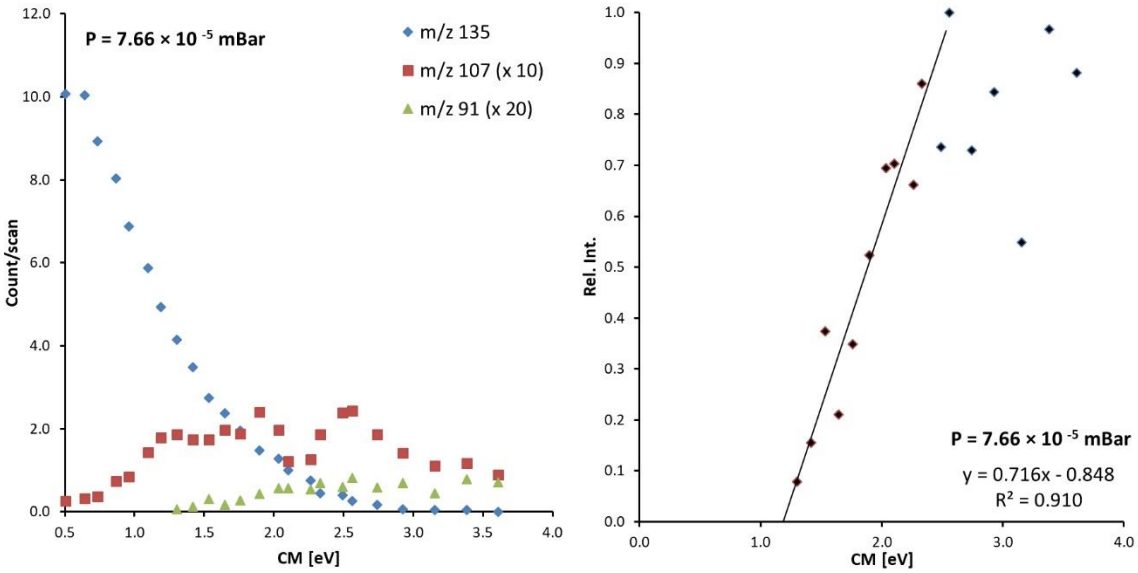

Figure S 33 Breakdown curve for $ClFe(CO_2)^-$ (*m/*z 135) (left) and extrapolation procedure for the decarboxylation of $ClFe(CO_2)^-$ (*m/*z 135) (right) recorded at argon collision gas pressure of 7.66×10^{-5} mBar.

Table S 34 Summary of the values from the extrapolation procedure for decarboxylation of $ClFe(CO_2)^-$ (*m/*z 135).

Pressure [mBar]:	Slope	Intercept	X at Y=0 [eV]	[kJ/mol]
7.66×10^{-5}	0.716	-0.848	1.184	113.7
1.07×10^{-4}	0.415	-0.474	1.143	109.7
1.97×10^{-4}	0.500	-0.559	1.118	107.4
2.80×10^{-4}	0.428	-0.447	1.046	100.4
3.45×10^{-4}	0.468	-0.456	0.974	93.5
Extrapolated pressure [mBar]:	Intercept	Slope	Y at X=0 [eV]	[kJ/mol]
0	-720.066	1.238	1.238	118.8

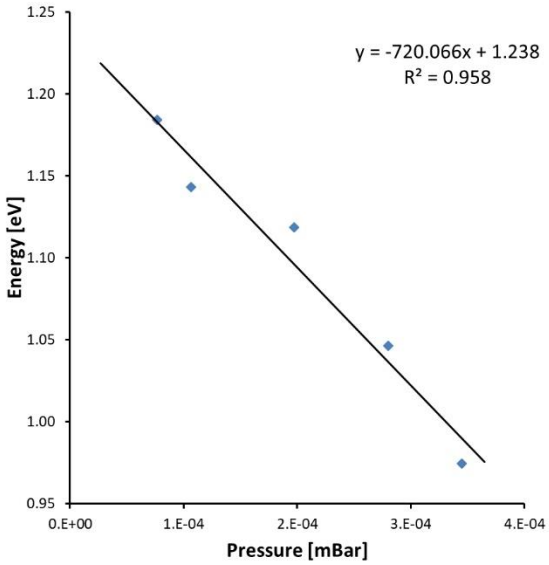

Figure S 35 Extrapolation procedure for the decarboxylation of $ClFe(CO_2)^-$ (*m/*z 135) at a gas pressure of 0 mbar.

1.3.4 Collision-induced dissociation (CID) of $ClCo(CO_2)^-$ (*m/*z 138)

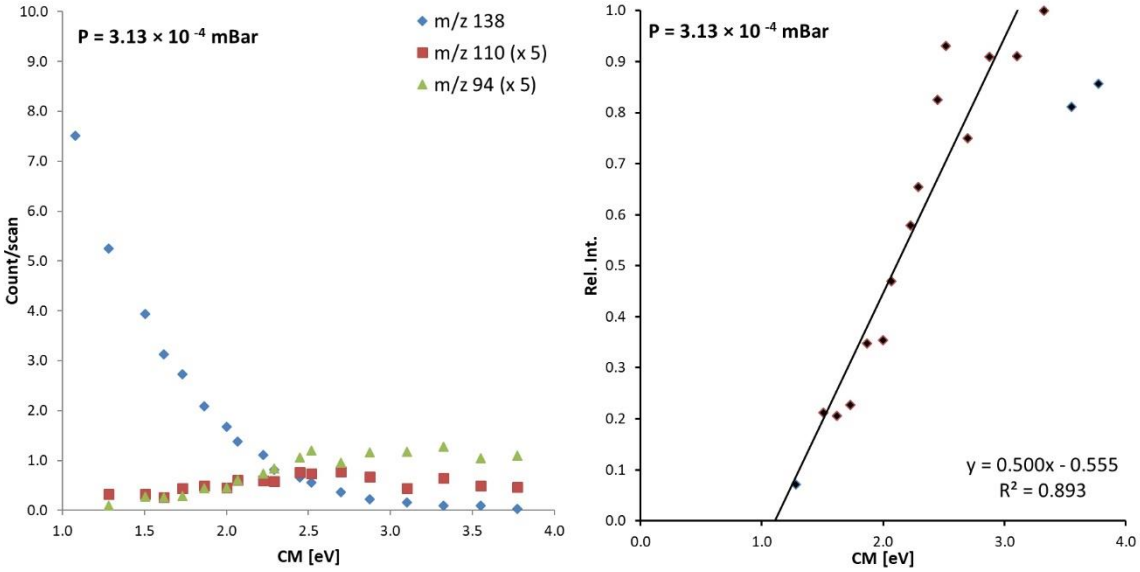

Figure S 36 Breakdown curve for $ClCo(CO_2)^-$ (*m/*z 138) (left) and extrapolation procedure for the decarboxylation of $ClCo(CO_2)^-$ (*m/*z 138) (right) recorded at argon collision gas pressure of 3.13×10^{-4} mBar.

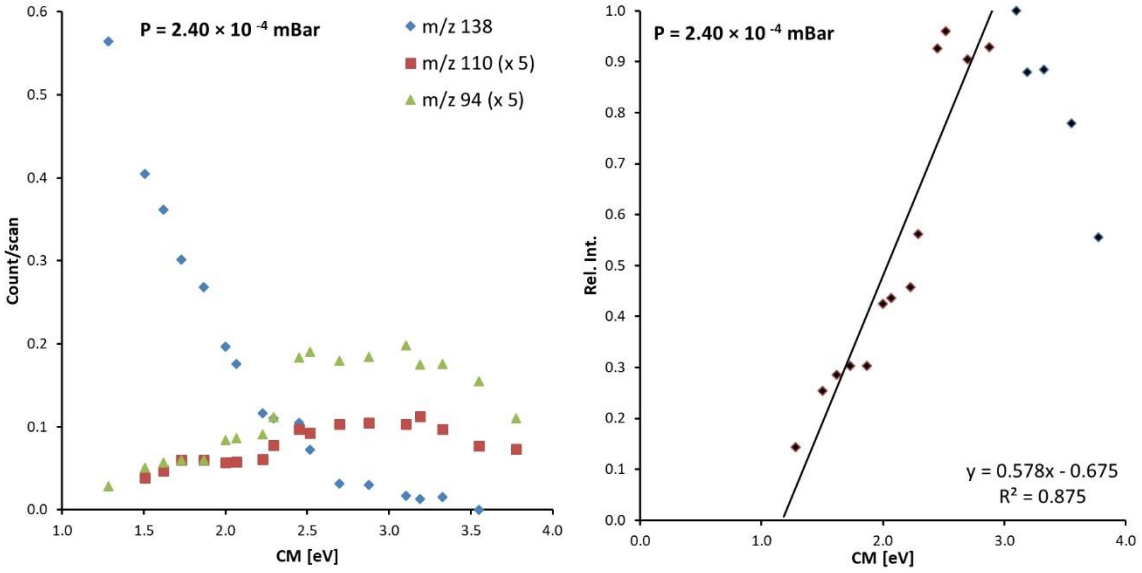

Figure S 37 Breakdown curve for $ClCo(CO_2)^-$ (*m/*z 138) (left) and extrapolation procedure for the decarboxylation of $ClCo(CO_2)^-$ (*m/*z 138) (right) recorded at argon collision gas pressure of 2.40×10^{-4} mBar.

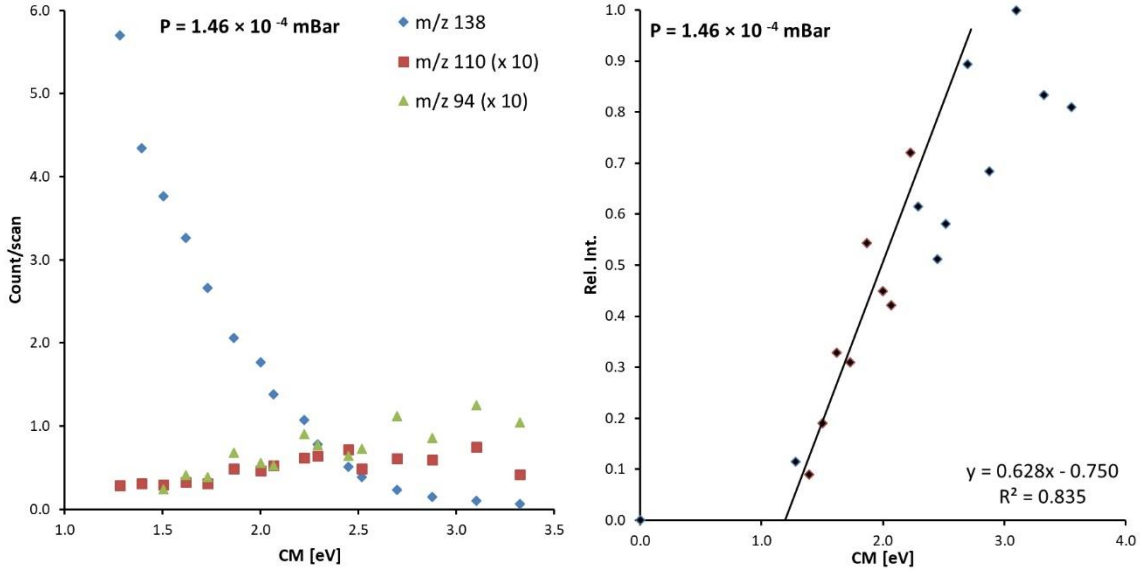

Figure S 38 Breakdown curve for $ClCo(CO_2)^-$ (*m/*z 138) (left) and extrapolation procedure for the decarboxylation of $ClCo(CO_2)^-$ (*m/*z 138) (right) recorded at argon collision gas pressure of 1.46×10^{-4} mBar.

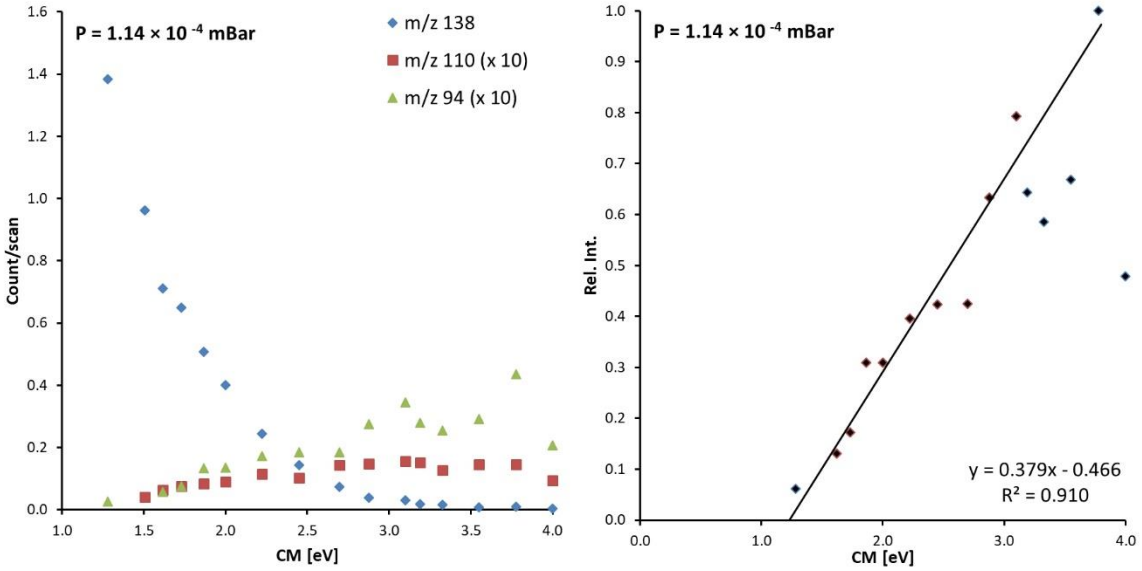

Figure S 39 Breakdown curve for $ClCo(CO_2)^-$ (*m/*z 138) (left) and extrapolation procedure for the decarboxylation of $ClCo(CO_2)^-$ (*m/*z 138) (right) recorded at argon collision gas pressure of 1.14×10^{-4} mBar.

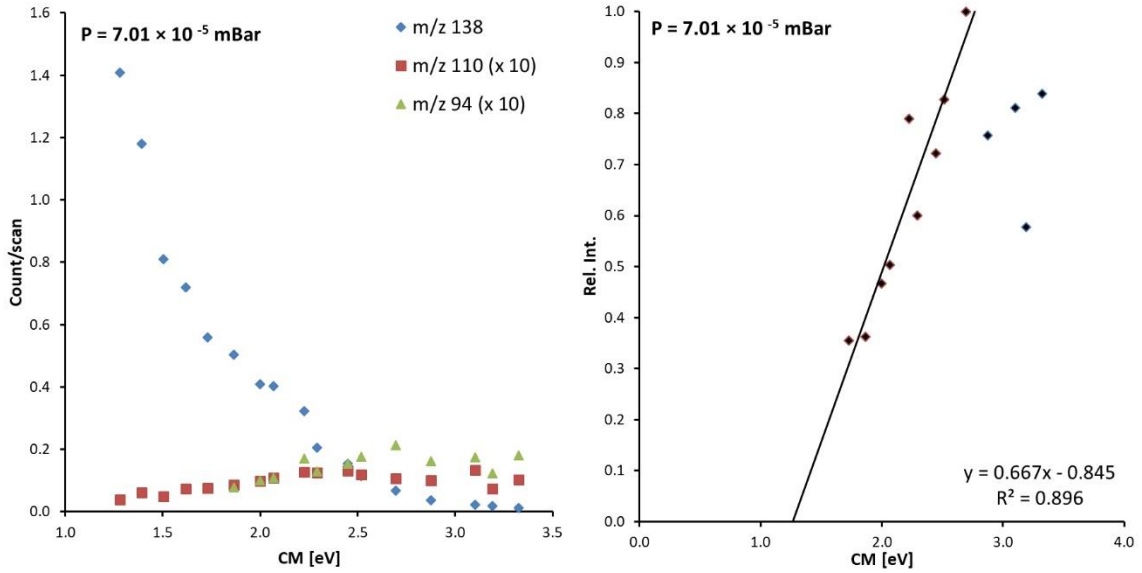

Figure S 40 Breakdown curve for $ClCo(CO_2)^-$ (*m/*z 138) (left) and extrapolation procedure for the decarboxylation of $ClCo(CO_2)^-$ (*m/*z 138) (right) recorded at argon collision gas pressure of 7.01×10^{-5} mBar.

Table S 41 Summary of the values from the extrapolation procedure for decarboxylation of $ClCo(CO_2)^-$ (*m/*z 138).

Pressure [mBar]:	Slope	Intercept	X at Y=0 [eV]	[kJ/mol]
7.01×10^{-5}	0.667	-0.845	1.267	121.6
1.14×10^{-4}	0.379	-0.466	1.231	118.2
1.46×10^{-4}	0.628	-0.750	1.193	114.6
2.40×10^{-4}	0.578	-0.675	1.169	112.2
3.13×10^{-4}	0.500	-0.555	1.109	106.5
Extrapolated pressure [mBar]:	Intercept	Slope	Y at X=0 [eV]	[kJ/mol]
0	-598.747	1.300	1.300	124.4

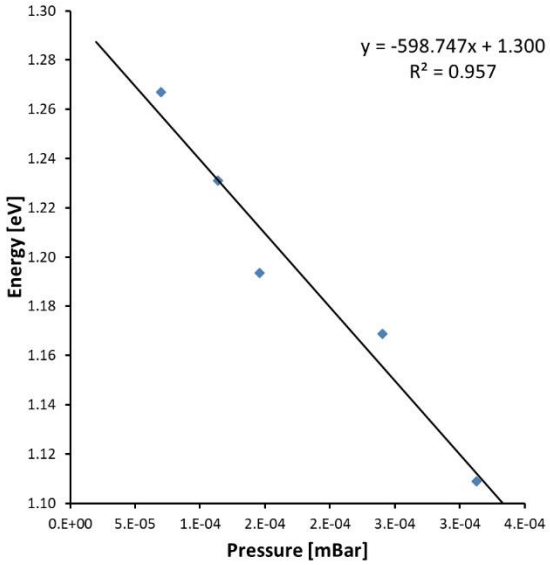

Figure S 42 Extrapolation procedure for the decarboxylation of $ClCo(CO_2)^-$ (*m/*z 138) at a gas pressure of 0 mbar.

1.3.5 Collision-induced dissociation (CID) of $ClNi(CO_2)^-$ (*m/z* 137)

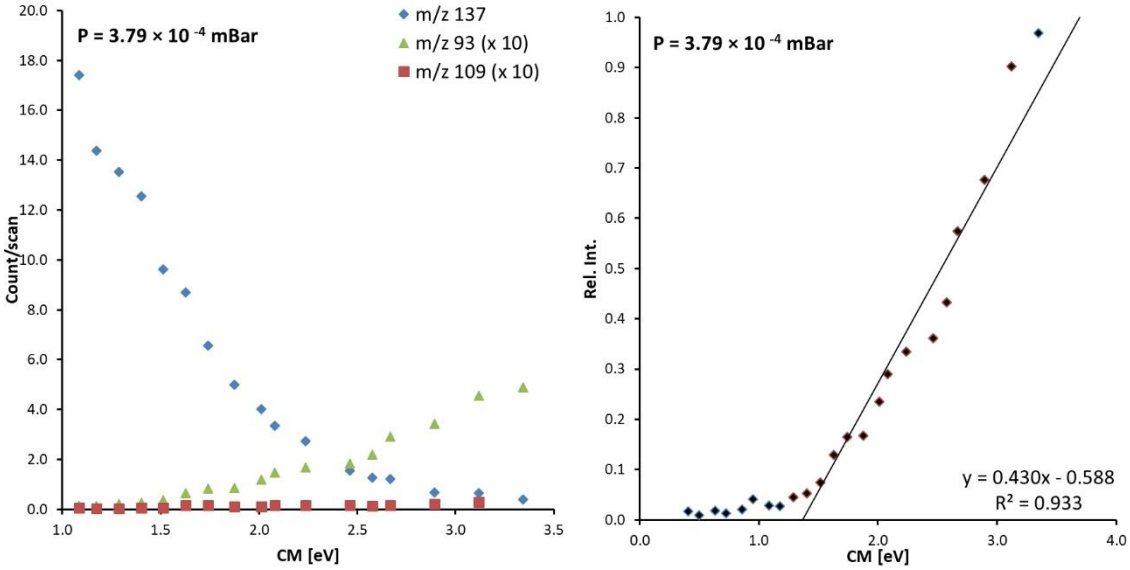

Figure S 43 Breakdown curve for $ClNi(CO_2)^-$ (*m/z* 137) (left) and extrapolation procedure for the decarboxylation of $ClNi(CO_2)^-$ (*m/z* 137) (right) recorded at argon collision gas pressure of 3.79×10^{-4} mBar.

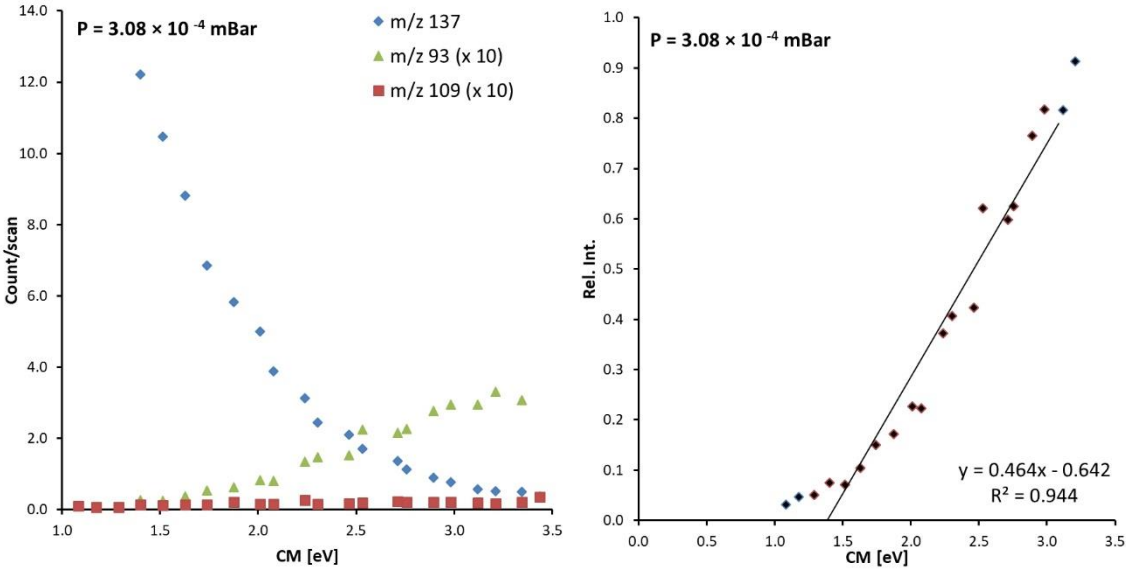

Figure S 44 Breakdown curve for $ClNi(CO_2)^-$ (*m/z* 137) (left) and extrapolation procedure for the decarboxylation of $ClNi(CO_2)^-$ (*m/z* 137) (right) recorded at argon collision gas pressure of 3.08×10^{-4} mBar.

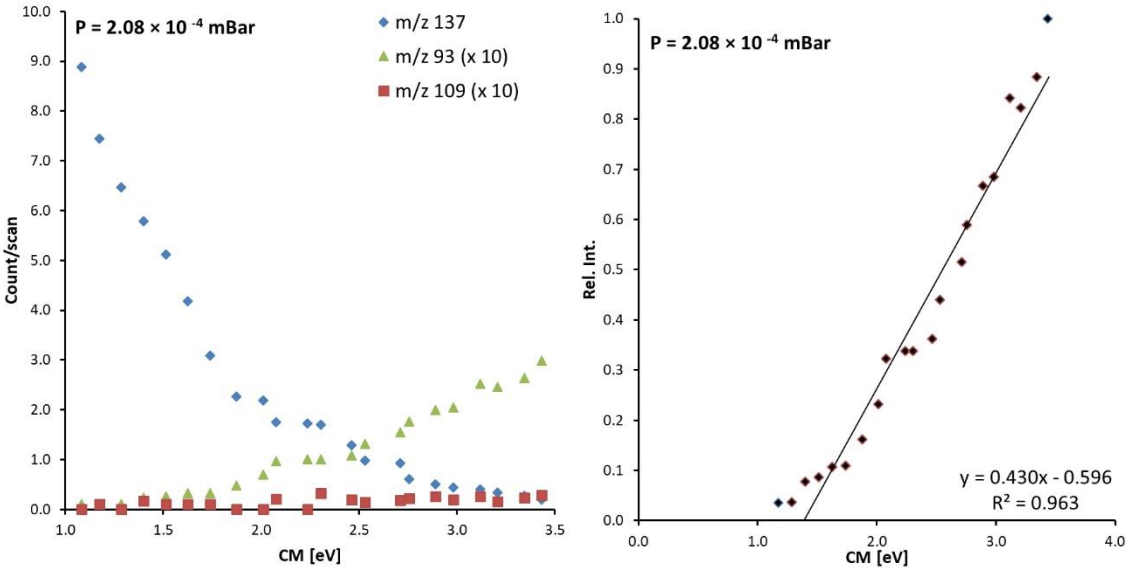

Figure S 45 Breakdown curve for $ClNi(CO_2)^-$ (*m/*z 137) (left) and extrapolation procedure for the decarboxylation of $ClNi(CO_2)^-$ (*m/*z 137) (right) recorded at argon collision gas pressure of 2.08×10^{-4} mBar.

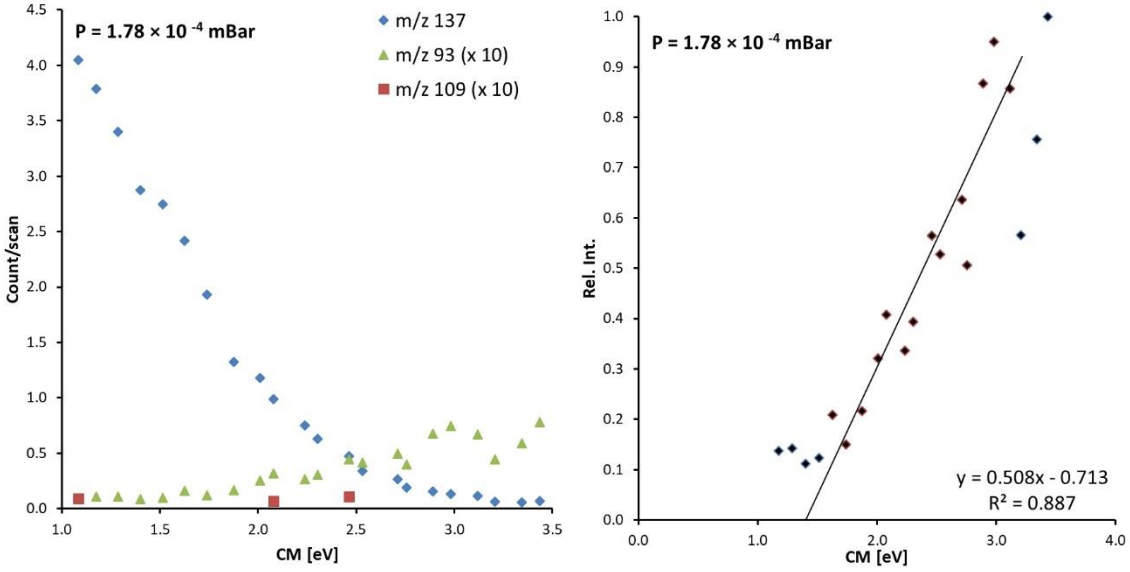

Figure S 46 Breakdown curve for $ClNi(CO_2)^-$ (*m/*z 137) (left) and extrapolation procedure for the decarboxylation of $ClNi(CO_2)^-$ (*m/*z 137) (right) recorded at argon collision gas pressure of 1.78×10^{-4} mBar.

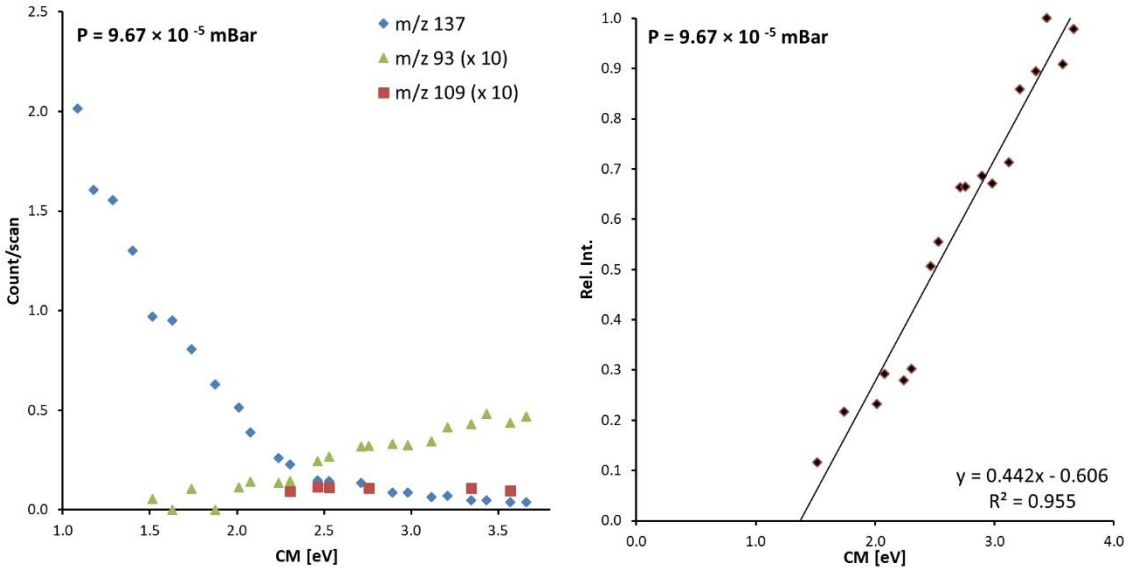

Figure S 47 Breakdown curve for $ClNi(CO_2)^-$ (*m/*z 137) (left) and extrapolation procedure for the decarboxylation of $ClNi(CO_2)^-$ (*m/*z 137) (right) recorded at argon collision gas pressure of 9.67×10^{-5} mBar.

Table S 48 Summary of the values from the extrapolation procedure for decarboxylation of $ClNi(CO_2)^-$ (*m/*z 137).

Pressure [mBar]:	Slope	Intercept	X at Y=0 [eV]	[kJ/mol]
9.67×10^{-5}	0.461	-0.650	1.410	135.3
1.78×10^{-4}	0.508	-0.713	1.404	134.8
2.08×10^{-4}	0.430	-0.596	1.387	133.2
3.08×10^{-4}	0.466	-0.646	1.385	133.0
3.79×10^{-4}	0.430	-0.588	1.368	131.4
Extrapolated pressure [mBar]:	**Intercept**	**Slope**	**Y at X=0 [eV]**	**[kJ/mol]**
0	-140.723	1.422	1.422	136.5

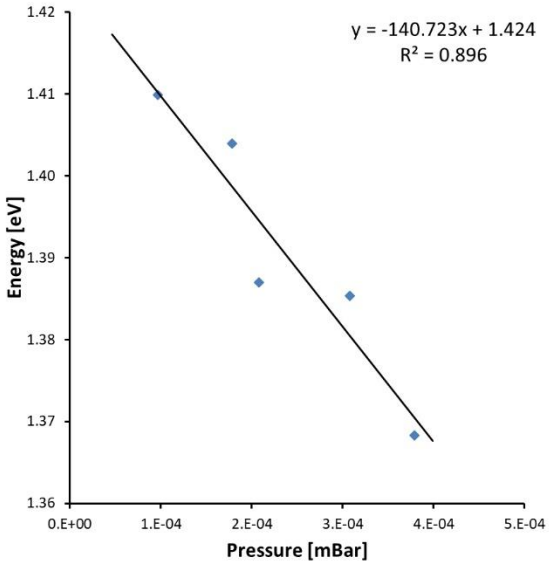

Figure S 49 Extrapolation procedure for the decarboxylation of $ClNi(CO_2)^-$ (*m/*z 137) at a gas pressure of 0 mbar.

1.3.6 Collision-induced dissociation (CID) of $ClCu(CO_2)^-$ (*m/*z 142)

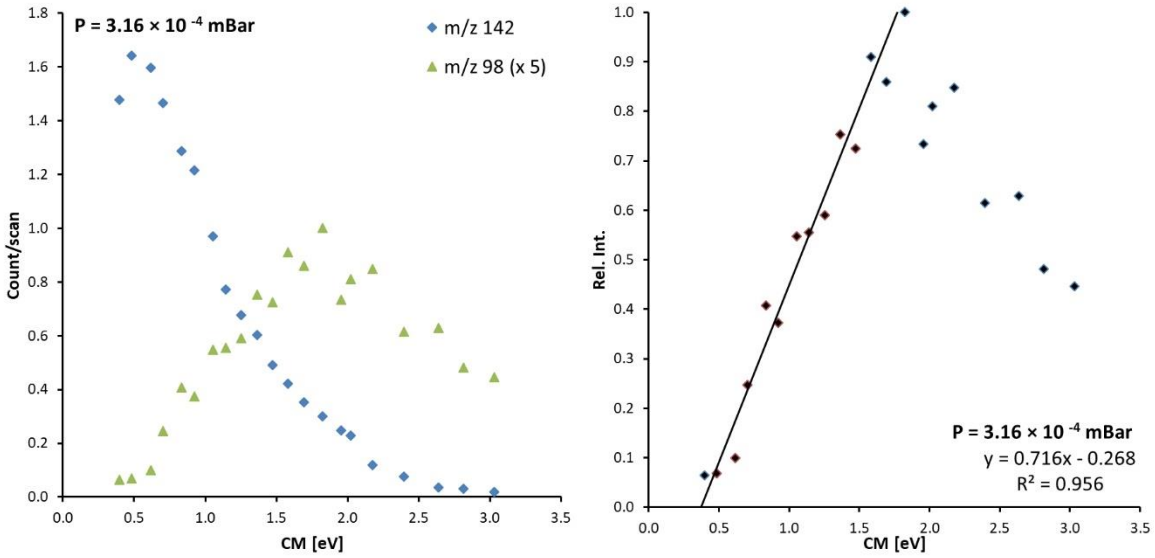

Figure S 50 Breakdown curve for $ClCu(CO_2)^-$ (*m/*z 142) (left) and extrapolation procedure for the decarboxylation of $ClCu(CO_2)^-$ (*m/*z 142) (right) recorded at argon collision gas pressure of 3.16×10^{-4} mBar.

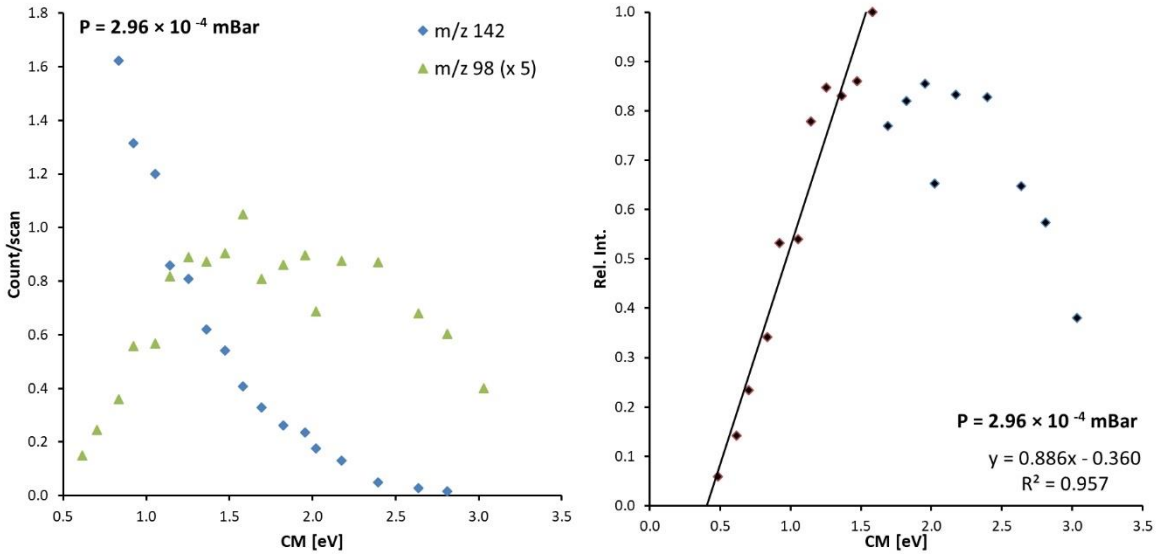

Figure S 51 Breakdown curve for $ClCu(CO_2)^-$ (*m/*z 142) (left) and extrapolation procedure for the decarboxylation of $ClCu(CO_2)^-$ (*m/*z 142) (right) recorded at argon collision gas pressure of 2.96×10^{-4} mBar.

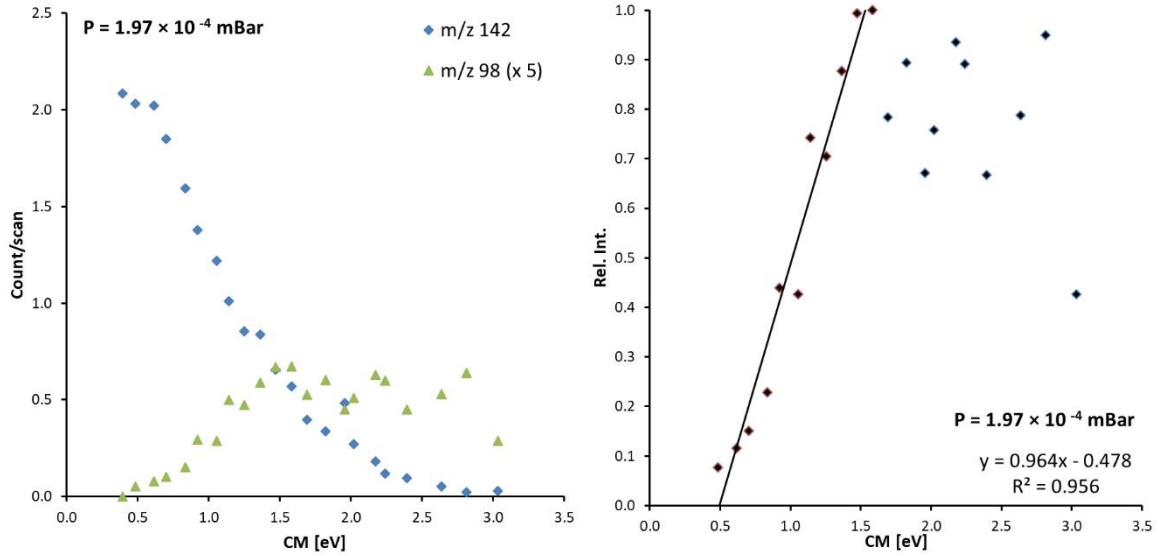

Figure S 52 Breakdown curve for $ClCu(CO_2)^-$ (*m/*z 142) (left) and extrapolation procedure for the decarboxylation of $ClCu(CO_2)^-$ (*m/*z 142) (right) recorded at argon collision gas pressure of 1.97×10^{-4} mBar.

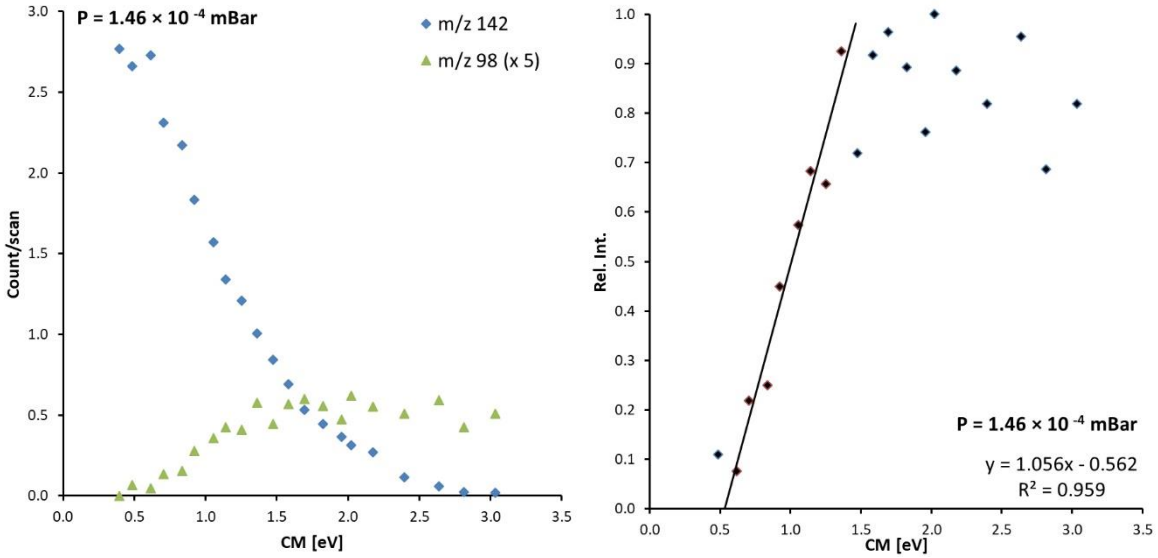

Figure S 53 Breakdown curve for $ClCu(CO_2)^-$ (*m/*z 142) (left) and extrapolation procedure for the decarboxylation of $ClCu(CO_2)^-$ (*m/*z 142) (right) recorded at argon collision gas pressure of 1.46×10^{-4} mBar.

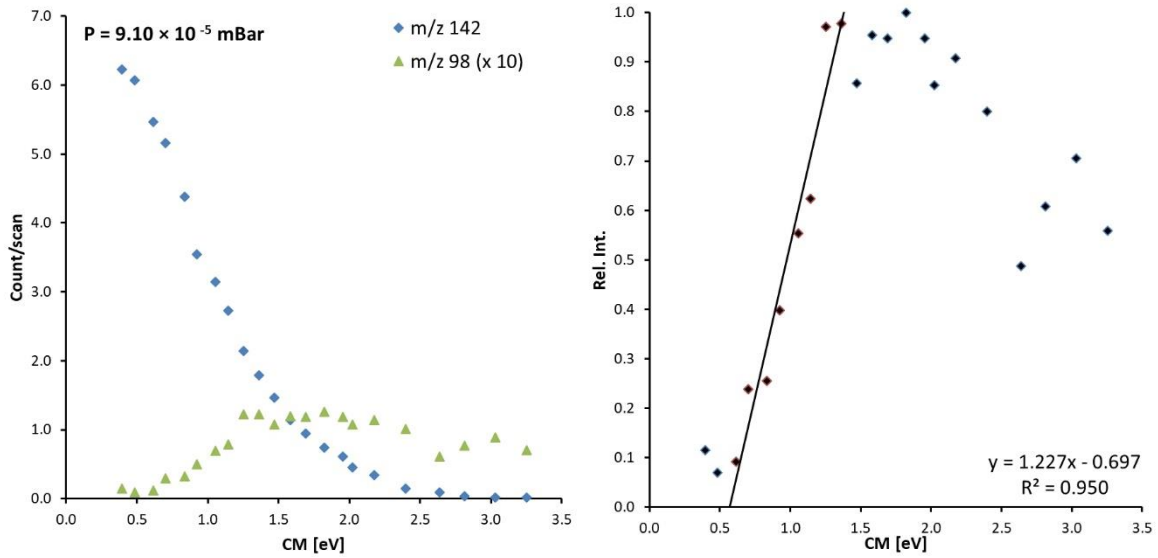

Figure S 54 Breakdown curve for $ClCu(CO_2)^-$ (*m/*z 142) (left) and extrapolation procedure for the decarboxylation of $ClCu(CO_2)^-$ (*m/*z 142) (right) recorded at argon collision gas pressure of 9.10×10^{-5} mBar.

Table S 55 Summary of the values from the extrapolation procedure for decarboxylation of $ClCu(CO_2)^-$ (*m/*z 142).

Pressure [mBar]:	Slope	Intercept	X at Y=0 [eV]	[kJ/mol]
9.10×10^{-5}	1.227	-0.697	0.568	54.5
1.46×10^{-4}	1.056	-0.562	0.532	51.1
1.97×10^{-4}	0.964	-0.478	0.496	47.6
2.96×10^{-4}	0.886	-0.360	0.406	39.0
3.16×10^{-4}	0.716	-0.268	0.374	36.0
Extrapolated pressure [mBar]:	Intercept	Slope	Y at X=0 [eV]	[kJ/mol]
0	-0.051	0.629	0.629	60.4

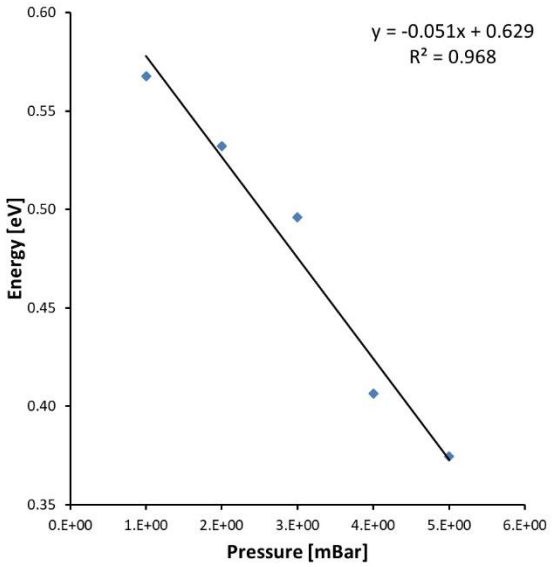

Figure S 56 Extrapolation procedure for the decarboxylation of $ClCu(CO_2)^-$ (*m/*z 142) at a gas pressure of 0 mbar.

1.3.7 Collision-induced dissociation (CID) of $ClZn(CO_2)^-$ (*m/z* 143)

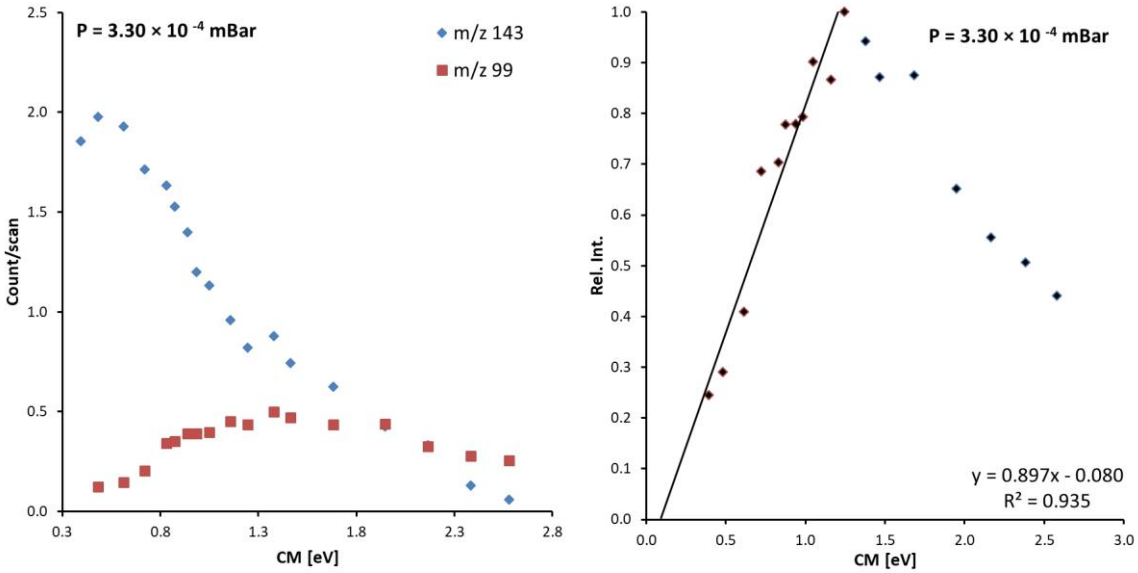

Figure S 57 Breakdown curve for $ClZn(CO_2)^-$ (*m/z* 143) (left) and extrapolation procedure for the decarboxylation of $ClZn(CO_2)^-$ (*m/z* 143) (right) recorded at argon collision gas pressure of 3.30×10^{-4} mBar.

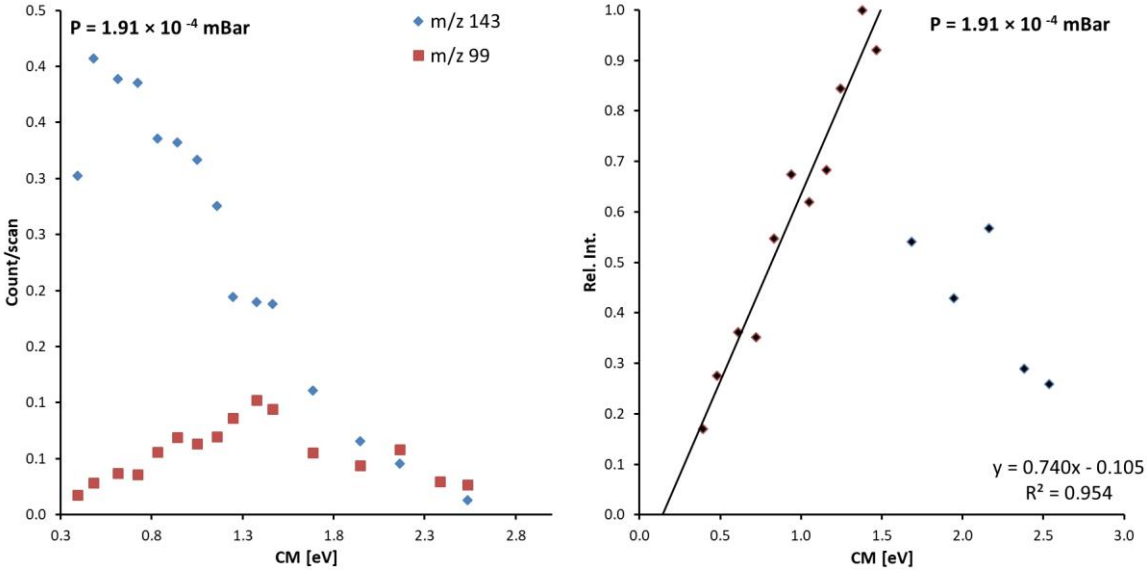

Figure S 58 Breakdown curve for $ClZn(CO_2)^-$ (*m/z* 143) (left) and extrapolation procedure for the decarboxylation of $ClZn(CO_2)^-$ (*m/z* 143) (right) recorded at argon collision gas pressure of 1.91×10^{-4} mBar.

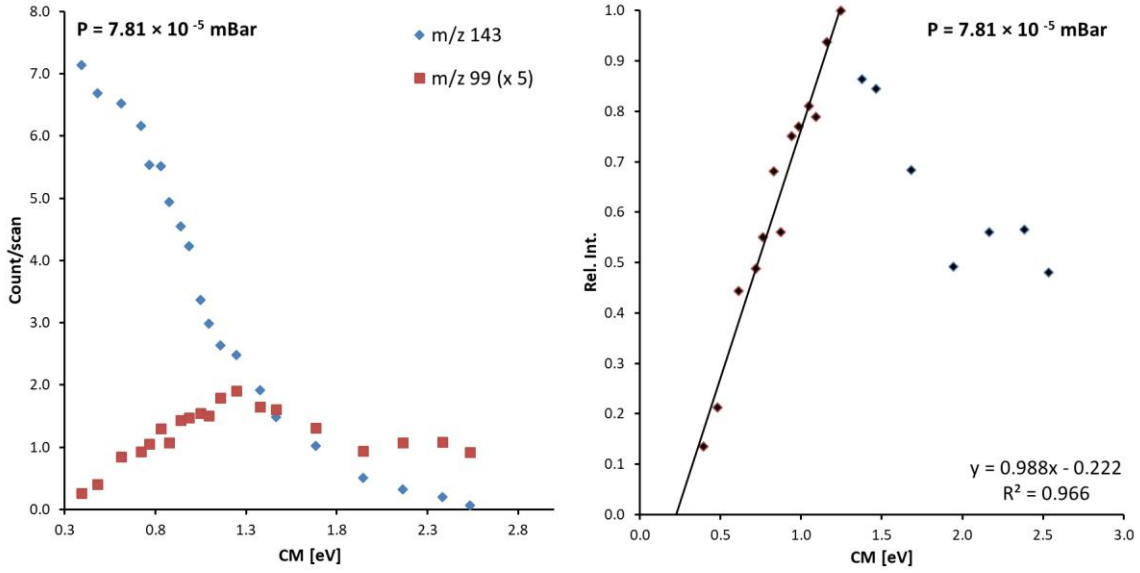

Figure S 59 Breakdown curve for $ClZn(CO_2)^-$ (*m/*z 143) (left) and extrapolation procedure for the decarboxylation of $ClZn(CO_2)^-$ (*m/*z 143) (right) recorded at argon collision gas pressure of 7.81×10^{-5} mBar.

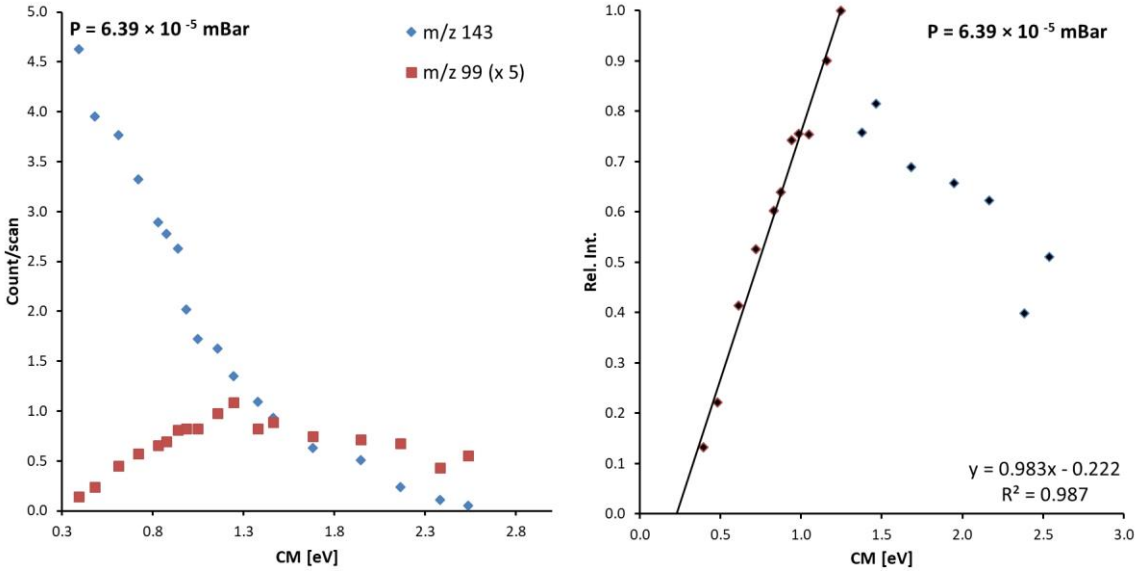

Figure S 60 Breakdown curve for $ClZn(CO_2)^-$ (*m/*z 143) (left) and extrapolation procedure for the decarboxylation of $ClZn(CO_2)^-$ (*m/*z 143) (right) recorded at argon collision gas pressure of 6.39×10^{-5} mBar.

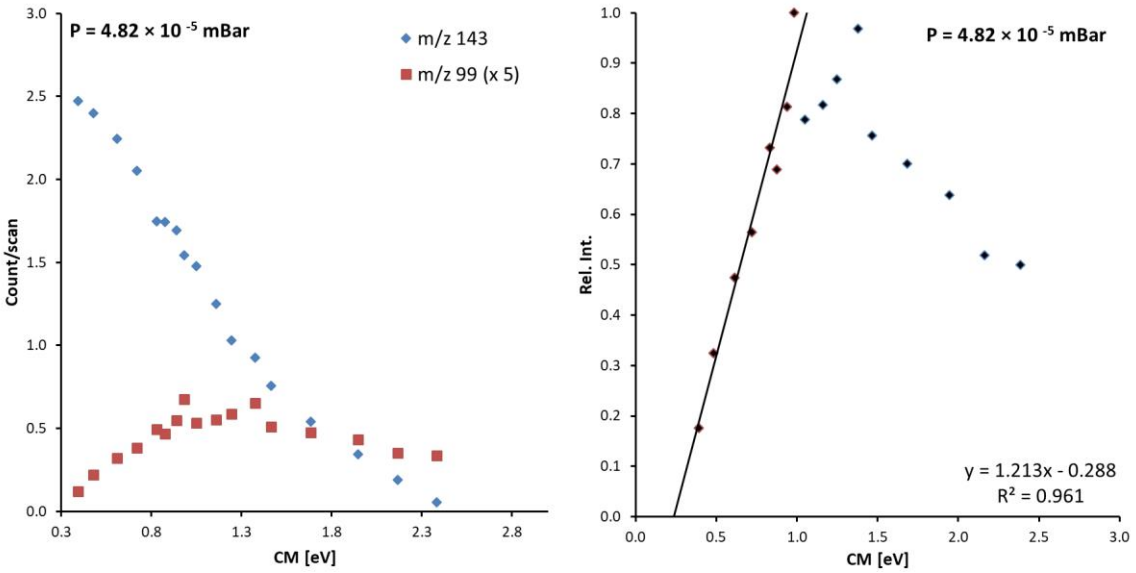

Figure S 61 Breakdown curve for $ClZn(CO_2)^-$ (*m/*z 143) (left) and extrapolation procedure for the decarboxylation of $ClZn(CO_2)^-$ (*m/*z 143) (right) recorded at argon collision gas pressure of 4.82×10^{-5} mBar.

Table S 62 Summary of the values from the extrapolation procedure for decarboxylation of $ClZn(CO_2)^-$ (*m/*z 143).

Pressure [mBar]	Slope	Intercept	X at Y=0 [eV]	[kJ/mol]
4.82×10^{-5}	1.213	-0.288	0.238	22.8
6.39×10^{-5}	0.983	-0.222	0.226	21.7
7.81×10^{-5}	0.988	-0.222	0.225	21.6
1.91×10^{-4}	0.740	-0.105	0.142	13.6
3.30E-04	0.897	-0.080	0.090	8.6
Extrapolated pressure [mBar]:	**Intercept**	**Slope**	**Y at X=0 [eV]**	**[kJ/mol]**
0	-543.23	0.261	0.261	25.1

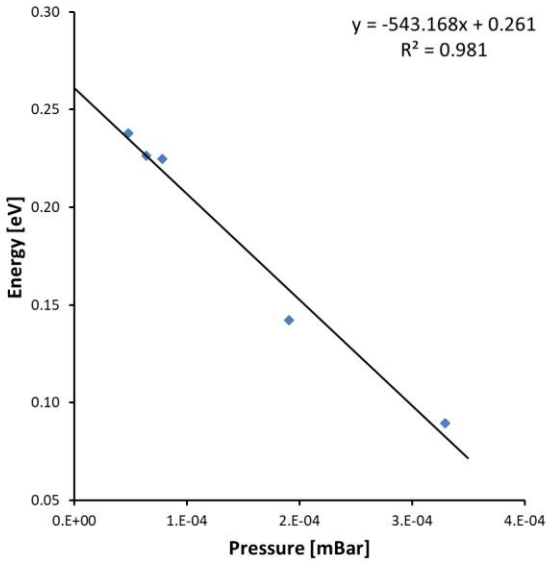

Figure S 63 Extrapolation procedure for the decarboxylation of $ClZn(CO_2)^-$ (*m/*z 143) at a gas pressure of 0 mbar.

1.4 L-CID simulations

In order to apply the L-CID software[1] for T-CID (threshold collision-induced dissociation) measurements, the ion kinetic energy distribution (IKED) was calculated on the basis of retardation curve measured as a function of parent ion intensities and ion energies, in the lab frame [eV] (Figure S64). The ion source parameters and ion optics were adjusted to afford a narrow Gaussian distribution with FWHM at 0.213 eV. The experimental breakdown curves of model $ClZnCO_2^-$ ion, recorded at five different argon pressures were introduced into the L-CID simulations. The reactive cross-sections for each data set were calculated using methodology described elsewhere.[1-2] Data inputs containing the calculated cross-sections and collision energies were used for further L-CID simulations, including a number of other parameters required by the software: number of reaction channels: CH=1, no transition state TS1=0, parent ion weight: M_p = 142.8, collision gas weight: M_t = 39.9628, polarizability of collision gas atoms (argon): polar=1.6e-24, fwhm_kinetic= 0.213, temperature: T=298.15, number of degrees of freedom of the parent ion: s=9, number of free rotors in the parent ion structure: rotors=0, number of ions used in simulations: mxions=100000, number of interactions: mxint=25. The simulations were repeated four times for each data set in order to avoid the numerical and statistical errors.

Simulated energy values for each gas pressure are summarized in Table S69. In order to impose single-collision conditions, extrapolation to zero-pressure was also performed (Figure S68).

***Comment*:**

Final analysis leads us to the conclusion that for breakdown curves recorded for ions of such low abundance, the methodology does not apply well. It can be seen on Figures S65, S66 that simulated curves (black lines) do not follow properly the experimental data points and bend at irregular places, indicating wrong onset energies. In this respect, also the zero-pressure extrapolation shown in Figure S67 is encumbered with a significant error. We assumed that for such simulations, the experimental curves have to be smooth and possess more or less ideal sinusoidal shape, with well described front and back plateaus. Due to very low intensity of the $[ClM(CO_2)]^-$ ions, we decided to use a very straightforward method for energy extrapolation, which reproduced correctly the theoretical predictions presented in the main part of this paper. The procedure and results are presented above in Chapter 1.3.

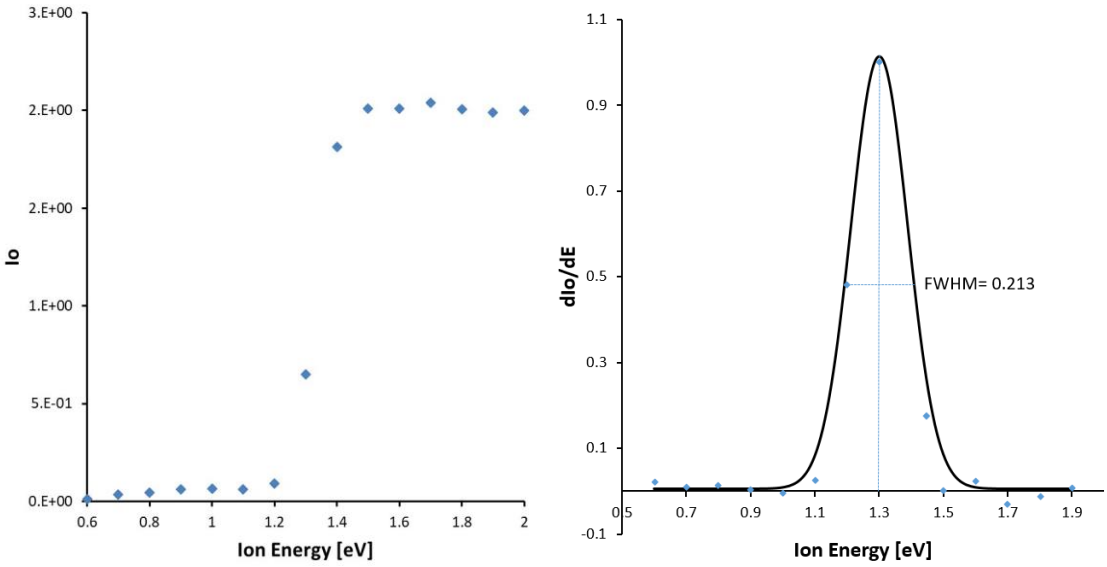

Figure S 64 Ion intensity (*Io)* of $ClZnCO_2^-$ as function of ion energy in the lab frame [eV] (left), and ion kinetic energy distribution (blue points) with Gaussian fit (black) (right).

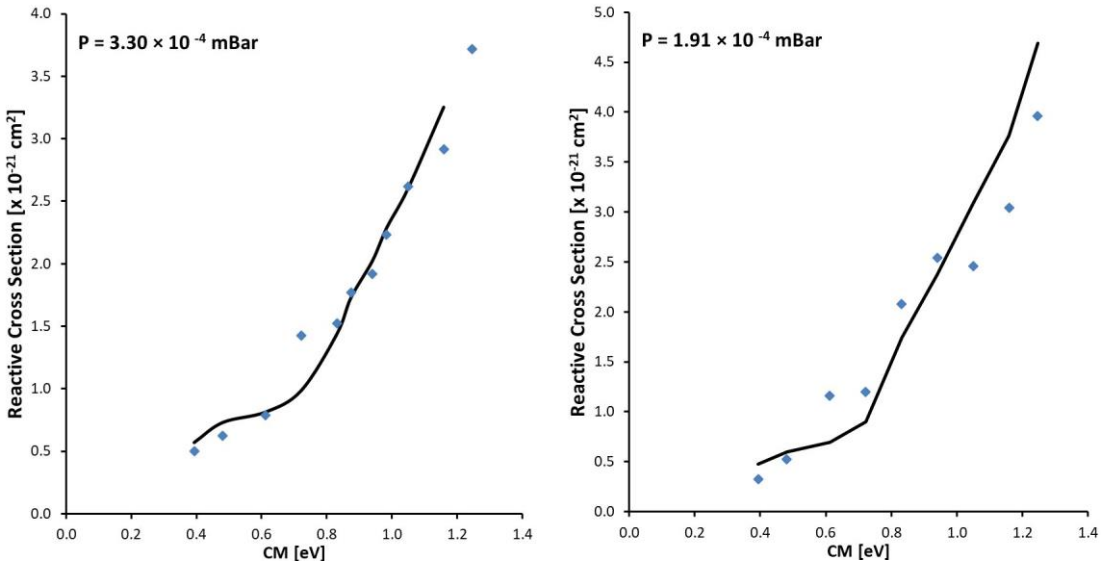

Figure S 65 Experimental (blue points) and simulated (black line) reactive cross-sections at the pressure of 3.3×10^{-4} (left) and 1.91×10^{-4} mBar (right) as a function of collision energy in the center-of-mass frame [eV].

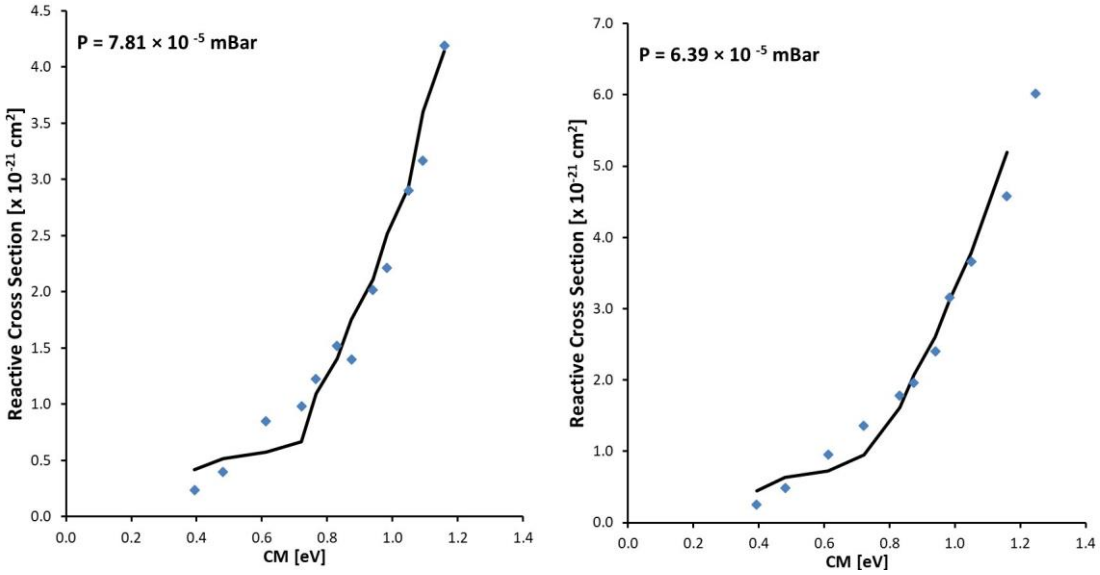

Figure S 66 Experimental (blue points) and simulated (black line) reactive cross-sections at the pressure of 7.81×10^{-5} (left) and 6.39×10^{-5} mBar (right) as a function of collision energy in the center-of-mass frame [eV].

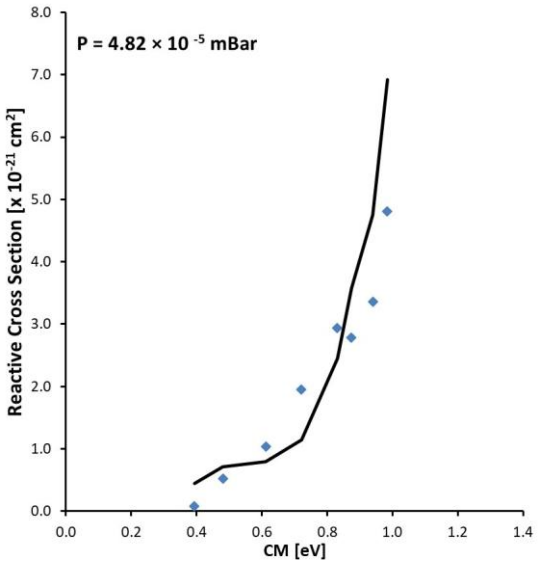

Figure S 67 Experimental (blue points) and simulated (black line) reactive cross-sections at the pressure of 4.82×10^{-5} mBar as a function of collision energy in the center-of-mass frame [eV].

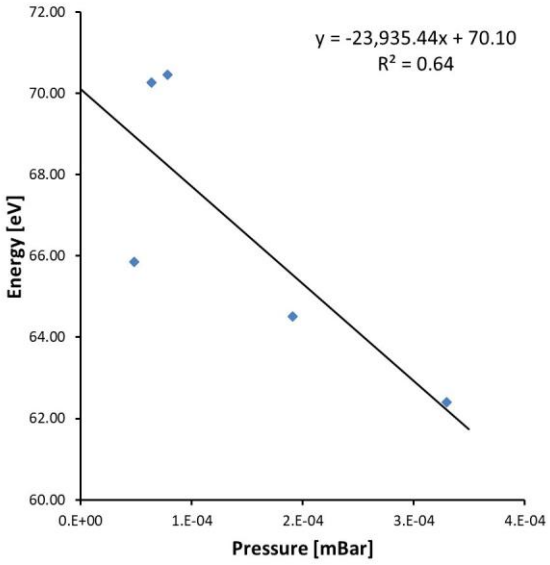

Figure S 68 Extrapolation procedure for the decarboxylation of $ClZn(CO_2)^-$ (*m/*z 143) at a gas pressure of 0 mbar.

Table S 69 Summary of the values from the simulation procedure for decarboxylation of $ClZn(CO_2)^-$ (*m/*z 143).

Pressure [mBar]	**Extrapolated energies by L-CID software**	
	[eV]	**[kJ/mol]**
4.81×10^{-5}	0.69	65.86
6.39×10^{-5}	0.73	70.27
7.81×10^{-5}	0.73	70.46
1.91×10^{-4}	0.67	64.51
3.30×10^{-4}	0.65	62.40
0	0.64	61.44

2. Computational details

The theoretical results were obtained using the Gaussian 09 package[3] and the initial molecular geometries were created using GaussView 5.0.[4] The optimization of the equilibrium $[ClM(CO_2)]^-$ structures was performed at 6 different DFT and *ab initio* levels of theory, listed in the tables below. No geometry constraints were applied during the optimizations. Energies were corrected for zero-point vibrational energy. A frequency analysis was performed at the optimized geometries to ensure that there were no imaginary frequencies. All possible spin states for each metallic ionic complex were computed and summarized in Tables S70 – S79.

Charge densities of the CO_2 moieties in $[ClM(CO_2)]^-$ complexes were calculated in relation to the charge density of the neutral CO_2 molecule in its $^1A_1$ electronic state, according to the equation:

$$\delta^-(CO_2) = [\delta(CO_2)_{[ClM(CO2)]-}] - [\delta(CO_2)_{[CO2]}],$$

,where
$\delta^-(CO_2)$ – relative charge density of CO_2 moiety in $[ClM(CO_2)]^-$;
$[\delta^-(CO_2)_{[ClM(CO2)]-}]$ – charge density of CO_2 moiety in $[ClM(CO_2)]^-$;
$[\delta^-(CO_2)_{[CO2]}]$ – charge density of neutral CO_2 in the $^1A_1$ electronic state.

Electron density distributions were computed at CAM-B3LYP/AUG-cc-pVTZ level using the Hirshfeld method[5] and the results are shown in Figures S87-S89 and in Table S86.

In addition, potential energy surfaces of $^1A_1$ and $^3B_2$ electronic states of neutral carbon dioxide as a function of bond angle (∠OCO) were calculated at the CASSCF/aug-cc-pVDZ level, including 16 valence electrons and 12 reactive orbitals. The number of configurations generated in the full valence space were 122760 and 174240 for the $^1A_1$ and $^3B_2$ electronic states, respectively. The spin state crossover points were estimated using a simple interpolation method, by solving a system of two linear equations corresponding to the $^1A_1$ and $^3B_2$ potential energy surface curves (Figures S82, S83).

The electronic energies of the isolated neutral CO_2 moieties taken from $[ClM(CO_2)]^-$ complexes optimized at CAM-B3LYP/AUG-cc-pVTZ level were computed at the single-point CASSCF/aug-cc-pVDZ level with analogous active space restrictions. The energy distribution of all "*frozen*" CO_2 moieties was plotted in Figure S84.

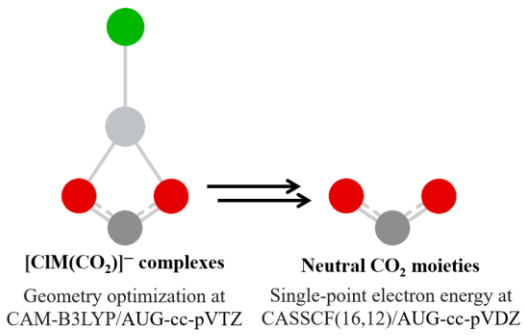

2.1. Calculated relative complexation energies

Table S 70 Relative energies in [kJ/mol] for substrates and products (for different spin states), calculated for the reaction between $ClSc^-$ and CO_2. For all methods, the aug-cc-pVTZ basis set was used.

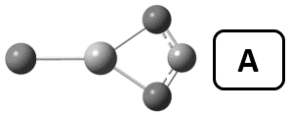

M= Sc	Doublet	Quartet	Sextet	Octet	Doublet	Quartet	Sextet	Octet	Doublet	Quartet	Sextet	Octet
MP2	0	206	717	1478	-212	-54	487	-	-157	-62	483	-
B3LYP	0	151	655	1508	-219	-68	387	-	-176	-83	387	-
M11	0	152	709	1622	-233	-103	392	-	-175	-101	398	-
wB97XD	0	95	785	1531	-231	-80	390	-	-226	-88	391	-
CAM-B3LYP	0	88	640	1508	-257	-106	360	-	-244	-127	366	-
M06-2X	0	185	722	1554	-229	-71	412	-	-165	-80	414	-

"-" SCF convergence issues.

Table S 71 Relative energies in [kJ/mol] for substrates and products (for different spin states), calculated for the reaction between $ClTi^-$ and CO_2. For all methods, the aug-cc-pVTZ basis set was used.

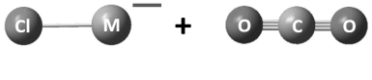

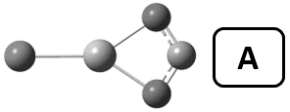

M= Ti	Singlet	Triplet	Quintet	Septet	Singlet	Triplet	Quintet	Septet	Singlet	Triplet	Quintet	Septet
MP2	84	0	1375	1387	-168	-257	-111	-	-233	-257	-111	-
B3LYP	86	0	1451	541	-179	-223	-130	349	-174	-257	-123	-
M11	54	0	687	1500	-212	-249	-125	361	-205	-267	-136	-
wB97XD	120	0	1465	582	-185	-221	-97	372	-183	-254	-107	-
CAM-B3LYP	132	0	17	557	-193	-247	-131	339	-185	-275	-139	-
M06-2X	104	0	80	675	-157	-221	-97	384	-139	-237	-105	-

"-" SCF convergence issues.

Table S 72 Relative energies in [kJ/mol] for substrates and products (for different spin states), calculated for the reaction between ClV^- and CO_2. For all methods, the aug-cc-pVTZ basis set was used.

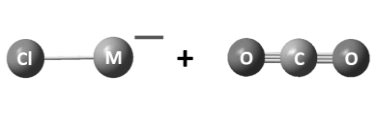

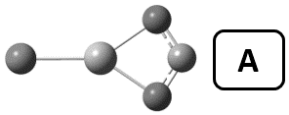

M= V	Doublet	Quartet	Sextet	Octet	Doublet	Quartet	Sextet	Octet	Doublet	Quartet	Sextet	Octet
MP2	252	0	18	690	112	-125	-70	-	-55	-198	-81	-
B3LYP	203	0	8	536	-68	-143	-95	396	-107	-218	-112	-
M11	208	12	0	549	-153	-214	-147	-	-190	-252	-148	-
wB97XD	186	148	0	554	-128	-185	-102	-	-179	-198	-117	-
CAM-B3LYP	161	0	19	561	-99	-195	-123	376	-131	-240	-132	-
M06-2X	214	0	46	604	-109	-225	-149	363	-118	-257	-149	-

"-" SCF convergence issues.

Table S 73 Relative energies in [kJ/mol] for substrates and products (for different spin states), calculated for the reaction between $ClCr^-$ and CO_2. For all methods, the aug-cc-pVTZ basis set was used.

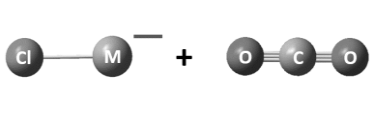

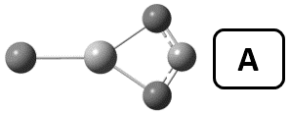

M= Cr	Singlet	Triplet	Quintet	Septet	Singlet	Triplet	Quintet	Septet	Singlet	Triplet	Quintet	Septet
MP2	692	335	52	0	254	225	-79	192	179	99	-119	-
B3LYP	428	238	9	0	176	13	-96	-	80	8	-162	-
M11	490	292	33	0	136	5	-105	143	80	-	-155	-
wB97XD	456	376	0	2	329	216	10	272	276	189	-28	61
CAM-B3LYP	486	390	0	7	161	45	-116	-	165	6	-172	-
M06-2X	597	208	0	32	169	56	-150	112	115	29	-188	-

"-" SCF convergence issues.

Table S 74 Relative energies in [kJ/mol] for substrates and products (for different spin states), calculated for the reaction between $ClMn^-$ and CO_2. For all methods, the aug-cc-pVTZ basis set was used.

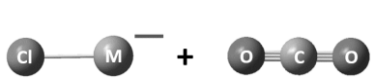

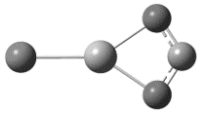

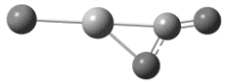

M= Mn	Doublet	Quartet	Sextet	Octet	Doublet	Quartet	Sextet	Octet	Doublet	Quartet	Sextet	Octet
MP2	645	116	73	0	424	41	-170	97	113	-64	-179	-99
B3LYP	323	150	0	145	142	65	-59	39	106	-29	-80	22
M11	393	131	0	96	115	33	-117	125	58	-55	-128	-35
wB97XD	400	344	0	158	151	68	-56	44	56	-48	-76	-
CAM-B3LYP	445	148	0	146	132	54	-79	19	108	-56	-94	5
M06-2X	483	193	0	172	453	129	-78	23	26	60	-75	24

"-" SCF convergence issues.

Table S 75 Relative energies in [kJ/mol] for substrates and products (for different spin states), calculated for the reaction between $ClFe^-$ and CO_2. For all methods, the aug-cc-pVTZ basis set was used.

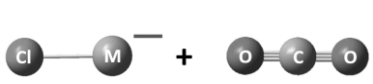

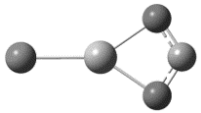

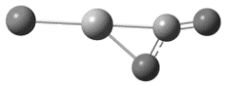

M= Fe	Singlet	Triplet	Quintet	Septet	Singlet	Triplet	Quintet	Septet	Singlet	Triplet	Quintet	Septet
MP2	248	61	0	4	318	-54	-221	57	-1	-121	-230	-114
B3LYP	212	0	70	116	141	-25	-142	7	-18	-122	-161	-21
M11	303	0	36	85	253	33	-178	72	4	-170	-192	-65
wB97XD	249	76	0	191	139	-3	-101	50	21	-138	-128	28
CAM-B3LYP	307	68	0	174	165	-1	-119	25	20	-145	-142	-1
M06-2X	613	97	0	179	426	159	-82	31	157	-	-96	18

"-" SCF convergence issues.

Table S 76 Relative energies in [kJ/mol] for substrates and products (for different spin states), calculated for the reaction between $ClCo^-$ and CO_2. For all methods, the aug-cc-pVTZ basis set was used.

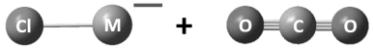

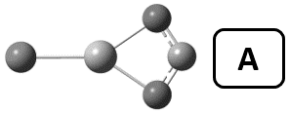

M= Co	Doublet	Quartet	Sextet	Octet	Doublet	Quartet	Sextet	Octet	Doublet	Quartet	Sextet	Octet
MP2	3	0	296	781	86	-36	337	-	-48	-58	62	-
B3LYP	26	0	305	774	43	-50	100	570	-129	-104	79	589
M11	165	0	234	750	-3	-93	150	546	-140	-131	11	525
wB97XD	0	31	329	862	4	-72	73	-	-163	-139	56	-
CAM-B3LYP	77	0	318	769	-	-74	169	539	-166	-143	-	-
M06-2X	7	0	223	745	61	-101	19	531	-	-106	219	525

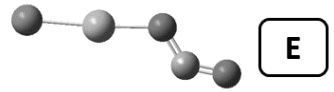

M= Co	Doublet	Quartet	Sextet	Octet
MP2	-28	-	-	665
B3LYP	-5	-20	-	680
M11	-	-112	11	525
wB97XD	-	-96	-	-
CAM-B3LYP	-107	-118	78	-
M06-2X	-	-97	68	561

"-" SCF convergence issues.

Table S 77 Relative energies in [kJ/mol] for substrates and products (for different spin states), calculated for the reaction between $ClNi^-$ and CO_2. For all methods, the aug-cc-pVTZ basis set was used.

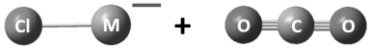

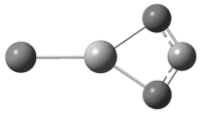

A

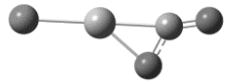

B

M= Ni	Singlet	Triplet	Quintet	Septet	Singlet	Triplet	Quintet	Septet	Singlet	Triplet	Quintet	Septet
MP2	284	0	335	1131	161	70	185	742	-	33	177	-
B3LYP	54	0	293	878	39	-60	275	601	-154	-93	123	605
M11	103	0	280	953	36	-21	112	625	-137	-107	112	627
wB97XD	42	0	306	943	27	-81	249	624	-166	-	119	612
CAM-B3LYP	67	0	493	955	31	-78	128	613	-155	-103	112	634
M06-2X	137	0	255	838	58	-28	89	589	-69	-82	146	591

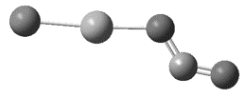

E

M= Ni	Singlet	Triplet	Quintet	Septet
MP2	B	-87	-	0
B3LYP	B	-83	125	649
M11	B	-109	112	690
wB97XD	B	-94	121	752
CAM-B3LYP	B	-100	112	-
M06-2X	B	-83	87	-

"-" SCF convergence issues.

Table S 78 Relative energies in [kJ/mol] for substrates and products (for different spin states), calculated for the reaction between $ClCu^-$ and CO_2. For all methods, the aug-cc-pVTZ basis set was used.

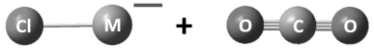

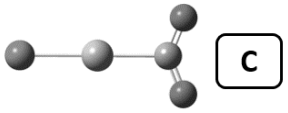

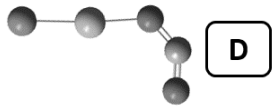

M= Cu	Doublet	Quartet	Sextet	Octet	Doublet	Quartet	Sextet	Octet	Doublet	Quartet	Sextet	Octet
MP2	0	506	1406	1847	-87	498	-	-	-85	564	-	-
B3LYP	0	395	1071	1801	-71	350	713	1290	-74	225	719	1279
M11	0	408	1165	2079	-96	217	764	-	-98	234	787	-
wB97XD	0	416	1017	2048	-88	234	791	-	-80	255	-	-
CAM-B3LYP	0	411	1116	1838	-90	218	775	-	-89	239	785	-
M06-2X	0	379	1147	1758	-72	192	746	-	-72	206	749	-

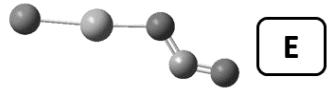

M= Cu	Doublet	Quartet	Sextet	Octet
MP2	-92	344	905	-
B3LYP	-80	330	882	1325
M11	-101	218	804	-
wB97XD	-84	234	-	-
CAM-B3LYP	-94	218	-	-
M06-2X	-74	192	-	-

"-" SCF convergence issues.

Table S 79 Relative energies in [kJ/mol] for substrates and products (for different spin states), calculated for the reaction between $ClZn^-$ and CO_2. For all methods, the aug-cc-pVTZ basis set was used.

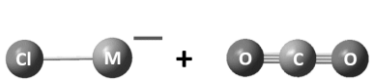

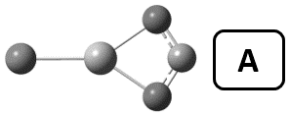

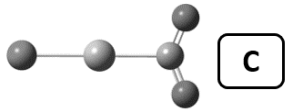

M= Zn	Singlet	Triplet	Quintet	Septet	Singlet	Triplet	Quintet	Septet	Singlet	Triplet	Quintet	Septet
MP2	0	210	758	1538	11	305	654	-	-37	221	698	-
B3LYP	0	227	780	1611	41	184	586	-	-20	108	583	-
M11	0	204	749	1602	-18	245	587	-	-41	64	671	-
wB97XD	0	246	815	1674	40	129	607	-	-13	243	813	-
CAM-B3LYP	0	227	783	1624	20	88	578	-	-25	88	579	-
M06-2X	0	214	767	1601	-2	86	593	-	-29	75	687	-

"-" SCF convergence issues.

2.2. CO_2 potential energy surfaces for $^1A_1$ and $^3B_2$ states

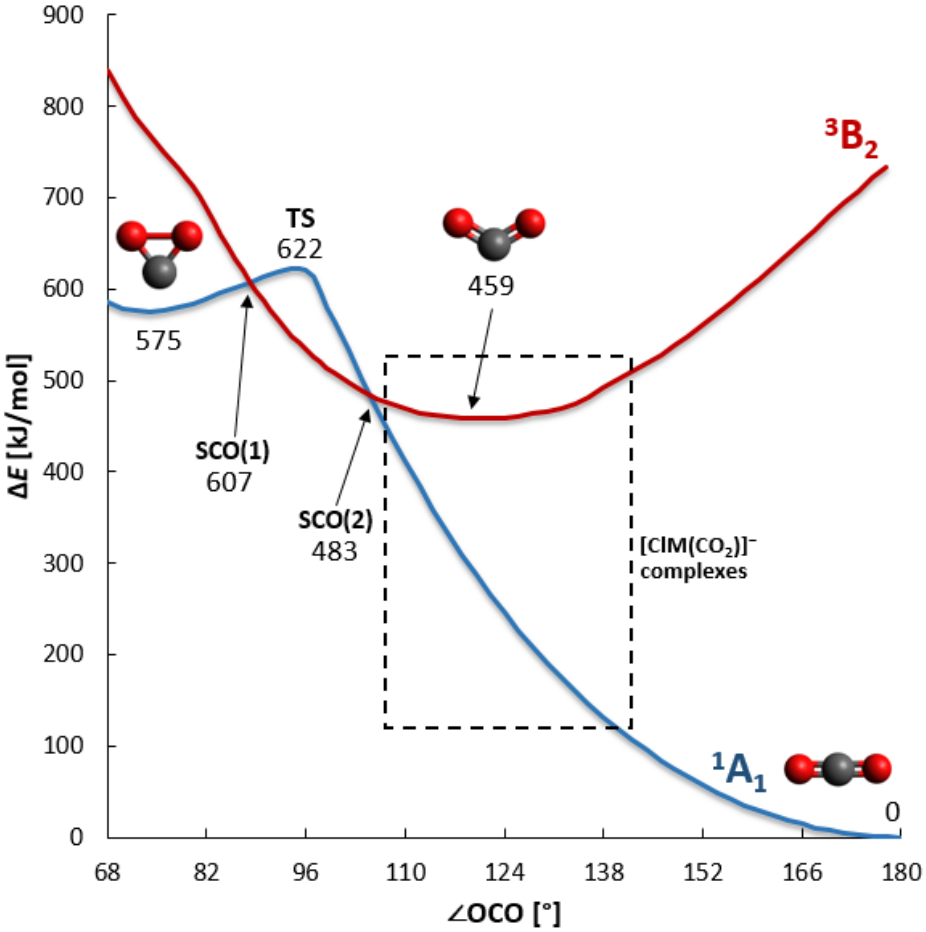

Figure S 80 Potential energy surfaces of $^1A_1$ and $^3B_2$ states along bending coordinate of symmetric CO_2 (C_{2v}). Calculations were performed at CASSCF/AUG-cc-pVDT level of theory by including 16 electrons and 12 valence orbitals.

Table S 81 Geometry and energy parameters calculated for neutral CO_2 molecule at CASSCF(16,12)/AUG-cc-pVDT

	∠OCO [°]	**$R_{C\text{-}O}$** [Å]	**$R_{O\text{-}O}$** [Å]	**ΔE** [kJ/mol]	**Symmetry**	**Electronic state**
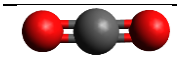	180	1.174	-	0	$D_{\infty h}$	$^1\Sigma_g$
TS	74.2	1.328	1.945	622	C_{2v}	$^1A_1$
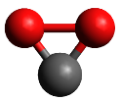	73.5	1.338	1.599	575	C_{2v}	$^1A_1$
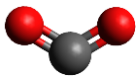	118.2	1.257	2.160	459	C_{2v}	$^3B_2$
SCO (1)	88.1	-	-	607	C_{2v}	$^1A_1/^3B_2$
SCO (2)	105.1	-	-	483	C_{2v}	$^1A_1/^3B_2$

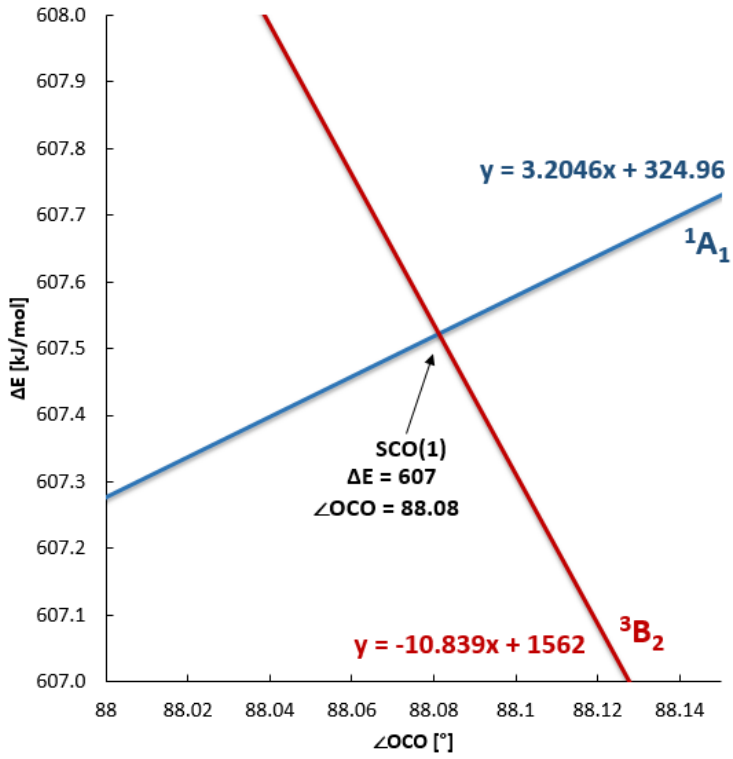

Figure S 82 Interpolation procedure and estimated spin crossover point SCO(1) between $^1A_1$ and $^3B_2$ electronic states.

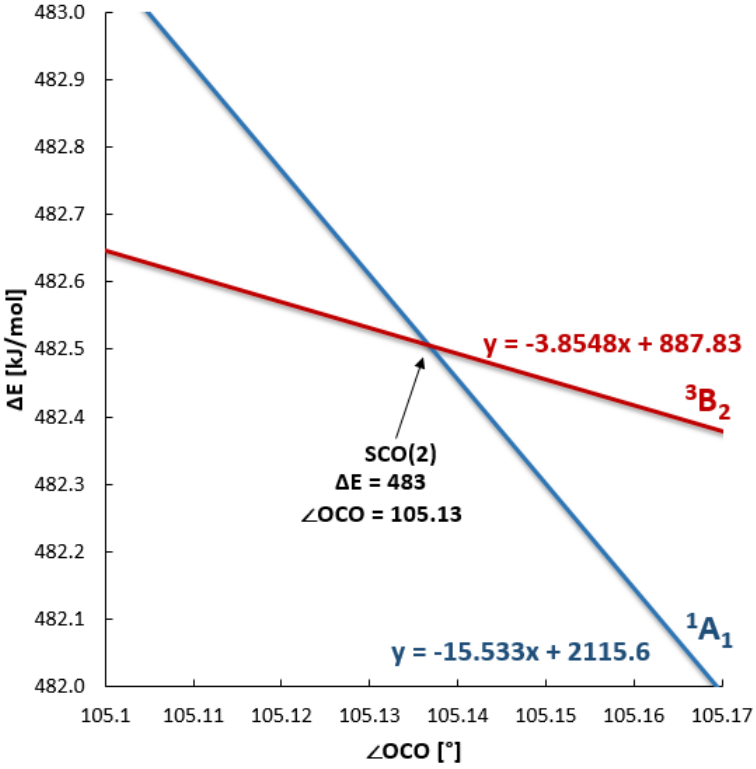

Figure S 83 Interpolation procedure and estimated spin crossover point SCO(1) between $^3B_2$ and $^1A_1$ electronic states.

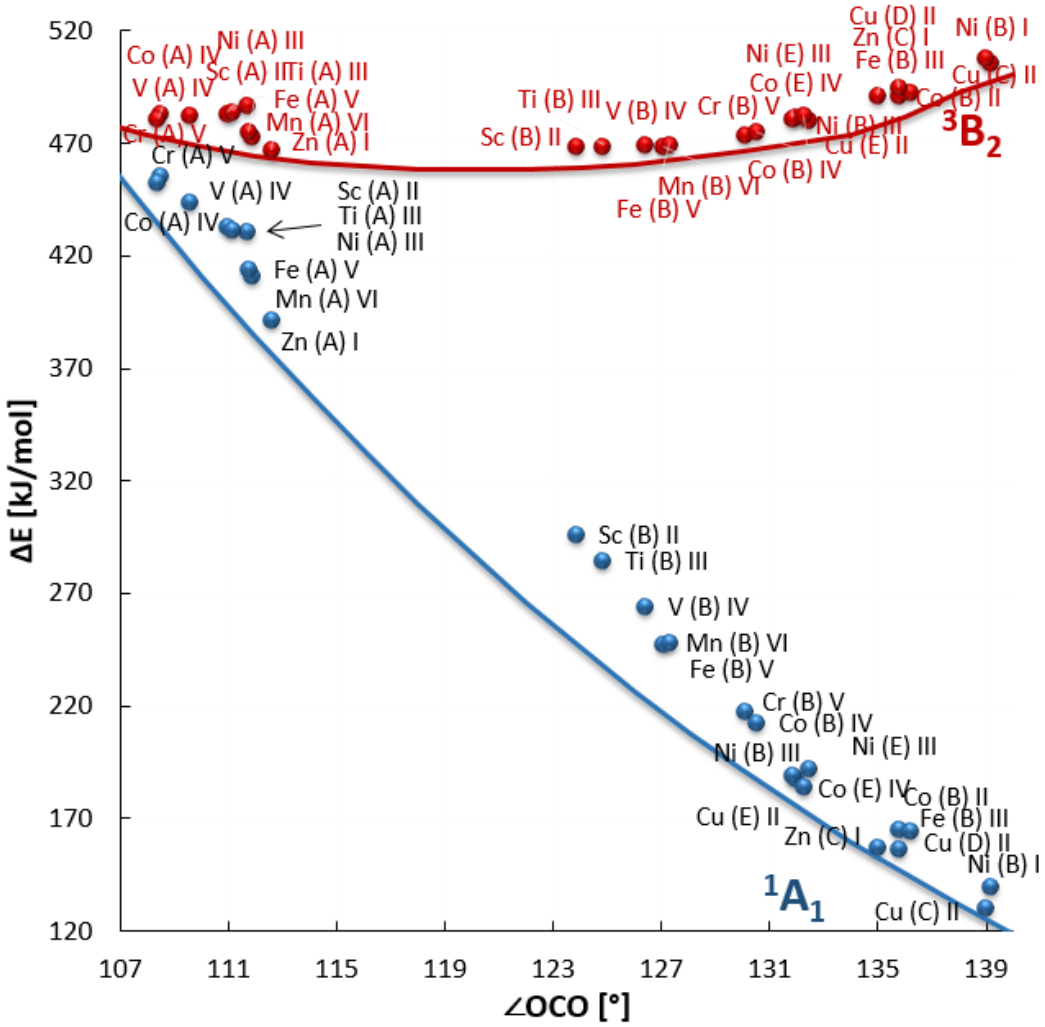

Figure S 84 Single point electron energy distribution of CO_2 moieties from [$ClMCO_2^-$] structures, calculated for $^1A_1$ and $^3B_2$ electronic states at CASSCF(16,12)/AUG-cc-pVDT level of theory

Table S 85 Relative energies and geometry parameters of CO_2 moieties taken from [$ClMCO_2^-$] structures, calculated for $^1A_1$ and $^3B_2$ electronic states at CASSCF(16,12)/aug-cc-pVDZ level of theory.

Structure:	**ΔE, $^1A_1$ [kJ/mol]**	**ΔE, $^3B_2$ [kJ/mol]**	**∠OCO [°]**	***d*(C-O^1) [Å]**	***d*(C-O^2) [Å]**
Co (A) IV	453	481	108.39	1.318	1.318
Cr (A) V	456	484	108.49	1.325	1.325
V (A) IV	444	482	109.56	1.326	1.326
Ti (A) III	433	484	110.96	1.331	1.331
Ni (A) III	432	484	111.16	1.332	1.332
Sc (A) II	431	487	111.66	1.337	1.337
Fe (A) V	414	475	111.75	1.318	1.318
Mn (A) VI	411	474	111.89	1.316	1.316
Zn (A) I	392	467	112.57	1.298	1.298
Sc (B) II	296	469	123.85	1.368	1.208
Ti (B) III	285	469	124.83	1.360	1.210
V (B) IV	264	470	126.41	1.344	1.210
Mn (B) VI	248	469	127.07	1.323	1.213
Fe (B) V	249	470	127.30	1.328	1.209
Cr (B) V	218	474	130.07	1.306	1.210
Co (B) IV	213	475	130.50	1.302	1.209
Ni (E) III	190	481	131.83	1.272	1.203
Co (E) IV	188	482	131.95	1.270	1.204
Cu (E) II	184	483	132.26	1.266	1.205
Ni (B) III	193	481	132.45	1.289	1.207
Zn (C) I	157	492	134.98	1.226	1.226
Cu (D) II	157	495	135.77	1.254	1.205
Fe (B) III	166	492	135.80	1.278	1.205
Co (B) II	164	493	136.19	1.281	1.203
Cu (C) II	131	508	138.98	1.222	1.223
Ni (B) I	140	507	139.20	1.267	1.200

Relative energy ΔE was calculated in relation to the $^1A_1$ linear CO_2 molecule.

2.3. Calculated partial charges of CO_2 moieties in $[ClM(CO_2)]^-$ complexes

Table S 86 Calculated partial charges of CO_2 moieties in $[ClM(CO_2)]^-$ complexes in relation to the neutral CO_2 molecule at $^1A_1$ electronic state

Isomer:	$\delta^-(CO_2)$ [Rho]#
Sc (A) II	0.868
Ti (A) III	0.850
V (A) IV	0.837
Cr (A) V	0.900
Mn (A) VI	0.896
Fe (A) V	0.854
Co (A) IV	0.867
Zn (A) I	0.912
Ni (A) III	0.742
Sc (B) II	0.815
Ti (B) III	0.779
V (B) IV	0.736
Cr (B) V	0.742
Mn (B) VI	0.794
Fe (B) V	0.752
Fe (B) III	0.558
Co (B) IV	0.670
Co (B) II	0.535
Ni (B) III	0.657
Ni (B) I	0.517
Zn (C) I	0.771
Cu (C) II	0.604
Cu (D) II	0.609
Co (E) IV	0.545
Ni (E) III	0.574
Cu (E) II	0.607

#Charge density of the CO_2 moiety in $[ClM(CO_2)]^-$ complexes was calculated in relation to the neutral CO_2 molecule in $^1A_1$ electronic state at CAM-B3LYP/ CAM-B3LYP/AUG-cc-pVTZ level using the Hirshfeld method.[5] $\delta^-(CO_2) = [\delta(CO_2)_{[ClM(CO2)]}] - [\delta(CO_2)_{[CO2]}]$

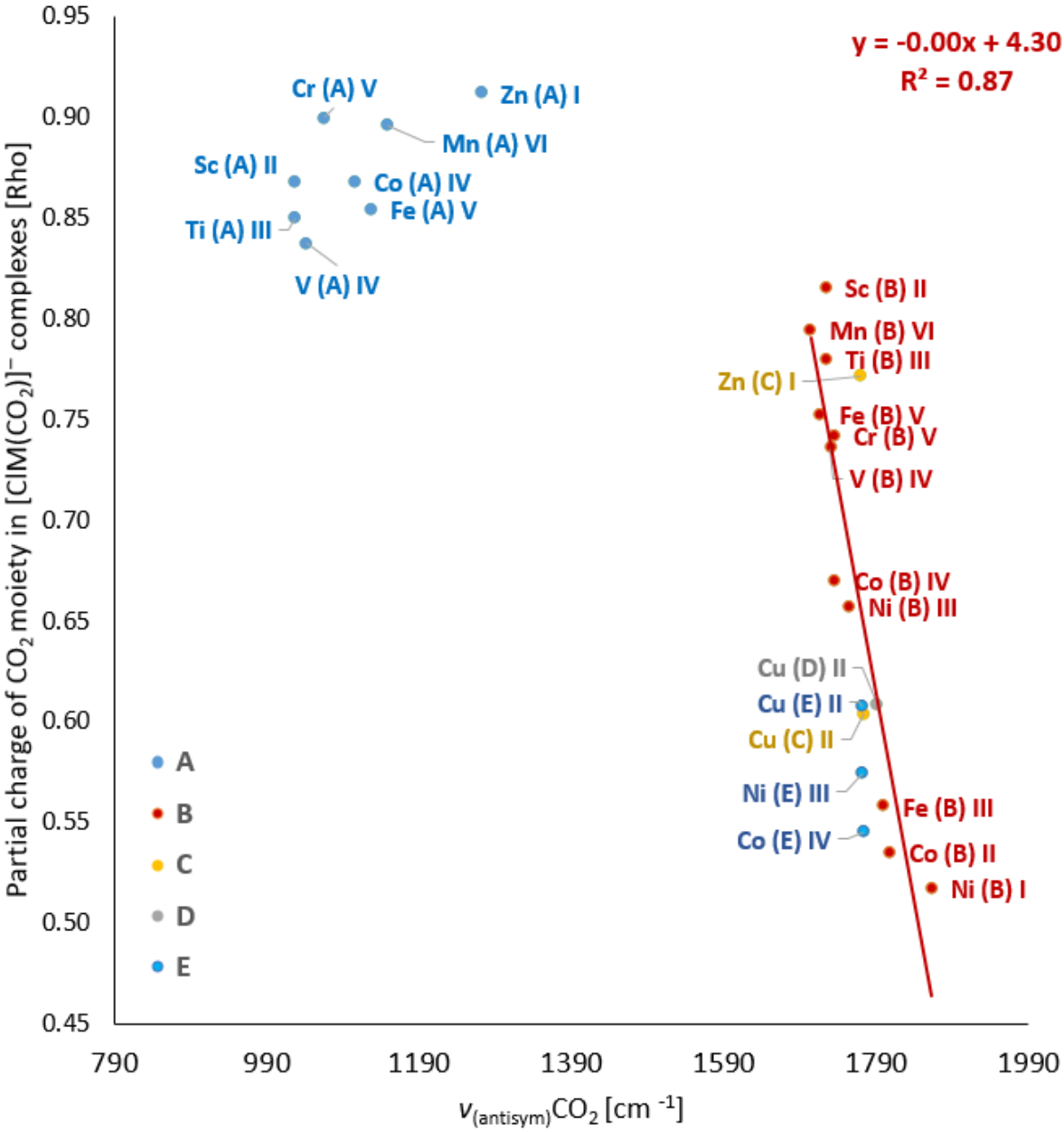

Figure S 87 Partial charge of CO_2 moieties in $[ClM(CO_2)]^-$ complexes as a function of calculated antisymmetric stretch $\nu_{(antisym)}CO_2$ [cm $^{-1}$]

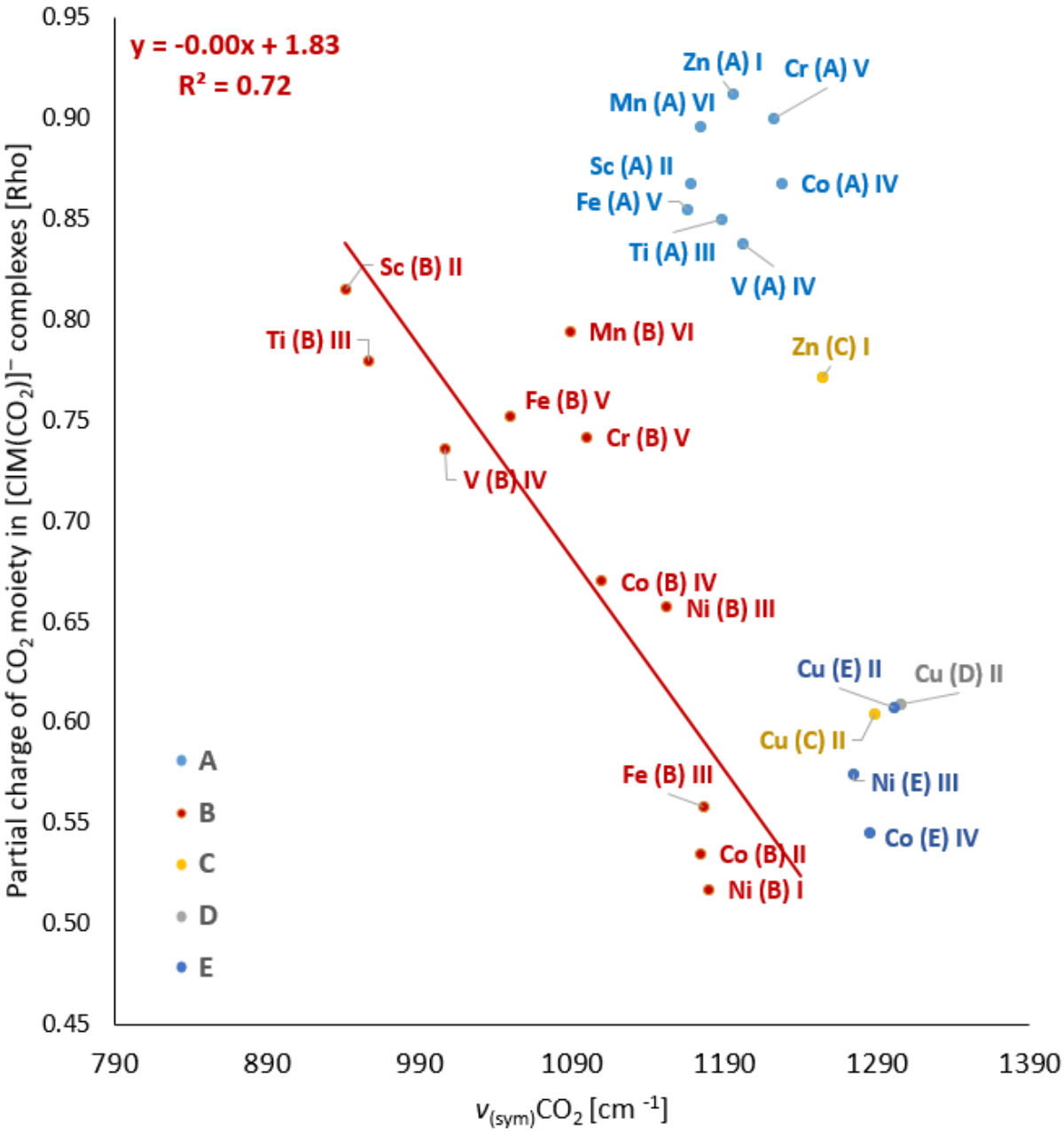

Figure S 88 Partial charge of CO_2 moieties in $[ClM(CO_2)]^-$ complexes as a function of calculated symmetric stretch $\nu_{(sym)}CO_2$ [cm $^{-1}$]

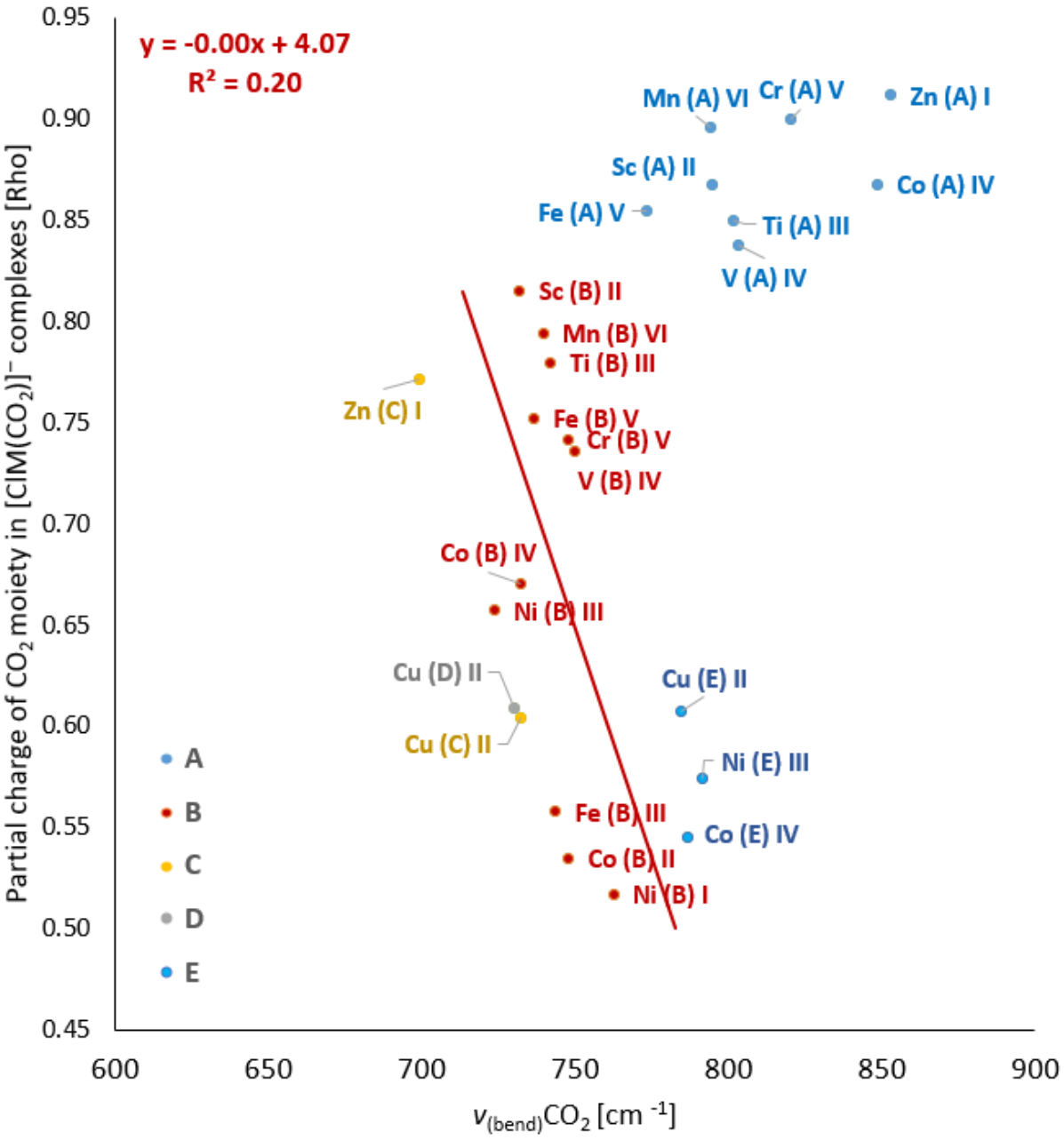

Figure S 89 Partial charge of CO_2 moieties in $[ClM(CO_2)]^-$ complexes as a function of calculated bending stretches $\nu_{(antisym)}CO_2$ [cm $^{-1}$]

2.4. Population Analysis

Table S 90 Natural population analysis of the metal atoms at the $[ClM(CO_2)]^-$ structures at the CASSCF/aug-cc-pVTZ//CAM-B3LYP/aug-cc-pVTZ level of theory.

Metal	Population Analysis	
Sc	$\mathbf{A^{II}}$: $3d^{0.95}4s^{0.60}4p^{0.23}$	$\mathbf{B^{II}}$: $3d^{1.02}4s^{0.79}4p^{0.46}$
Ti	$\mathbf{B^{III}}$: $3d^{2.41}4s^{0.65}4p^{0.22}$	$\mathbf{A^{III}}$: $3d^{2.31}4s^{0.50}4p^{0.12}$
V	$\mathbf{B^{IV}}$: $3d^{3.44}4s^{0.58}4p^{0.29}$	$\mathbf{A^{IV}}$: $3d^{3.29}4s^{0.41}4p^{0.23}$
Cr	$\mathbf{B^{V}}$: $3d^{4.53}4s^{0.59}4p^{0.23}$	$\mathbf{A^{V}}$: $3d^{4.23}4s^{0.36}4p^{0.26}$
Mn	$\mathbf{B^{VI}}$: $3d^{5.12}4s^{0.72}4p^{0.40}$	$\mathbf{A^{VI}}$: $3d^{5.11}4s^{0.38}4p^{0.26}$
Fe	$\mathbf{B^{III}}$: $3d^{6.56}4s^{0.88}4p^{0.18}$ $\mathbf{A^{V}}$: $3d^{6.19}4s^{0.35}4p^{0.28}$	$\mathbf{B^{V}}$: $3d^{6.16}4s^{0.67}4p^{0.35}$
Co	$\mathbf{B^{II}}$: $3d^{7.66}4s^{0.77}4p^{0.17}$ $\mathbf{E^{IV}}$: $3d^{7.66}4s^{0.66}4p^{0.16}$	$\mathbf{B^{IV}}$: $3d^{7.27}4s^{0.75}4p^{0.32}$ $\mathbf{A^{IV}}$: $3d^{7.09}4s^{0.49}4p^{0.24}$
Ni	$\mathbf{B^{I}}$: $3d^{8.82}4s^{0.61}4p^{0.12}$ $\mathbf{E^{III}}$: $3d^{8.75}4s^{0.51}4p^{0.13}$	$\mathbf{B^{III}}$: $3d^{8.14}4s^{0.88}4p^{0.34}$ $\mathbf{A^{III}}$: $3d^{8.80}4s^{0.49}4p^{0.12}$
Cu	$\mathbf{E^{II}}$: $3d^{9.73}4s^{0.46}4p^{0.11}$ $\mathbf{D^{II}}$: $3d^{9.84}4s^{0.39}4p^{0.11}$	$\mathbf{C^{II}}$: $3d^{9.88}4s^{0.48}4p^{0.13}$
Zn	$\mathbf{C^{I}}$: $3d^{10.0}4s^{1.21}4p^{0.25}$	$\mathbf{A^{I}}$: $3d^{10.0}4s^{0.60}4p^{0.23}$

Table S 91 Main coefficients of the CASSCF configuration states at the CASSCF/aug-cc-pVTZ//CAM-B3LYP/aug-cc-pVTZ level of theory of the $[ClM(CO_2)]^-$ structures.

Sc	0.983|2+00000000> (A^{II})	0.983|2+00000000> (B^{II})
Ti	0.976|2++0000000> (B^{III})	0.981|2++0000000> (A^{III})
V	0.973|2+++000000> (B^{IV})	0.992|2+++000000> (A^{IVI})
Cr	0.954|2++++00000> (B^{V})	0.971|2++++00000> (A^{V})
Mn	0.977|2+++++0000> (B^{VI})	0.996|2+++++0000> (A^{VI})
Fe	0.908|222++00000> -0.249|220++20000> (B^{III}) 0.990|22++++0000> (A^{V})	0.980|22++++0000> (B^{V})
Co	0.920|2222+00000>-0.246|2220+20000> (B^{II}) 0.971|222+++0000> (E^{IV})	0.974|222+++0000> (B^{IV}) 0.989|222+++0000> (A^{IV})
Ni	0.919|2222200000>-0.330|2222020000> (B^{I}) 0.980|2222++0000> (E^{III})	0.969|2222++0000> (B^{III}) 0.980|2222++0000> (A^{III})
Cu	0.950|22222+0000> (E^{II}) 0.981|22222+0000> (D^{II})	0.976|22222+0000> (C^{II})
Zn	0.974|2222220000> (C^{I})	0.976|2222220000> (A^{I})

Table S 92 Atomic natural population charges of the atoms at the $[ClM(CO_2)]^-$ structures at the CASSCF/aug-cc-pVTZ//CAM-B3LYP/aug-cc-pVTZ level of theory.

	q_{Cl}	q_M	q_C	q_{O1}	q_{O2}	q_{CO_2}
Sc(A^{II})	-0.65	+1.11	-0.18	-0.64	-0.64	-1.46
Sc(B^{II})	-0.62	+0.61	+0.33	-0.70	-0.62	-0.99
Ti(B^{III})	-0.69	+0.62	+0.21	-0.56	-0.59	-0.94
Ti(A^{III})	-0.69	+0.97	-0.27	-0.50	-0.50	-1.27
V(B^{IV})	-0.70	+0.65	+0.32	-0.63	-0.63	-0.94
V(A^{III})	-0.70	+0.97	-0.24	-0.52	-0.52	-1.28
Cr(B^{V})	-0.68	+0.59	+0.31	-0.58	-0.63	-0.9
Cr(A^{V})	-0.69	+1.06	-0.25	-0.56	-0.56	-1.37
Mn(B^{VI})	-0.76	+0.70	+0.36	-0.65	-0.65	-0.94
Mn(A^{VI})	-0.72	+1.17	-0.29	-0.59	-0.59	-1.47
Fe(B^{III})	-0.76	+0.34	+0.59	-0.54	-0.62	-0.57
Fe(B^{V})	-0.72	+0.77	+0.21	-0.65	-0.61	-1.05
Fe(A^{V})	-0.72	+1.12	+0.01	-0.70	-0.70	-1.39
Co(B^{II})	-0.76	+0.36	+0.57	-0.59	-0.58	-0.6
Co(B^{IV})	-0.73	+0.62	+0.33	-0.66	-0.57	-0.9
Co(E^{IV})	-0.75	+0.55	+0.24	-0.47	-0.57	-0.8
Co(A^{IV})	-0.71	+1.13	-0.19	-0.62	-0.62	-1.43
Ni(B^{I})	-0.80	+0.43	+0.49	-0.61	-0.51	-0.63
Ni(B^{III})	-0.72	+0.61	+0.21	-0.68	-0.43	-0.9
Ni(E^{III})	-0.75	+0.60	+0.23	-0.50	-0.58	-0.85
Ni(A^{III})	-0.81	+0.56	+0.38	-0.56	-0.56	-0.74
Cu(E^{II})	-0.78	+0.68	+0.18	-0.55	-0.54	-0.91
Cu(D^{II})	-0.80	+0.65	+0.14	-0.49	-0.50	-0.85
Cu(C^{II})	-0.73	+0.28	+0.39	-0.47	-0.47	-0.55
Zn(C^{I})	-0.81	+0.50	0.29	-0.56	-0.43	-0.70
Zn(A^{I})	-070	+1.15	-0.14	-0.66	-0.66	-1.46

2.5. Prototype species

Table S 93 Calculated geometries and natural population analysis at the CAM-B3LYP/aug-cc-pVTZ level of theory.

	R(C-O)	∠OCO	q_C	q_O	q_O
$HCOO^-$	1.246	130.2	+0.64	-0.80	-0.80
H_2CO	1.196		+0.29	-0.50	
HCOOH	1.194, 1338[a]	124.8	+0.66	-0.58	-0.68[a.b]
CO_2 ($^1A_1$)	1.156	180.0	+1.01	-0.50	-0.50
CO_2 ($^3B_2$)	1.234	118.4	+0.60	-0.30	-0.30
CO_2^-	1.225	137.6	+0.51	-0.76	-0.76

[a] Single C-O bond. [b] Total charge on OH is -0.19.

2.6. Cartesian coordinates

Structures of $[ClM(CO_2)]^-$ ions optimized with CAM-B3LYP/aug-cc-pVTZ.

$ClSc(CO_2)^-$:

Complex A (Charge: -1, Multiplicity: 2):

C	-0.01705000	-0.20517500	-0.01175700
O	-0.04334400	-0.02507700	1.31256600
O	1.21028600	-0.02504300	-0.50989600
Sc	1.90876800	0.33720900	1.31297200
Cl	3.55392200	1.72482900	2.44417600

Complex B (Charge: -1, Multiplicity: 2):

C	0.00099100	0.03575600	-0.08824900
O	-0.01895900	-0.19885700	1.09674900
O	1.12166000	-0.06406700	-0.86584200
Sc	-0.19657000	0.50563300	-2.17270600
Cl	-1.04381200	-0.28002200	-4.30216400

$ClTi(CO_2)^-$:

Complex A (Charge: -1, Multiplicity: 3):

C	0.01192200	-0.00037200	0.00848300
O	0.01355200	0.00010200	1.33937100
O	1.25418400	0.00010300	-0.46923700
Ti	1.98899200	0.00122800	1.36350000
Cl	3.93580900	0.00240600	2.69726300

Complex B (Charge: -1, Multiplicity: 3):

C	-0.00227600	-0.00000100	-0.00604700
O	-0.00089600	0.00000300	1.20375200
O	1.11323800	0.00000500	-0.78416000
Ti	-0.31297100	-0.00001800	-2.05299100
Cl	-1.38695500	-0.00032400	-4.16788500

$ClV(CO_2)^-$:

Complex A (Charge: -1, Multiplicity: 4):

C	-0.00606300	-0.00766600	-0.00443000
O	-0.00031900	-0.00231800	1.32126000
O	1.24117600	-0.00218900	-0.45367300
V	1.92326200	-0.33866000	1.34504400
Cl	3.81137400	-0.04334500	2.66403200

Complex B (Charge: -1, Multiplicity: 4):

C	-0.00214200	0.00000600	0.01086200
O	0.00689800	-0.00000700	1.22096500
O	1.07381400	-0.00001200	-0.79526700
V	-0.41446800	0.00003800	-1.97076600
Cl	-1.78779300	0.00014300	-3.84994400

$ClCr(CO_2)^-$:

Complex A (Charge: -1, Multiplicity: 5):

C	0.01125300	0.00000000	0.00808600
O	0.01525200	0.00000000	1.33308800
O	1.26656300	0.00000000	-0.41599200
Cr	1.93904000	0.00000000	1.38725500
Cl	3.82213200	0.00000000	2.73474600

Complex B (Charge: -1, Multiplicity: 5):

C	-0.01178800	-0.00000900	-0.00113600
O	0.00650800	0.00000700	1.20915900
O	0.97484800	0.00001000	-0.85692900
Cr	-0.64106600	-0.00004000	-1.91948200
Cl	-2.23227200	-0.00018100	-3.59545500

$ClMn(CO_2)^-$:

Complex A (Charge: -1, Multiplicity: 6):

C	0.01566700	0.00000000	0.01068700
O	0.00982300	0.00000000	1.32639700
O	1.23873500	0.00000000	-0.47434200
Mn	2.00942500	0.00000100	1.37124700
Cl	3.90450800	0.00000500	2.66452000

Complex B (Charge: -1, Multiplicity: 6):

C	-0.00364000	-0.00006400	-0.00519200
O	0.01250000	0.00017600	1.20773100
O	1.04126400	0.00001400	-0.81662600
Mn	-0.61364000	-0.00057800	-1.94423900
Cl	-1.10822900	-0.00117500	-4.19138500

$ClFe(CO_2)^-$:

Complex A (Charge: -1, Multiplicity: 5):

C	-2.19121200	3.82915900	2.66142600
O	-1.02922800	4.40745800	2.43499400
O	-2.91194900	4.50597400	3.53285200
Fe	-1.49152700	5.81748900	3.68407400
Cl	-0.81829700	7.70970700	4.65648400

Complex B (Charge: -1, Multiplicity: 3):

C	-2.21944400	3.93536300	2.76503600
O	-1.86376400	3.12839700	1.94372100
O	-3.23122000	4.07582800	3.53347300
Fe	-2.03881900	5.53914100	3.81302700
Cl	-0.94553900	7.34077300	4.40470600

Complex B (Charge: -1, Multiplicity: 5):

C	-2.15737400	3.87636500	2.67603500
O	-2.09480900	2.92432500	1.93336700
O	-3.12233600	4.15782100	3.54428500
Fe	-1.82570100	5.57400000	3.69717700
Cl	-1.09856500	7.48698900	4.60909900

$ClCo(CO_2)^-$:

Complex A (Charge: -1, Multiplicity: 4):

C	-2.34044000	0.00000800	0.00005800
O	-1.56912100	1.06927300	0.00002400
O	-1.56913200	-1.06926600	0.00006300
Co	0.02729000	-0.00000500	-0.00001000
Cl	2.23533800	0.00000200	-0.00004300

Complex B (Charge: -1, Multiplicity: 2):

C	1.63342500	0.24904400	0.00001000
O	2.48733500	1.09675400	0.00000300
O	1.60209600	-1.03109700	0.00004900
Co	-0.14389500	-0.30023500	-0.00001500
Cl	-2.21120500	0.33489900	0.00001800

Complex B (Charge: -1, Multiplicity: 4):

C	-1.77698600	-0.18530200	0.00019400
O	-2.85193500	-0.73837800	0.00022500
O	-1.47794800	1.08224500	0.00023500
Co	0.18727000	0.08222000	0.00013200
Cl	2.36424300	-0.18889300	0.00009100

Complex E (Charge: -1, Multiplicity: 4):

C	2.32122700	-0.35868800	0.00000900
O	3.52439800	-0.32520000	0.00001700
O	1.44658200	0.56154400	-0.00001500
Co	-0.39870600	0.14500900	-0.00000800
Cl	-2.52530200	-0.21493300	0.00000800

$ClNi(CO_2)^-$:

Complex A (Charge: -1, Multiplicity: 3):

C	-2.25963200	0.00051400	0.00002600
O	-1.50639600	1.09912700	0.00008600
O	-1.50680200	-1.09855800	-0.00001100
Ni	0.01967600	-0.00044500	0.00002800
Cl	2.18308500	0.00028300	-0.00009100

Complex B (Charge: -1, Multiplicity: 1):

C	1.55037100	0.28877300	0.00000000
O	2.28868300	1.23443500	0.00000000
O	1.61277000	-0.97621500	0.00000000
Ni	-0.13698300	-0.34008600	0.00000000
Cl	-2.15529700	0.33997100	0.00000000

Complex B (Charge: -1, Multiplicity: 3):

C	-1.77052800	-0.21825100	0.00002600
O	-2.78872100	-0.86626200	0.00001900
O	-1.54728100	1.05153300	0.00008000
Ni	0.17487000	0.12193300	-0.00001800
Cl	2.31392800	-0.22014900	0.00003500

Complex E (Charge: -1, Multiplicity: 3):

C	2.33867900	-0.36959200	0.00001500
O	3.53973800	-0.30605900	0.00001500
O	1.44152100	0.53203600	-0.00001600
Ni	-0.38410700	0.13882200	-0.00000300
Cl	-2.48993000	-0.19730100	0.00000600

$ClCu(CO_2)^-$:

Complex C (Charge: -1, Multiplicity: 2):

C	-0.01314100	-1.79683100	0.00000000
O	1.13612800	-2.21626200	0.00000000
O	-1.15417400	-2.23424400	0.00000000
Cu	0.00000000	0.21273700	0.00000000
Cl	0.01313100	2.36562700	0.00000000

Complex D (Charge: -1, Multiplicity: 2):

C	2.53885800	-0.16782500	0.00000300
O	2.84920900	0.99702300	0.00000000
O	1.46232100	-0.81080100	0.00000400
Cu	-0.31942800	-0.19801400	0.00000000
Cl	-2.38011600	0.30938600	-0.00000300

Complex E (Charge: -1, Multiplicity: 2):

C	2.35062600	-0.35932000	0.00000000
O	3.55192400	-0.26667300	0.00000000
O	1.43009900	0.50911900	-0.00000200
Cu	-0.39892700	0.12116400	0.00000100
Cl	-2.49359100	-0.19396500	0.00000000

$ClZn(CO_2)^-$:

Complex A (Charge: -1, Multiplicity: 1):

C	0.00790000	0.00000200	0.00530300
O	-0.00484200	0.00000000	1.30351400
O	1.21154800	0.00000000	-0.48124100
Zn	1.97548700	-0.00000500	1.34633600
Cl	3.78555700	-0.00001100	2.57926800

Complex C (Charge: -1, Multiplicity: 1):

C	0.01686700	0.00000000	0.00722000
O	-0.00178200	0.00000000	1.23356300
O	0.89747100	0.00000000	-0.84646600
Zn	-1.89025300	0.00000100	-0.81706300
Cl	-3.93103600	0.00000200	-1.69868700

3. Principal Component Analysis of all (A-E) isomers

The Principal Component Analysis was performed for all $[ClM(CO_2)]^-$ structures optimized using CAM-B3LYP/aug-cc-pVTZ. The 15 structural, spectral, and one energetic variable, listed in Tables S86 and S87 were taken into account during the simulation according to the atomic numbering shown in Figure S90.

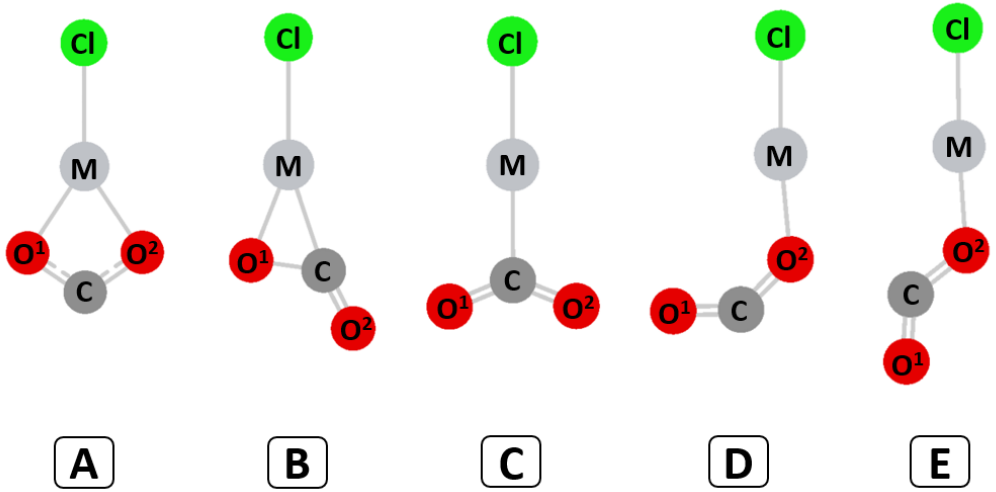

Figure S 94 Numbering of the atoms according to the variables presented in Tables S91-S92.

Table S 95 Variables taken into account for Principal Component Analysis from $[ClM(CO_2)]^-$ structures optimized at CAM-B3LYP/aug-cc-pVTZ level.

	ΔE [kJ/mol]	∠OCO [°]	d(C-O^1) [Å]	d(C-O^2) [Å]	d(O1-O2) [Å]	d(C-M) [Å]	d(M-Cl) [Å]
Observation:	**Var. 1**	**Var. 2**	**Var. 3**	**Var. 4**	**Var. 5**	**Var. 6**	**Var. 7**
Sc (A) II	-257	111.659	1.337	1.337	2.212	2.400	2.431
Sc (B) II	-244	123.849	1.368	1.208	2.274	2.146	2.423
Ti (A) III	-247	110.964	1.331	1.331	2.193	2.397	2.360
Ti (B) III	-275	124.832	1.360	1.210	2.279	2.070	2.372
V (A) IV	-195	109.559	1.326	1.326	2.166	2.378	2.322
V (B) IV	-240	126.413	1.344	1.210	2.281	2.024	2.328
Cr (A) V	-116	108.493	1.325	1.325	2.151	2.370	2.316
Cr (B) V	-172	130.072	1.306	1.210	2.282	2.019	2.311
Mn (A) VI	-151	111.886	1.316	1.316	2.180	2.414	2.294
Mn (B) VI	-164	127.069	1.323	1.213	2.271	2.033	2.301
Fe (A) V	-115	111.749	1.318	1.318	2.182	2.343	2.231
Fe (B) V	-142	127.299	1.328	1.209	2.274	2.009	2.241
Fe (B) III	-145	135.800	1.278	1.205	2.301	1.924	2.189
Co (A) IV	-115	108.391	1.318	1.318	2.139	2.368	2.208
Co (B) IV	-183	130.501	1.302	1.209	2.281	1.982	2.194
Co (B) II	-204	136.193	1.281	1.203	2.305	1.860	2.163
Co (E) IV	-170	131.951	1.270	1.204	2.259	2.766	2.157
Ni (A) III	-78	111.155	1.332	1.332	2.198	2.279	2.163
Ni (B) III	-103	132.446	1.289	1.207	2.285	1.975	2.166
Ni (B) I	-155	139.196	1.267	1.200	2.312	1.801	2.130
Ni (E) III	-100	131.830	1.272	1.203	2.259	2.770	2.132
Cu (C) II	-90	138.976	1.222	1.223	2.290	2.010	2.153
Cu (D) II	-89	135.767	1.254	1.205	2.279	2.858	2.122
Cu (E) II	-94	132.258	1.266	1.205	2.259	1.870	2.118
Zn (A) I	20	112.572	1.298	1.298	2.160	2.381	2.190
Zn (C) I	-25	134.982	1.226	1.226	2.266	2.078	2.223

Table S 96 Variables taken into account for Principal Component Analysis from $[ClM(CO_2)]^-$ structures optimized at CAM-B3LYP/aug-cc-pVTZ level.

	∠MCO^2 [°]	∠MO^{1}C [°]	δ$^-$(CO_2) [Rho]	$\nu_{1(bend)}$ CO_2 [cm^{-1}]	$\nu_{2(sym)}$ CO_2 [cm^{-1}]	$\nu_{3(antisym)}$ CO_2 [cm^{-1}]	ν_4 M-(CO_2) [cm^{-1}]
Observation:	**Var. 8**	**Var. 9**	**Var. 10**	**Var. 11**	**Var. 12**	**Var. 13**	**Var. 14**
Sc (A) II	55.834	90.313	0.868	794.85	1167.16	1025.97	484.53
Sc (B) II	173.593	78.753	0.815	732.04	941.36	1723.58	520.4
Ti (A) III	55.460	90.770	0.850	801.69	1188.48	1026.05	488.96
Ti (B) III	171.435	76.555	0.779	742.12	956.83	1724.18	505.91
V (A) IV	55.213	90.903	0.837	803.14	1201.85	1042.84	493.16
V (B) IV	168.674	75.144	0.736	749.75	1006.26	1729.56	539.13
Cr (A) V	54.247	91.785	0.900	820.28	1222.18	1064.58	515.7
Cr (B) V	162.705	74.265	0.742	747.54	1099.73	1734.57	489.98
Mn (A) VI	55.944	91.033	0.896	794.15	1174.57	1148.27	453.81
Mn (B) VI	163.299	72.101	0.794	739.53	1088.41	1703.61	462.09
Fe (A) V	55.883	89.903	0.854	773.15	1165.58	1127.03	470.88
Fe (B) V	165.746	73.658	0.752	736.56	1049.27	1716.32	482.02
Fe (B) III	154.363	71.199	0.558	743.75	1175.79	1799.56	442.79
Co (A) IV	54.195	91.991	0.867	848.58	1227.43	1105.45	490.74
Co (B) IV	160.529	72.288	0.670	732.1	1109.24	1735.94	431.09
Co (B) II	152.382	68.688	0.535	747.94	1173.98	1807.85	442.32
Co (E) IV	167.914	120.825	0.545	786.76	1284.54	1773.00	421.85
Ni (A) III	55.566	88.662	0.742	627.35	946.29	997.90	464.49
Ni (B) III	157.445	71.612	0.657	723.64	1151.91	1753.82	403.92
Ni (B) I	148.420	67.197	0.517	762.48	1179.5	1862.19	539.55
Ni (E) III	166.395	122.703	0.574	791.48	1274.1	1770.95	429.39
Cu (C) II	109.675	43.774	0.604	732.35	1288.47	1772.98	354.96
Cu (D) II	105.524	130.172	0.609	729.97	1305.6	1791.42	450.43
Cu (E) II	10.017	124.692	0.607	784.76	1301.34	1770.76	420.43
Zn (A) I	56.287	90.676	0.912	853.07	1195.17	1272.14	431.58
Zn (C) I	112.515	43.514	0.771	699.31	1254.37	1768.48	357.18

Table S 97 Mean and standard deviation values of the variables.

Variable	Mean	Std. deviation
ΔE [kJ/mol]	-148.467	70.169
∠OCO [°]	124.456	10.695
***d*C-O^1 [Å]**	1.302	0.037
***d*C-O^2 [Å]**	1.248	0.055
***d*O^1-O^2 [Å]**	2.244	0.053
***d*C-M [Å]**	2.212	0.285
***d*M-Cl [Å]**	2.240	0.093
∠MCO^2 [°]	113.433	53.029
∠MO^{1}C [°]	84.738	21.276
δ$^-$(CO_2) [Rho]	0.730	0.126
$\nu_{1(bend)}CO_2$ [cm^{-1}]	761.475	46.555
$\nu_{2(sym)}CO_2$ [cm^{-1}]	1158.823	105.696
$\nu_{3(antisym)}CO_2$ [cm^{-1}]	1528.808	324.253
ν_4M-(CO_2) [cm^{-1}]	461.050	47.036

Table S 98 Correlation coefficients between the variables (Pearson matrix). [#]

	Δ*E*	**∠OCO**	***d*C-O^1**	***d*C-O^2**	***d*O^1-O^2**	***d*C-M**	***d*M-Cl**	**∠MCO^2**	**∠MO^{1}C**	**δ$^-$(CO$_2$)**	**$\nu_{1(bend)}$**	**$\nu_{2(sym)}$**	**$\nu_{3(antisym)}$**	**ν_4**
ΔE [kJ/mol]	1													
∠OCO [°]	0.078	1												
***d*C-O^1 [Å]**	**-0.605**	**-0.654**	1											
***d*C-O^2 [Å]**	0.055	**-0.926**	**0.390**	1										
***d*O^1-O^2 [Å]**	-0.208	**0.930**	-0.361	**-0.917**	1									
***d*C-M [Å]**	0.133	-0.382	0.010	0.380	**-0.492**	1								
***d*M-Cl [Å]**	**-0.670**	**-0.516**	**0.766**	0.360	-0.257	-0.003	1							
∠MCO^2 [°]	-0.328	**0.661**	-0.015	**-0.796**	**0.780**	-0.266	-0.011	1						
∠MO^{1}C [°]	0.057	-0.222	0.053	0.140	-0.312	**0.711**	-0.191	-0.323	1					
δ$^-$(CO$_2$) [Rho]	-0.046	**-0.864**	**0.631**	**0.750**	**-0.774**	0.209	**0.690**	**-0.497**	-0.052	1				
$\nu_{1(bend)}$CO$_2$ [cm^{-1}]	-0.010	**-0.439**	0.106	0.380	**-0.567**	0.344	0.155	**-0.394**	0.379	0.360	1			
$\nu_{2(sym)}$CO$_2$ [cm^{-1}]	**0.468**	0.189	**-0.761**	0.028	-0.134	0.363	**-0.521**	-0.365	0.342	-0.277	**0.465**	1		
$\nu_{3(antisym)}$CO$_2$ [cm^{-1}]	0.000	**0.954**	**-0.472**	**-0.993**	**0.922**	**-0.392**	**-0.391**	**0.768**	-0.191	**-0.760**	-0.377	0.033	1	
ν_4M-(CO$_2$) [cm^{-1}]	**-0.592**	**-0.411**	**0.757**	0.222	-0.191	-0.025	**0.555**	0.044	0.120	0.327	0.210	**-0.531**	-0.284	1

In **bold**, significant values (except diagonal) at the level of significance alpha=0,050 (two-tailed test)

Table S 99 Results from the PCA for all principal components.

	F1	F2	F3	F4	F5	F6	F7
Eigenvalue	6.248	3.654	1.573	0.871	0.608	0.487	0.281
Variability (%)	44.625	26.096	11.237	6.223	4.343	3.480	2.010
Cumulative %	44.625	70.722	81.958	88.181	92.524	96.004	98.014
	F8	**F9**	**F10**	**F11**	**F12**	**F13**	**F14**
Eigenvalue	0.195	0.032	0.028	0.017	0.006	0.000	0.000
Variability (%)	1.395	0.227	0.197	0.124	0.040	0.002	0.001
Cumulative %	99.409	99.636	99.833	99.956	99.997	99.999	100.000

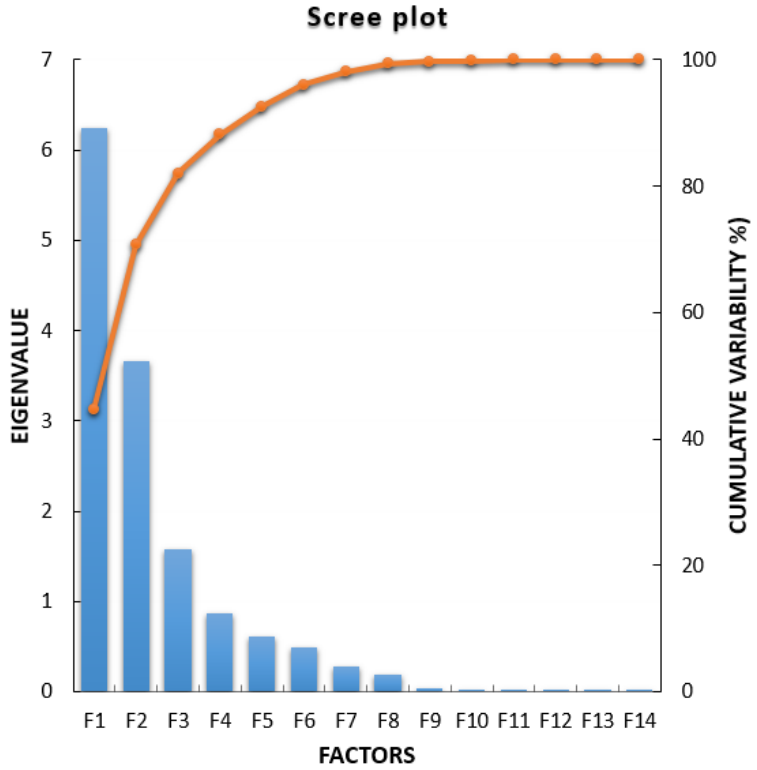

Figure S 100 Scree plot of the calculated eigenvalues, cumulative variability of the factors.

Table S 101 Eigenvectors.

	F1	F2	F3	F4	F5	F6	F7	F8	F9	F10	F11	F12	F13	F14
ΔE [kJ/mol]	0.052	0.393	-0.328	-0.222	-0.077	0.609	0.022	0.275	-0.274	0.360	-0.010	0.166	0.004	-0.016
∠OCO [°]	0.395	0.005	0.066	0.087	0.027	-0.053	0.047	0.210	-0.122	-0.088	0.111	0.051	-0.351	0.788
***d*C-O^1 [Å]**	-0.256	-0.369	0.117	-0.150	-0.087	0.170	0.180	-0.309	0.103	0.147	0.210	0.693	0.040	0.199
***d*C-O^2 [Å]**	-0.368	0.102	-0.186	-0.048	-0.030	-0.266	-0.278	-0.043	-0.269	0.122	0.238	-0.156	0.569	0.418
***d*O^1-O^2 [Å]**	0.368	-0.173	0.077	0.014	0.026	-0.159	0.108	0.153	-0.407	0.028	0.673	0.067	0.095	-0.367
***d*C-M [Å]**	-0.168	0.247	0.428	-0.356	0.522	0.014	-0.314	0.159	-0.164	-0.332	-0.019	0.250	-0.043	-0.049
***d*M-Cl [Å]**	-0.227	-0.350	0.027	0.228	0.447	-0.144	0.273	0.355	-0.270	0.413	-0.330	0.007	-0.012	-0.002
∠MCO^2 [°]	0.272	-0.278	0.187	-0.034	0.335	0.348	-0.436	-0.259	0.193	0.414	0.114	-0.305	0.055	0.065
∠MO^{1}C [°]	-0.108	0.228	0.596	-0.320	-0.191	-0.007	0.479	-0.030	0.023	0.264	0.072	-0.357	0.039	0.086
δ$^-$(CO$_2$) [Rho]	-0.347	-0.083	-0.209	0.071	0.299	0.328	0.274	0.244	0.348	-0.296	0.451	-0.271	-0.038	0.072
$\nu_{1(bend)}$CO$_2$ [cm^{-1}]	-0.204	0.174	0.302	0.679	-0.059	0.351	-0.022	-0.284	-0.381	-0.128	0.047	-0.029	-0.058	0.000
$\nu_{2(sym)}$CO$_2$ [cm^{-1}]	0.051	0.458	0.133	0.397	0.101	-0.224	-0.071	0.207	0.494	0.343	0.192	0.306	0.101	-0.040
$\nu_{3(antisym)}$CO$_2$ [cm^{-1}]	0.377	-0.074	0.139	0.093	0.061	0.241	0.235	0.128	0.090	-0.285	-0.252	0.098	0.722	0.089
ν_4M-(CO$_2$) [cm^{-1}]	-0.181	-0.323	0.297	0.053	-0.506	0.142	-0.383	0.584	0.083	-0.019	-0.001	-0.015	0.002	-0.031

Table S 102 Factor loadings.

	F1	F2	F3	F4	F5	F6	F7	F8	F9	F10	F11	F12	F13	F14
ΔE [kJ/mol]	0.130	0.752	-0.412	-0.207	-0.060	0.425	0.012	0.122	-0.049	0.060	-0.001	0.012	0.000	0.000
∠OCO [°]	0.987	0.009	0.083	0.081	0.021	-0.037	0.025	0.093	-0.022	-0.015	0.015	0.004	-0.006	0.010
***d*C-O¹ [Å]**	-0.641	-0.705	0.147	-0.140	-0.067	0.119	0.095	-0.137	0.018	0.024	0.028	0.052	0.001	0.002
***d*C-O² [Å]**	-0.919	0.196	-0.234	-0.045	-0.024	-0.186	-0.147	-0.019	-0.048	0.020	0.031	-0.012	0.010	0.005
***d*O¹-O² [Å]**	0.920	-0.331	0.096	0.013	0.021	-0.111	0.057	0.067	-0.072	0.005	0.089	0.005	0.002	-0.005
***d*C-M [Å]**	-0.421	0.471	0.536	-0.332	0.407	0.010	-0.166	0.070	-0.029	-0.055	-0.003	0.019	-0.001	-0.001
***d*M-Cl [Å]**	-0.566	-0.668	0.034	0.213	0.349	-0.100	0.145	0.157	-0.048	0.069	-0.043	0.001	0.000	0.000
∠MCO² [°]	0.679	-0.531	0.234	-0.031	0.261	0.243	-0.231	-0.115	0.034	0.069	0.015	-0.023	0.001	0.001
∠MO¹C [°]	-0.269	0.436	0.748	-0.299	-0.149	-0.005	0.254	-0.013	0.004	0.044	0.009	-0.027	0.001	0.001
δ⁻(CO₂) [Rho]	-0.867	-0.159	-0.262	0.066	0.233	0.229	0.145	0.108	0.062	-0.049	0.059	-0.020	-0.001	0.001
$\nu_{1(bend)}$CO₂ [cm^{-1}]	-0.511	0.332	0.379	0.634	-0.046	0.245	-0.012	-0.126	-0.068	-0.021	0.006	-0.002	-0.001	0.000
$\nu_{2(sym)}$CO₂ [cm^{-1}]	0.126	0.875	0.167	0.371	0.079	-0.156	-0.038	0.092	0.088	0.057	0.025	0.023	0.002	0.000
$\nu_{3(antisym)}$CO₂ [cm^{-1}]	0.943	-0.141	0.174	0.087	0.047	0.168	0.125	0.056	0.016	-0.047	-0.033	0.007	0.013	0.001
ν_4M-(CO₂) [cm^{-1}]	-0.453	-0.617	0.372	0.050	-0.395	0.099	-0.203	0.258	0.015	-0.003	0.000	-0.001	0.000	0.000

Table S 103 Contribution of the variables (%). #

	F1	F2	F3	F4	F5	F6	F7	F8	F9	F10	F11	F12	F13	F14
ΔE [kJ/mol]	0.269	**15.468**	10.782	4.929	0.587	37.125	0.050	7.565	7.483	12.955	0.011	2.745	0.002	0.026
∠OCO [°]	**15.597**	0.002	0.436	0.753	0.074	0.284	0.220	4.394	1.476	0.775	1.231	0.259	12.343	62.155
***d*C-O^1 [Å]**	6.573	**13.612**	1.376	2.255	0.749	2.888	3.239	9.540	1.055	2.154	4.399	48.053	0.157	3.950
***d*C-O^2 [Å]**	**13.508**	1.050	3.471	0.232	0.091	7.074	7.729	0.188	7.219	1.493	5.668	2.448	32.365	17.465
***d*O^1-O^2 [Å]**	**13.560**	3.004	0.586	0.021	0.070	2.521	1.159	2.330	16.548	0.079	45.345	0.444	0.893	13.440
***d*C-M [Å]**	2.833	6.078	18.279	12.683	27.290	0.021	9.845	2.523	2.690	11.023	0.037	6.270	0.186	0.243
***d*M-Cl [Å]**	5.134	**12.222**	0.075	5.217	19.977	2.062	7.479	12.593	7.263	17.077	10.881	0.005	0.015	0.001
∠MCO^2 [°]	7.380	7.730	3.495	0.114	11.201	12.115	19.045	6.731	3.726	17.163	1.297	9.286	0.299	0.417
∠MO^{1}C [°]	1.158	5.193	35.529	10.240	3.657	0.005	22.986	0.089	0.052	6.957	0.521	12.720	0.149	0.746
δ$^-$(CO_2) [Rho]	**12.037**	0.689	4.357	0.498	8.951	10.775	7.513	5.968	12.099	8.748	20.342	7.356	0.146	0.521
***ν*$_{1(bend)}$$CO_2$ [cm^{-1}]**	4.174	3.025	9.133	46.142	0.348	12.305	0.050	8.065	14.479	1.634	0.222	0.082	0.341	0.000
***ν*$_{2(sym)}$$CO_2$ [cm^{-1}]**	0.255	**20.975**	1.765	15.767	1.016	5.026	0.506	4.287	24.411	11.758	3.706	9.350	1.023	0.157
***ν*$_{3(antisym)}$$CO_2$ [cm^{-1}]**	**14.234**	0.547	1.920	0.867	0.367	5.796	5.518	1.631	0.809	8.148	6.339	0.961	52.081	0.783
***ν*$_4$M-(CO_2) [cm^{-1}]**	3.288	**10.404**	8.797	0.282	25.623	2.003	14.662	34.096	0.690	0.038	0.000	0.022	0.000	0.095

Table S 104 Factor scores.

	F1	F2	F3	F4	F5	F6	F7	F8	F9	F10	F11	F12	F13	F14
Sc (A) II	-3.706	-0.857	0.412	0.676	0.732	-1.430	0.238	0.153	-0.345	0.163	0.198	0.002	0.021	0.005
Sc (B) II	-0.344	-4.048	0.684	-0.417	0.603	0.470	0.533	0.288	-0.134	-0.038	-0.216	0.107	-0.002	0.013
Ti (A) III	-3.593	-0.322	0.452	0.660	0.296	-1.204	-0.085	-0.075	-0.008	-0.049	0.127	-0.014	-0.028	-0.012
Ti (B) III	0.032	-3.815	0.665	-0.109	0.356	0.112	0.421	-0.238	-0.047	-0.294	-0.092	-0.001	0.007	0.017
V (A) IV	-3.585	0.268	0.204	0.506	-0.044	-0.630	-0.272	-0.031	0.174	0.091	-0.193	0.033	-0.028	-0.012
V (B) IV	0.355	-3.303	0.729	0.142	-0.366	0.315	-0.122	0.267	-0.011	-0.148	-0.053	0.015	0.020	-0.036
Cr (A) V	-3.953	0.750	-0.001	0.620	-0.290	0.443	-0.320	0.538	0.192	0.319	-0.135	0.082	0.007	0.012
Cr (B) V	1.059	-1.729	0.038	0.363	0.176	0.353	0.071	0.493	-0.018	0.207	-0.004	-0.206	-0.038	0.002
Mn (A) VI	-3.043	0.737	-0.303	0.109	0.454	-0.149	0.205	-0.103	0.018	-0.193	0.072	-0.124	0.009	0.015
Mn (B) VI	0.730	-1.703	-0.374	0.058	0.531	0.553	0.339	0.031	0.223	0.160	0.143	-0.002	-0.004	0.000
Fe (A) V	-2.727	0.874	-0.606	-0.414	-0.280	0.040	-0.139	-0.024	0.126	-0.068	0.158	0.015	0.040	-0.016
Fe (B) V	0.984	-1.734	-0.309	-0.357	-0.178	0.903	0.047	-0.054	0.104	0.045	0.190	0.077	-0.015	-0.019
Fe (B) III	2.798	-0.242	-0.279	0.412	-0.385	-0.241	-0.238	-0.216	-0.200	0.302	-0.048	0.063	0.017	0.005
Co (A) IV	-3.578	1.561	0.054	0.782	-0.630	0.726	-0.505	-0.365	0.281	-0.206	-0.083	0.037	-0.002	0.014
Co (B) IV	1.901	-0.923	-0.407	-0.088	0.066	-0.089	0.052	-0.722	0.243	-0.126	0.114	-0.082	-0.008	0.003
Co (B) II	2.950	-0.560	-0.100	0.693	-0.610	-0.741	-0.315	-0.645	0.010	-0.054	0.011	0.018	0.015	0.010
Co (E) IV	1.761	1.942	2.714	-0.407	0.903	-0.195	-0.368	-0.566	0.031	0.043	-0.204	-0.081	0.017	-0.008
Ni (A) III	-1.879	-0.245	-2.047	-3.728	-1.035	-0.632	-0.325	-0.153	-0.127	0.047	-0.114	-0.036	-0.008	0.001
Ni (B) III	2.439	0.090	-0.990	-0.310	0.175	0.297	0.159	-0.564	0.117	0.255	0.184	0.072	-0.001	0.012
Ni (B) I	3.046	-0.684	0.277	0.990	-1.988	0.012	-1.155	0.727	-0.134	-0.079	0.053	-0.071	0.004	0.008
Ni (E) III	1.696	2.282	2.501	-0.647	0.667	0.530	-0.348	-0.334	-0.126	0.147	-0.021	-0.010	-0.006	-0.006
Cu (C) II	3.379	1.874	-2.158	0.894	0.800	-0.804	-0.318	-0.065	-0.168	-0.228	-0.084	0.130	-0.031	-0.006
Cu (D) II	1.851	2.764	2.244	-1.541	0.335	-0.217	0.081	1.095	0.095	-0.209	0.198	0.089	-0.009	0.011
Cu (E) II	1.493	2.680	0.433	0.508	-1.851	-0.483	2.028	0.036	0.036	0.022	-0.105	-0.014	0.000	-0.006
Zn (A) I	-2.582	2.683	-0.918	0.402	0.002	2.025	0.209	-0.250	-0.487	-0.100	0.049	-0.019	-0.006	-0.003
Zn (C) I	2.516	1.658	-2.915	0.203	1.559	0.036	0.125	0.778	0.154	-0.011	-0.145	-0.080	0.029	-0.004

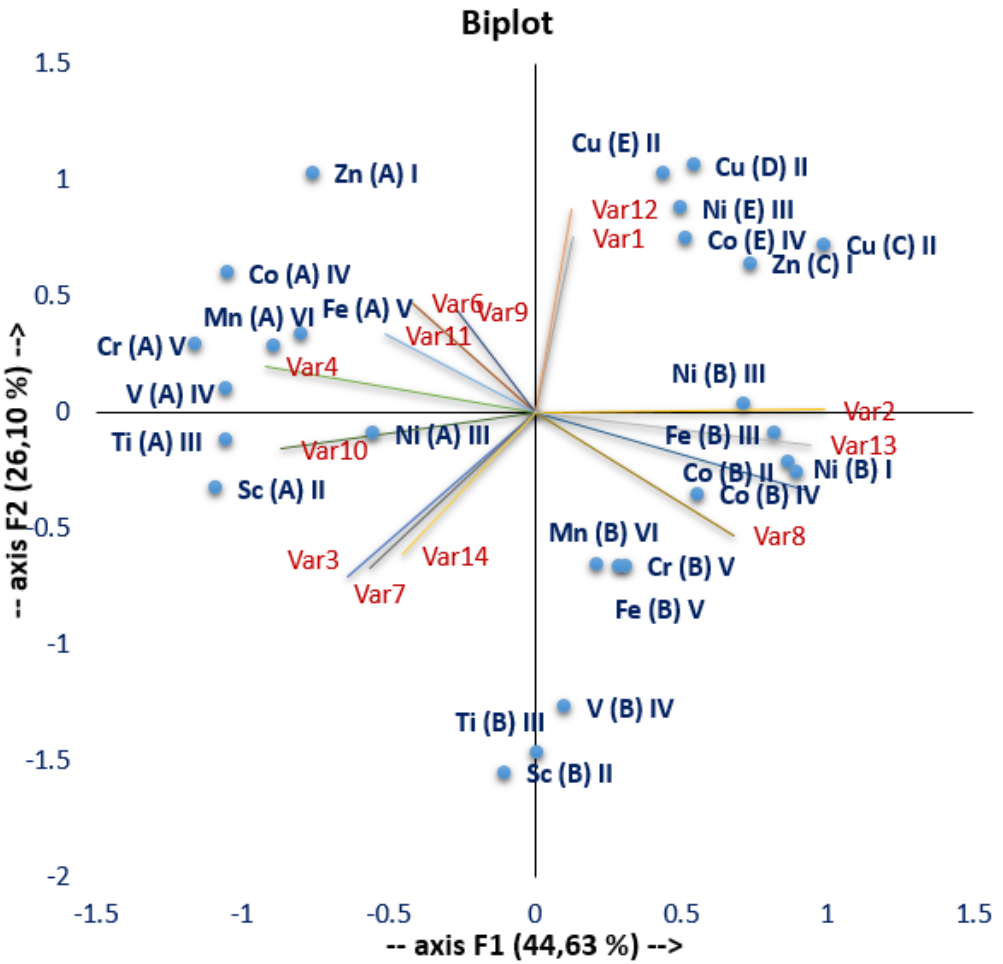

Figure S 105 Factor and object distribution for first two principal components.

Table S 106 Contribution of the observations (%)

	F1	F2	F3	F4	F5	F6	F7	F8	F9	F10	F11	F12	F13	F14
Sc (A) II	8.456	0.773	0.416	2.018	3.393	16.144	0.775	0.459	14.406	3.702	8.729	0.003	5.092	0.560
Sc (B) II	0.073	17.252	1.145	0.768	2.301	1.743	3.886	1.629	2.162	0.196	10.378	7.866	0.039	4.302
Ti (A) III	7.947	0.109	0.499	1.926	0.553	11.441	0.098	0.111	0.007	0.332	3.576	0.141	9.132	3.445
Ti (B) III	0.001	15.322	1.082	0.052	0.800	0.099	2.418	1.112	0.271	12.064	1.891	0.001	0.600	7.149
V (A) IV	7.913	0.076	0.102	1.130	0.012	3.133	1.011	0.019	3.650	1.146	8.245	0.768	8.702	3.778
V (B) IV	0.078	11.482	1.300	0.089	0.847	0.783	0.202	1.405	0.015	3.070	0.633	0.150	4.533	32.905
Cr (A) V	9.619	0.593	0.000	1.699	0.530	1.550	1.398	5.705	4.469	14.178	4.028	4.593	0.633	3.817
Cr (B) V	0.691	3.148	0.004	0.581	0.196	0.983	0.069	4.785	0.039	6.001	0.004	29.039	16.517	0.114
Mn (A) VI	5.702	0.572	0.225	0.052	1.306	0.176	0.577	0.211	0.040	5.219	1.146	10.510	0.887	5.989
Mn (B) VI	0.328	3.053	0.342	0.015	1.787	2.412	1.568	0.019	6.018	3.574	4.542	0.003	0.194	0.001
Fe (A) V	4.577	0.805	0.898	0.757	0.497	0.013	0.263	0.012	1.916	0.638	5.556	0.148	18.440	6.664
Fe (B) V	0.596	3.167	0.234	0.564	0.201	6.435	0.030	0.057	1.313	0.277	7.995	4.059	2.430	8.995
Fe (B) III	4.818	0.062	0.191	0.749	0.936	0.457	0.772	0.919	4.861	12.760	0.509	2.705	3.307	0.666
Co (A) IV	7.882	2.566	0.007	2.700	2.514	4.156	3.483	2.620	9.582	5.905	1.541	0.958	0.063	4.839
Co (B) IV	2.225	0.896	0.405	0.034	0.028	0.062	0.038	10.273	7.162	2.201	2.886	4.561	0.806	0.291
Co (B) II	5.359	0.330	0.024	2.122	2.355	4.333	1.353	8.199	0.013	0.413	0.029	0.218	2.536	2.490
Co (E) IV	1.909	3.971	18.007	0.732	5.162	0.301	1.856	6.312	0.118	0.263	9.263	4.501	3.252	1.550
Ni (A) III	2.173	0.063	10.241	61.358	6.772	3.151	1.442	0.462	1.954	0.312	2.902	0.893	0.662	0.015
Ni (B) III	3.664	0.008	2.396	0.425	0.193	0.698	0.344	6.259	1.650	9.086	7.503	3.596	0.010	3.764
Ni (B) I	5.711	0.493	0.188	4.331	25.005	0.001	18.230	10.397	2.179	0.875	0.633	3.411	0.192	1.662
Ni (E) III	1.770	5.482	15.289	1.850	2.812	2.221	1.660	2.194	1.919	3.029	0.099	0.075	0.437	0.991
Cu (C) II	7.027	3.695	11.389	3.529	4.050	5.097	1.386	0.082	3.431	7.220	1.566	11.563	10.941	1.021
Cu (D) II	2.109	8.045	12.314	10.483	0.711	0.372	0.090	23.588	1.102	6.066	8.693	5.424	0.911	3.320
Cu (E) II	1.371	7.563	0.459	1.139	21.664	1.844	56.238	0.026	0.159	0.065	2.432	0.134	0.001	0.972
Zn (A) I	4.104	7.577	2.062	0.713	0.000	32.386	0.597	1.227	28.695	1.389	0.544	0.255	0.406	0.210
Zn (C) I	3.897	2.896	20.781	0.182	15.375	0.010	0.214	11.917	2.868	0.017	4.676	4.425	9.279	0.492

4. Artificial Neural Network Analysis (ANNA).

In order to further analyze the relationship between the stability of the complexes and other physical factors, an artificial neural network (ANN) was constructed based on calculated Pearson's[6] correlation coefficients (ρ) between the 14 variables describing the full set of 26 structures including all (A-E) isomers (Figure 6, left, and S103). For a better understanding of the presented results, it needs to be stated that in the Pearson's correlation analysis if two variables are positively correlated with each other this means that if one variable increases the other does also. The strength of the linear relationship is measured between $\rho \in [0,1]$, with the value of 0 meaning that there is no linear correlation between the given variables. On the other hand, a negative correlation occurs when one of the variables decreases while the other increases. In this case, the correlation is measured in the range of $\rho \in [-1:0]$, with -1 indicating a maximum strength of the negative linear correlation.

Several positive and negative correlations between the complexation energies (ΔE) and other variables were found. First, a negative correlation was found between ΔE and $d(\text{C-O}^1)$ (ρ=−0.6) and d(Cl-M) (ρ=−0.7) bond distances, as well as the ν_4(M-CO_2) vibrational frequency (ρ=−0.6). This means that when the ν_4(M-CO_2) frequency value and the metal-chloride and carbon-oxygen bond lengths decrease, the $[ClM(CO_2)]^-$ complexes become less stable since ΔE increases in value and becomes less negative. A second, weak and positive correlation between ΔE of all (A-E) isomers and the symmetric vibrational stretch (ρ=0.5) of CO_2 moiety ($\nu_2^{sym}(CO_2)$) was found. In addition, correlation coefficients were calculated independently for nine (A) and eleven (B) isomers and artificial neural networks for those connections were constructed and plotted in Figure 6. A strong positive correlation between ΔE and the antisymmetric stretch (ρ=0.7) for (A)-type isomers was found (See S104, S105). This means that when ΔE increases, making the complexes less stable, the $\nu_3^{antisym}(CO_2)$ frequency also increases. A number of strong negative correlations were identified between the ΔE of the (A) isomers and four bond distances $d(\text{C-O}^1)$ (ρ=−0.8), $d(\text{C-O}^2)$ (ρ=−0.8), $d(\text{O}^1\text{-O}^2)$ (ρ=−0.5), d(M-Cl) (ρ=−0.9), as well as one positive correlation with the vibrational frequency ν_4(M-CO_2) (ρ=0.6). Furthermore, several correlations were found for the (B)-type isomers. Significant positive correlations were found between ΔE and the symmetric stretch of the CO_2 moiety (ρ=0.8) and the ∠OCO (ρ=0.6), $\angle MCO^1$ (ρ=0.7) valence angles. In addition, four negative correlations between the ΔE of the (B)-type isomers and $d(\text{C-O}^1)$ (ρ=−0.7), d(M-Cl) (ρ=−0.7), $\angle MCO^1$ (ρ=−0.6), ν_4(M-CO_2) (ρ=−0.6) were identified.

The neural network analysis shows that there is no strong overall simple linear, two-dimensional relationship between the energy of complexation (ΔE) and any other single variable. On the other hand, a multidimensional relationship between a number of structural and spectral factors and the ΔE values was found. The theoretically predicted periodic trend and relationships between the relative stability of the $[ClM(CO_2)]^-$ ions and the vibrational and geometric parameters of the CO_2 ligand can be related to the infrared spectroscopy measurements of the first-row transition metal-CO_2 cluster ions $[M(CO_2)_{2\text{-}8}]^-$, published in a series of papers by Weber and co-workers[7]. The authors have presented photodissociation action spectra recorded for $[M(CO_2)_3]^-$ ions with characteristic spectral features between 1600−1900 cm^{-1}. The main IR peaks correspond to the antisymmetric stretches of two CO_2 molecules bonded to the metal core in a "butterfly" mode, where both CO_2 molecules coordinate to the metal atom in a (B)-type motif. The key spectral features recorded for manganese containing[7e] cluster ions were located at 1680 and 1724 cm-1, for iron[7d] at 1699 and 1749 cm^{-1}, and for cobalt[7c] at ~1750 and ~1780 cm^{-1}. Nickel[7b] and copper[7a] core–CO_2 clusters were characterized by three spectral features corresponding to overlapping antisymmetric CO_2 stretches of two very similar cluster isomers at ~1740; ~1770 and ~1790 cm-1 and at ~1750; ~1780 and ~1820 cm^{-1}, respectively. It can be seen that experimentally measured band origins of the main features are clearly red-shifted in the periodic trend Mn<Fe<Co<Ni<Cu. Furthermore, these authors have suggested that the observed red shift of the antisymmetric stretches of asymmetric, (B)-like isomers can be correlated to the amount of negative charge deposited on the partially reduced CO_2 moiety.[7d, 8] It can be seen in the presented connection network constructed for (B)-type isomers (Figure 6, right) that the partial charges of the CO_2 ligand in (B)-type isomers are strongly negatively correlated with the symmetric (ρ=−0.9) and antisymmetric CO_2 stretches (ρ=−0.85). Additionally, a large linear correlation

coefficient (R^2=0.87) was found between $\delta^-(CO_2)$ and the latter variable (see S87), showing that highly negatively charged CO_2 moieties result in lower antisymmetric vibrational frequencies. The extent of the experimentally observed red shifts[7-8] strongly supports the proposed trend derived from the statistical analysis and the computed CO_2 partial charges.

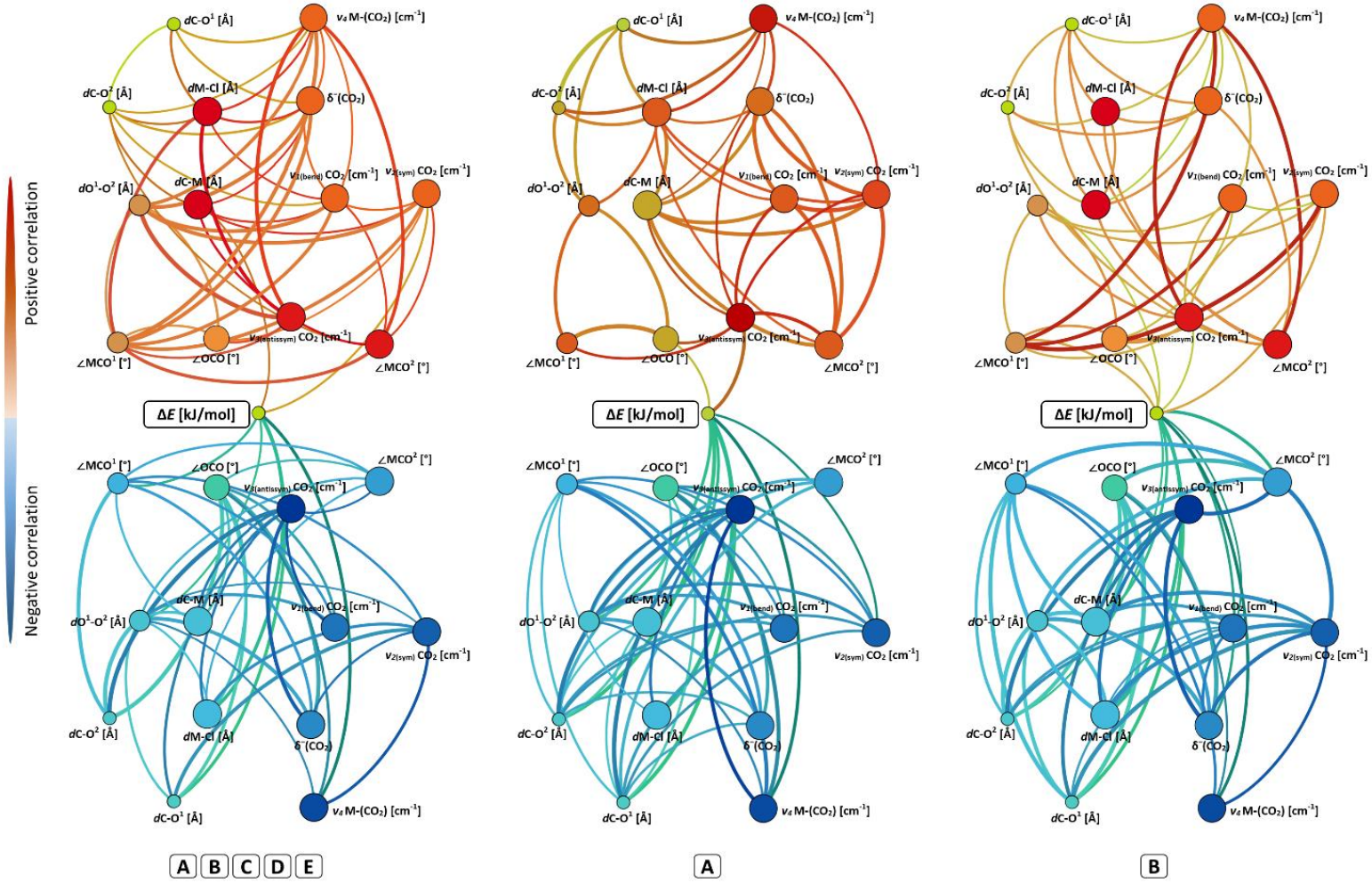

Figure S 107 Artificial neural networks constructed based on the calculated Pearson's correlation coefficients between 14 variables for all twenty-six (A)-(E) isomers (left), nine A isomers (middle) and eleven B isomers (right). Note that different shades of the principal blue and red colors were introduced just to enhance visibility and they do not indicate the strength of the connections.

4.1. Correlation coefficients calculated for all (A-E) isomers

Table S 108 Correlation coefficients between 14 variables for 26 (A-E) isomers (Pearson matrix). [#]

	Δ*E*	**∠OCO**	***d*C-O^1**	***d*C-O^2**	***d*O^1-O^2**	***d*C-M**	***d*M-Cl**	**∠MCO^2**	**∠MO^{1}C**	**δ$^-$(CO$_2$)**	**$\nu_{1(bend)}$**	**$\nu_{2(sym)}$**	**$\nu_{3(antisym)}$**	**ν_4**
Δ*E* [kJ/mol]	1													
∠OCO [°]	0.078	1												
***d*C-O^1 [Å]**	**-0.605**	**-0.654**	1											
***d*C-O^2 [Å]**	0.055	**-0.926**	**0.390**	1										
***d*O^1-O^2 [Å]**	-0.208	**0.930**	-0.361	**-0.917**	1									
***d*C-M [Å]**	0.133	-0.382	0.010	0.380	**-0.492**	1								
***d*M-Cl [Å]**	**-0.670**	**-0.516**	**0.766**	0.360	-0.257	-0.003	1							
∠MCO^2 [°]	-0.328	**0.661**	-0.015	**-0.796**	**0.780**	-0.266	-0.011	1						
∠MO^{1}C [°]	0.057	-0.222	0.053	0.140	-0.312	**0.711**	-0.191	-0.323	1					
δ$^-$(CO$_2$) [Rho]	-0.046	**-0.864**	**0.631**	**0.750**	**-0.774**	0.209	**0.690**	**-0.497**	-0.052	1				
$\nu_{1(bend)}$CO$_2$ [cm^{-1}]	-0.010	**-0.439**	0.106	0.380	**-0.567**	0.344	0.155	**-0.394**	0.379	0.360	1			
$\nu_{2(sym)}$CO$_2$ [cm^{-1}]	**0.468**	0.189	**-0.761**	0.028	-0.134	0.363	**-0.521**	-0.365	0.342	-0.277	**0.465**	1		
$\nu_{3(antisym)}$CO$_2$ [cm^{-1}]	0.000	**0.954**	**-0.472**	**-0.993**	**0.922**	**-0.392**	**-0.391**	**0.768**	-0.191	**-0.760**	-0.377	0.033	1	
ν_4M-(CO$_2$) [cm^{-1}]	**-0.592**	**-0.411**	**0.757**	0.222	-0.191	-0.025	**0.555**	0.044	0.120	0.327	0.210	**-0.531**	-0.284	1

In **bold**, significant values (except diagonal) at the level of significance alpha=0,050 (two-tailed test)

4.2. Correlation coefficients calculated for (A) type isomers

Table S 109 Correlation coefficients between 14 variables for 9 (A) isomers (Pearson matrix). [#]

	Δ*E*	**∠OCO**	***d*C-O^1**	***d*C-O^2**	***d*O^1-O^2**	***d*C-M**	***d*M-Cl**	**∠MCO^2**	**∠MO^{1}C**	**δ$^-$(CO$_2$)**	**$\nu_{1(bend)}$**	**$\nu_{2(sym)}$**	**$\nu_{3(antisym)}$**	**ν_4**
Δ*E* [kJ/mol]	1													
∠OCO [°]	0.144	1												
***d*C-O^1 [Å]**	**-0.772**	-0.269	1											
***d*C-O^2 [Å]**	**-0.773**	-0.271	**1.000**	1										
***d*O^1-O^2 [Å]**	-0.500	0.631	0.577	0.575	1									
***d*C-M [Å]**	-0.429	0.070	-0.171	-0.168	-0.079	1								
***d*M-Cl [Å]**	**-0.865**	-0.046	0.563	0.565	0.413	**0.666**	1							
∠MCO^2 [°]	0.098	**0.982**	-0.251	-0.253	0.631	0.087	-0.009	1						
∠MO^{1}C [°]	0.088	0.009	-0.559	-0.558	-0.445	**0.799**	0.287	-0.027	1					
δ$^-$(CO$_2$) [Rho]	-0.105	-0.607	-0.261	-0.257	**-0.724**	0.664	0.267	-0.615	**0.745**	1				
$\nu_{1(bend)}$CO$_2$ [cm^{-1}]	-0.017	-0.219	-0.489	-0.486	-0.580	**0.781**	0.283	-0.217	**0.897**	**0.857**	1			
$\nu_{2(sym)}$CO$_2$ [cm^{-1}]	-0.181	-0.322	-0.339	-0.338	-0.548	**0.791**	0.405	-0.307	**0.859**	**0.882**	**0.964**	1		
$\nu_{3(antisym)}$CO$_2$ [cm^{-1}]	**0.690**	0.388	**-0.973**	**-0.974**	-0.456	0.293	-0.425	0.355	0.659	0.254	0.543	0.387	1	
ν_4M-(CO$_2$) [cm^{-1}]	-0.566	**-0.822**	0.644	0.644	-0.180	0.054	0.496	**-0.803**	-0.046	0.432	0.117	0.302	**-0.680**	1

In **bold**, significant values (except diagonal) at the level of significance alpha=0,050 (two-tailed test)

4.3. Correlation coefficients calculated for (B) type isomers

Table S 110 Correlation coefficients between 14 variables for 11 (B) isomers (Pearson matrix). [#]

	Δ*E*	**∠OCO**	***d*C-O^1**	***d*C-O^2**	***d*O^1-O^2**	***d*C-M**	***d*M-Cl**	**∠MCO^2**	**∠MO^{1}C**	**δ$^-$(CO$_2$)**	**$\nu_{1(bend)}$**	**$\nu_{2(sym)}$**	**$\nu_{3(antisym)}$**	**ν_4**
Δ*E* [kJ/mol]	1													
∠OCO [°]	0.549	1												
***d*C-O^1 [Å]**	**-0.710**	**-0.961**	1											
***d*C-O^2 [Å]**	-0.237	**-0.839**	**0.677**	1										
***d*O^1-O^2 [Å]**	0.229	**0.925**	**-0.788**	**-0.924**	1									
***d*C-M [Å]**	-0.469	**-0.954**	**0.904**	**0.811**	**-0.902**	1								
***d*M-Cl [Å]**	**-0.711**	**-0.894**	**0.933**	**0.681**	**-0.719**	**0.901**	1							
∠MCO^2 [°]	**0.711**	**0.886**	**-0.946**	-0.581	**0.684**	**-0.885**	**-0.920**	1						
∠MO^{1}C [°]	**-0.629**	**-0.983**	**0.982**	**0.760**	**-0.855**	**0.954**	**0.930**	**-0.956**	1					
δ$^-$(CO$_2$) [Rho]	-0.405	**-0.968**	**0.891**	**0.881**	**-0.957**	**0.943**	**0.872**	**-0.805**	**0.930**	1				
$\nu_{1(bend)}$CO$_2$ [cm^{-1}]	-0.185	0.454	-0.306	-0.461	**0.622**	-0.568	-0.178	0.273	-0.395	-0.448	1			
$\nu_{2(sym)}$CO$_2$ [cm^{-1}]	**0.746**	**0.924**	**-0.989**	-0.594	**0.724**	**-0.868**	**-0.921**	**0.963**	**-0.966**	**-0.847**	0.243	1		
$\nu_{3(antisym)}$CO$_2$ [cm^{-1}]	0.271	**0.919**	**-0.777**	**-0.959**	**0.983**	**-0.892**	**-0.716**	**0.686**	**-0.852**	**-0.932**	**0.607**	**0.704**	1	
ν_4M-(CO$_2$) [cm^{-1}]	-0.570	-0.284	0.460	-0.033	-0.021	0.171	0.503	-0.481	0.370	0.260	**0.613**	-0.537	0.036	1

In **bold**, significant values (except diagonal) at the level of significance alpha=0,050 (two-tailed test)

4. References

[1] S. Narancic, A. Bach, P. Chen, *J. Phys. Chem. A* **2007**, *111*, 7006-7013.

[2] S. K. Loh, D. A. Hales, L. Lian, P. B. Armentrout, *J. Chem. Phys.* **1989**, *90*, 5466-5485.

[3] M. J. Frisch, G. W. Trucks, H. B. Schlegel, G. E. Scuseria, M. A. Robb, J. R. Cheeseman, G. Scalmani, V. Barone, B. Mennucci, G. A. Petersson, H. Nakatsuji, M. Caricato, X. Li, H. P. Hratchian, A. F. Izmaylov, J. Bloino, G. Zheng, J. L. Sonnenberg, M. Hada, M. Ehara, K. Toyota, R. Fukuda, J. Hasegawa, M. Ishida, T. Nakajima, Y. Honda, O. Kitao, H. Nakai, T. Vreven, J. A. Montgomery Jr., J. E. Peralta, F. Ogliaro, M. J. Bearpark, J. Heyd, E. N. Brothers, K. N. Kudin, V. N. Staroverov, R. Kobayashi, J. Normand, K. Raghavachari, A. P. Rendell, J. C. Burant, S. S. Iyengar, J. Tomasi, M. Cossi, N. Rega, N. J. Millam, M. Klene, J. E. Knox, J. B. Cross, V. Bakken, C. Adamo, J. Jaramillo, R. Gomperts, R. E. Stratmann, O. Yazyev, A. J. Austin, R. Cammi, C. Pomelli, J. W. Ochterski, R. L. Martin, K. Morokuma, V. G. Zakrzewski, G. A. Voth, P. Salvador, J. J. Dannenberg, S. Dapprich, A. D. Daniels, Ö. Farkas, J. B. Foresman, J. V. Ortiz, J. Cioslowski, D. J. Fox, Gaussian, Inc., Wallingford, CT, USA, **2009**.

[4] K. GaussView ver.5; Dennington R. ; Keith T.; Millam J.; Semichem Inc.; Shawnee Mission, 2009.

[5] F. L. Hirshfeld, *Theor. Chim. Acta* **1977**, *44*, 129-138.

[6] K. Pearson, *Notes on regression and inheritance in the case of two parents*, Royal Society, London, **1895**.

[7] a) B. J. Knurr, J. M. Weber, *J. Phys. Chem. A* **2014**, *118*, 10246-10251; b) B. J. Knurr, J. M. Weber, *J. Phys. Chem. A* **2014**, *118*, 8753-8757; c) B. J. Knurr, J. M. Weber, *The Journal of Physical Chemistry A* **2014**, *118*, 4056-4062; d) M. C. Thompson, L. G. Dodson, J. M. Weber, *J. Phys. Chem. A* **2017**, *121*, 4132-4138; e) M. C. Thompson, J. Ramsay, J. M. Weber, *J. Phys. Chem. A* **2017**, *121*, 7534-7542.

[8] a) B. J. Knurr, J. M. Weber, *J. Am. Chem. Soc.* **2012**, *134*, 18804-18808; b) B. J. Knurr, J. M. Weber, *The Journal of Physical Chemistry A* **2013**, *117*, 10764-10771.